NEI-NO-459

DE95723910

NTIS
One Source. One Search. One Solution.

HYDROGENATION OF CO ON SUPPORTED COBALT CATALYSTS STUDIED BY IN SITU FOURIER TRANSFORM INFRARED (FTIR) SPECTROSCOPY

NORGES TEKNISKE HOEGSKOLE, TRONDHEIM

DEC 1993

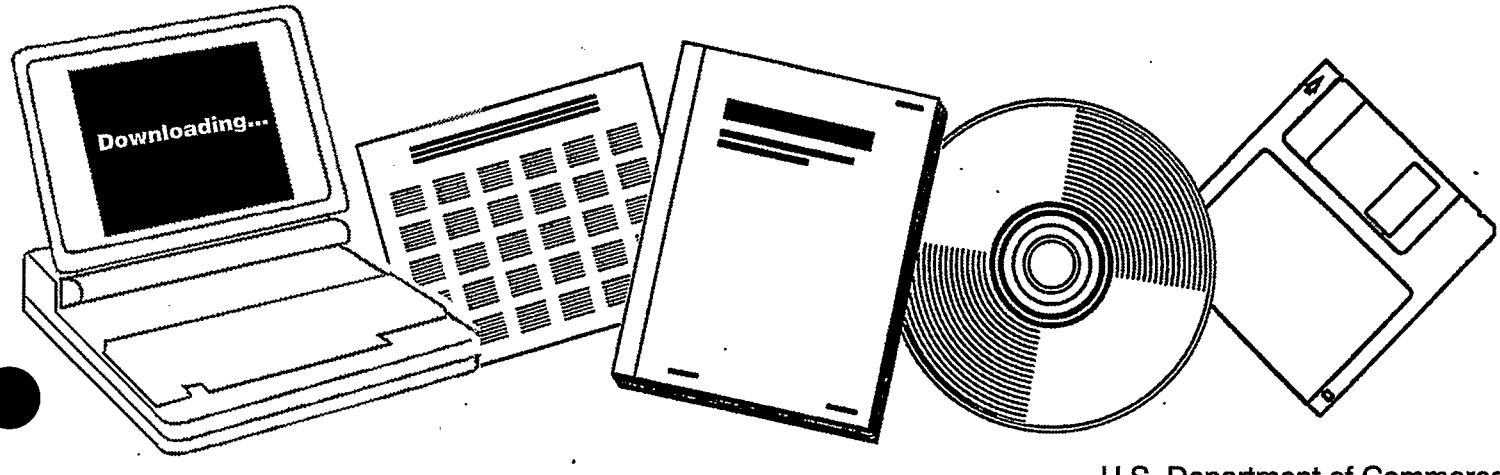

U.S. Department of Commerce
National Technical Information Service

One Source. One Search. One Solution.

NTIS

Providing Permanent, Easy Access to U.S. Government Information

National Technical Information Service is the nation's largest repository and disseminator of government-initiated scientific, technical, engineering, and related business information. The NTIS collection includes almost 3,000,000 information products in a variety of formats: electronic download, online access, CD-ROM, magnetic tape, diskette, multimedia, microfiche and paper.

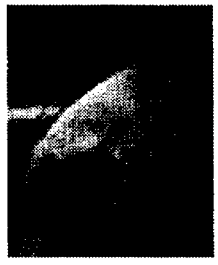

Search the NTIS Database from 1990 forward

NTIS has upgraded its bibliographic database system and has made all entries since 1990 searchable on **www.ntis.gov.** You now have access to information on more than 600,000 government research information products from this web site.

Link to Full Text Documents at Government Web Sites

Because many Government agencies have their most recent reports available on their own web site, we have added links directly to these reports. When available, you will see a link on the right side of the bibliographic screen.

Download Publications (1997 - Present)

NTIS can now provides the full text of reports as downloadable PDF files. This means that when an agency stops maintaining a report on the web, NTIS will offer a downloadable version. There is a nominal fee for each download for most publications.

For more information visit our website:

www.ntis.gov

U.S. DEPARTMENT OF COMMERCE
Technology Administration
National Technical Information Service
Springfield, VA 22161

Hydrogenation of CO on Supported Cobalt Catalysts Studied by *in situ* FTIR Spectroscopy

by

Geir Remo Fredriksen

A Thesis Submitted to
The Department of Industrial Chemistry
The Norwegian Institute of Technology
The University of Trondheim

In Partial Fulfilment of the Requirements
For the Degree
DOCTOR OF ENGINEERING
December 1993

TRYKK
93

ABSTRACT

Hydrogenation of CO over silica and alumina supported cobalt catalysts has been investigated by the use of different experimental techniques; temperature programmed reduction, *in situ* infrared spectroscopy, gravimetry and measurements of activity and selectivity.

Temperature Programmed Reduction (TPR) was used to characterize uncalcined silica and alumina supported cobalt catalysts with different metal loading, 0.82% and 4.7% Co/SiO_2 together with 1% and 4.6% $Co/\gamma\text{-}Al_2O_3$.

In addition to reduction peaks attributed to the reductive decomposition of cobalt nitrate (the metal precursor), TPR-profiles of all the catalysts except 1% $Co/\gamma\text{-}Al_2O_3$ featured peaks which have been assigned to the reduction of cobalt oxide, Co_3O_4. The lack of the cobalt oxide reduction peak for 1% $Co/\gamma\text{-}Al_2O_3$ has been interpreted as being a result of cobalt located in interstices of the alumina lattice, forming a cobalt aluminate spinel phase.

Peaks appearing at higher reduction temperatures have been ascribed to the presence of cobalt ions, Co^{2+}/Co^{3+}, exhibiting varying degree of interaction with the support.

The total extent of reduction of the catalysts increased with increasing cobalt loading. A higher degree of reduction for the silica supported catalysts compared to the alumina supported cobalt catalysts was found.

CO hydrogenation on silica supported cobalt catalysts studied by *in situ* infrared spectroscopy revealed absorption bands characteristic of linearly adsorbed CO on metallic cobalt. The constant frequency (2068 ± 4 cm^{-1}) of this band at different reaction conditions ($H_2/CO=2$, $P_{Tot}=2.5$, 6 or 11 bar, T=473K) has been discussed in terms of a high local coverage of adsorbed CO, akin to the formation of islands of carbon monoxide.

A decrease in the linear CO band intensity accompanied by a dowscale shift in frequency with increasing CO hydrogenation temperature, indicated a decrease in the coverage of adsorbed CO. The reduced coverage of CO at higher reaction temperatures is partly due to the deposition of carbon or carbonaceous species.

Absorption bands observed in the spectral region 2000-1800 cm^{-1} can be associated with silica overtone bands (lattice vibrations) and not bridgebonded CO.

At the reaction conditions of 2.5-11 bar, $H_2/CO=2$ and 473-573K, the heat of adsorption of CO on 4.7% Co/SiO_2 has been estimated to 40 ± 30 kJ/mole.

CO hydrogenation over 1% $Co/\gamma\text{-}Al_2O_3$ did not reveal absorption bands attributable to molecularly adsorbed CO. UV-VIS diffuse reflectance and TPR-measurements indicated that cobalt was located in the alumina lattice, occupying tetrahedral lattice sites, hence being inaccessible for adsorption of CO.

Infrared spectra of 4.6% $Co/\gamma\text{-}Al_2O_3$ during CO hydrogenation ($H_2/CO=2$, 6 bar, 473K) showed the presence of linearly adsorbed CO at 2062 cm^{-1} in addition to a pair of bands located at 1996 and 1952 cm^{-1}. The two bands have tentatively been attributed to bridgebonded CO, and are suggested to be associated with the mixed cobalt oxide phase. The intensity of the doublet decreased with time of reaction (at 473K) and upon an increase in the CO hydrogenation temperature.

Absorption bands appearing in the frequency regions 3050-2700 and 1800-1200 cm^{-1} during CO hydrogenation over the silica and alumina supported cobalt catalysts have been assigned to hydrocarbon structures and various compounds such as surface formates and carbonates. The variation of the band intensities with time during CO hydrogenation and subsequent treatment with He and/or hydrogen indicated that these structures could be regarded as spectator species, and not reaction intermediates in the Fischer-Tropsch synthesis.
Adsorption on the support was suggested by the lack of any influence of the growth of these bands on the linear CO band position and intensity, in addition to the absence of any reasonable reactivity in hydrogen at reaction conditions.

CO hydrogenation activity measurements were found to result in a negligible activity for 1% $Co/\gamma\text{-}Al_2O_3$ at reaction conditions (523K, $H_2/CO=2$, 6 bar).
The activity of 4.7% Co/SiO_2 decreased with time of reaction. In contrast, the 4.6% $Co/\gamma\text{-}Al_2O_3$ catalyst showed a low initial activity, but the activity increased with time during exposure to synthesis gas.

The distribution of the hydrocarbon products followed reasonably well the chain polymerization model of Anderson, Schulz and Flory, with characteristic deviations at C_1 (positive) and at C_2 (negative).

Microbalance investigations of 4.7% Co/SiO_2 during CO hydrogenation revealed decreasing amounts of deposited material with increasing reaction temperature (473-573K). The development of the weight curves with temperature has been discussed in terms of accumulation of hydrocarbons on the catalyst.

For 4.6% $Co/\gamma\text{-}Al_2O_3$, increasing CO hydrogenation temperature was found to result in increasing amounts of deposited species. Also, a significant weight increase could be observed over alumina alone when CO hydrogenation was carried out at 523K ($H_2/CO=2$, 6 bar).

The observed weight changes over alumina alone and the alumina supported cobalt catalyst are predominantly due to the formation of stable formate and carbonate species, as indicated from the *in situ* infrared investigations.

The weight increase observed when CO hydrogenation was carried out at 723K ($H_2/CO=2$, 6 bar) over 4.7% Co/SiO_2 and 4.6% $Co/\gamma\text{-}Al_2O_3$ has been interpreted as due to the formation of inactive carbon, probably graphite.

ACKNOWLEDGEMENTS

I wish to thank Professor A. Holmen for initiating the present work and acting as supervisor during the course of this study. I also appreciate his help in the preparation of this manuscript.

Special thanks to Dr. A. Hoff and Dr. S.H. Skaare for helpful discussions, sharing of frustrations and viewpoints and their will to answer questions of varying stupidity.
Associate Professor E. A. Blekkan and Dr. D. Schanke are thanked for reading through the manuscript, providing comments regarding the content as well as the grammar.
I would also like to thank my former colleagues at SINTEF, Applied Chemistry and the staff at the Department of Industrial Chemistry at NTH for companionship and collaboration. A special thank to Associate Professor O. Tronstad for doing the BET measurements. Experimental contributions from T. Johansen is also acknowledged.

My colleagues at STATOIL's Research Centre, Downstream Technology, are acknowledged for support and friendship. In this respect, I am indebted to Dr. A. Jackson for trawling through the manuscript and pointing out the worst grammatical errors and blunders. Special thanks to L. de Ridder and Dr. E. E. Johnsen for performing the UV-VIS diffuse reflectance measurements.

I am grateful for the financial support from STATOIL making it possible to visit Professor P. Hollins at the University of Reading, England.

Last, but not least, I wish to express my sincere gratitude to my wife Trine, whose understanding, incredible endurance and patience during these years made everything more tolerable when times of distress arrived.

The present study was made possible through the financial support from the Royal Norwegian Council for Scientific and Industrial Research through the SPUNG programme, and from the Department of Industrial Chemistry at The University of Trondheim, NTH.

LIST OF SYMBOLS AND ABBREVIATIONS

A	absorbance of infrared peak (measured as peak height)
A_c	cross sectional area of IR wafer (cm^2)
A_{CO}	molar integrated infrared intensity (cm/mole)
AES	Auger Electron Spectroscopy
α	chain growth probability
ASF	Anderson Schulz Flory polymerization kinetics
β	heating rate (K/min.)
BET	measurement of surface area by the method of Brunauer, Emmet and Teller
B	rotational constant
bcc	body centered cubic
B_{CHx}	structural unit intensity of CH_x-groups (dm^3/cm^2-mole)
C_{CO}	concentration of CO (mole/cm^3)
cm^{-1}	wavenumber (frequency)
D	dispersion (%)
δ	optical pathlength
$-\Delta H_{CO}$	heat of adsorption for CO (kJ/mole)
d_p	particle diameter (nm)
DRS	Diffuse Reflectance Spectroscopy
DRIFTS	Diffuse Reflectance Infrared Fourier Transform Spectroscopy
EELS	Electron Energy Loss Spectroscopy
ε_γ	extinction coefficient at γ cm^{-1}
ε_i	discrete energy level i
EPR	Electron Paramagnetic Resonance
ESCA	Electron Spectroscopy for Chemical Analysis
fcc	face centered cubic
FID	Flame Ionization Detector
F-T	Fischer-Tropsch
FTIR	Fourier Transform InfraRed spectroscopy
g_i	number of states with energy ε_i

GC	Gas Cromatograph
GHSV	Gas Hourly Space Velocity [Nml(CO+H_2)/g catalyst-h]
h	Planck constant ($6.6262 \cdot 10^{-34}$ J-s)
HDS	HydroDeSulfurization
HREELS	High Resolution Electron Energy Loss Spectroscopy
I	moment of inertia of a molecule
IR	InfraRed spectroscopy
ISS	Ion Scattering Spectroscopy
k	force constant
k	Boltzman constant ($1.381 \cdot 10^{-23}$ J/K)
K_{CO}	equilibrium constant for CO adsorption
k_p	rate constant for chain propagation
k_t	rate constant for chain termination
L	infrared beam path length or sample thickness (cm)
LEED	Low Electron Energy Diffraction
MCT	Mercury Cadmium Telluride
μ	dipole moment
N_i	number of molecules with energy ε_i
NMR	Nuclear Magnetic Resonance spectroscopy
m_{cat}	mass of catalyst (mg)
μ_m	reduced mass
n	number of carbon atoms in the hydrocarbon product
N	number of atoms in a molecule
n_{CO}	molar uptake of CO (mol/g)
P	absolute pressure (bar)
Q	normal coordinate
R	gas constant (8.314 J/mol-K)
r_e	equilibrium bond length
r_p	rate of chain propagation
r_t	rate of chain termination
ρ	density (cm^3/g)
S_{CO}	integrated infrared absorbance of CO peak (cm^{-1})

SIMS	Secondary Ion Mass Spectroscopy
θ_{co}	coverage of CO
T	temperature (K)
TCD	Thermal Conductivity Detector
TOS	Time On Stream (min.)
TPD	Temperature Programmed Desorption
TPR	Temperature Programmed Reduction
TPSR	Temperature Programmed Surface Reaction
U	potential energy of a system
UV-VIS	UltraViolet-VISible spectroscopy
W_n	Weight fraction of hydrocarbon product containing n carbon atoms
Å	Ångstrøm, 1 Å = 10^{-10}m
XPS	X-ray Photoelectron Spectroscopy
XRD	X-Ray Diffraction
XRPD	X-Ray Powder Diffraction

TABLE OF CONTENTS

1. INTRODUCTION

1.1. THE FISCHER-TROPSCH PROCESS; HISTORY, PAST AND FUTURE PROSPECTS

At the early beginning of the century, Sabatier et al. /1/ reported the production of methane from mixtures of hydrogen and carbon monoxide using nickel and cobalt catalysts. BASF /2/ showed that a mixture of hydrocarbons and oxygenated compounds could be formed from H_2 and CO over cobalt catalysts using high pressures. The process was further developed by Fischer and coworkers, and in 1923 the synthesis of mainly oxygenated products (primary alcohols) and liquid hydrocarbons over alkalized iron or cobalt catalysts was reported /3/.
Ni, Co and Fe were investigated as potential catalysts, but Ni and Fe were discarded with time. Ni because of its high tendency to produce methane and loss of nickel as nickel carbonyl, while rapid deactivation of the iron catalyst at low pressure excluded further use of iron as a suitable catalyst. Thus, the early Fischer-Tropsch production plants commissioned in 1936 used cobalt catalysts with the composition Co:ThO_2:MgO:Kieselguhr 100:5:8:200 (in relative mass units) in fixed bed reactors with low pressure.
The reasons for the rapidly growing and considerable interest in the process was mainly the need for self-sufficiency in transportation fuels and the oil-to-coal price ratio of up to 10:1. Development of the iron catalysts continued, and the work of Pichler /4/ revealed that the lifetime of the iron catalysts could be improved by increasing the reaction pressure from atmospheric to about 15 bar. Still, cobalt was not replaced in the plants during the Second World War. By 1944, some nine plants were in operation in Germany with capacities of up to 700.000 tons per year.
Initially after the war research activity was continued, both in Germany and in the USA, but with the discovery of huge oil fields in the Middle East, the production of chemicals and fuels from coal became economically unattractive. The greater availability of crude oil eroded the cost advantage of coal. Also factors like the multistep nature and the relative thermal inefficiency of the process contributed to a decreasing interest in the synthesis.
Only in South Africa was the coal-to-oil price maintained due to the lack of local oil fields, the abundant reserves of coal and the unique political situation. In 1955, the worlds first large commercial F-T operated plant, SASOL I, commenced production based on a precipitated iron

catalyst in fixed bed and moving bed reactors. The fixed bed reactors produce mainly waxes and heavy liquids olefins and paraffins. SASOL II, with ten times the capacity of SASOL I, and SASOL III became operational in 1980 and 1982, respectively. All SASOL Fischer-Tropsch catalysts are iron based. The SASOL II plant produces mainly gaseous olefins and light oils in Synthol recirculated fluidized bed reactors operating around 335°C and 22 bar.

The interruption in the supplies of crude oil as a result of the Middle East crisis during the 1970's led to a renewed interest in the Fischer-Tropsch process. During the years to follow, the research effort was mainly focused on maximizing the selectivity to hydrocarbons in the gasoline range (C_5-C_{11}) or to light olefins (C_2-C_4) /5/.
The use of zeolites represents a possible mean of improving the production of gasoline range hydrocarbons. This can possibly be accomplished by using /6/:

1) a typical Fischer-Tropsch catalyst supported on or physically mixed with a zeolite
2) a two step process consisting of a Fischer-Tropsch step followed by an upgrading step involving an oxide or zeolitic catalyst.

In either case, the role of the zeolite (or oxide) is to crack or hydrocrack heavy paraffins to lighter hydrocarbons and convert α-olefins to gasoline range branched and aromatic hydrocarbons /6/.

In the second generation Fischer-Tropsch processes now emerging, the interest has focused on maximizing the yield of heavy liquids and wax /7/. These products can then be hydrocracked to middle distillates under relatively mild conditions. This approach takes advantage of the nature of the Fischer-Tropsch polymerization kinetics. The final products obtained after hydrocracking exhibit excellent diesel properties, characterized by high cetane number, low sulphur content, free of aromatics and better low-temperature properties than todays diesel fuel.

The Fischer-Tropsch synthesis over normal catalysts inevitably produce a broad range of hydrocarbons, the carbon number distribution determined by Anderson-Schulz-Flory polymerization kinetic. The selectivity can be shifted considerably to the desired product

spectrum by the appropriate choice of catalyst and/or process conditions, but only within the constraints of the mechanism. Considerable research efforts have been and still are carried out in catalyst development, reactor design and process optimalization in order to overcome the mechanism and improve the selectivity to intermediate products, but with limited success. Further knowlegde and understanding of the relationship between the catalyst structure and activity and selectivity is a highly desirable objective.

1.2. THE SPUNG RESEARCH PROGRAMME

The Norwegian Ministries of Oil and Energy (OED) and Industry initiated in 1987 a 6 years State-financed Research and Development programme for the Utilization of Natural Gas, SPUNG. The activity has concentrated on three main areas, Chemical Conversion, Gas in Energy Systems, and Storage, Transportation and Distribution.

The background and the reason for the SPUNG programme are the fact that the dominating share of the proven petroleum reserves on the Norwegian Continental Shelf is natural gas. Norway possesses some 50% of the known Western European reserves of natural gas. These reserves are about twice as large as those of oil. It is expected that the gas resources will last some 100 years with the present rate of production, while known reserves of oil will be exhausted in about 45 years. Probably more than 50% of the undiscovered petroleum reserves is natural gas. Presently, 100% of the natural gas produced in Norway is exported to Europe. It is therefore an important challenge to develop technology aimed at increasing the utilization of natural gas as a source for f.ex. the production of liquid energy carriers. This has also been one of the major goals of the SPUNG programme; to support initiatives towards developing alternative processes for optimal use of the large quantities of natural gas through cooperation between research environments and the industry, both locally and abroad.

Chemical Conversion of natural gas into liquid products constitutes the largest main programme within SPUNG. The programme aims at developing technology for production of fuels and petrochemicals, which may provide an alternative to process routes using other raw materials in the production of the same petrochemicals. Also, research of fundamental character in order to provide basic competence and knowledge of the different chemical and

technological aspects have been an integrated part of the Chemical Conversion programme.

1.3. SCOPE OF THE CURRENT INVESTIGATION

The Fischer-Tropsch process represents a possible route for the conversion of natural gas to transportation fuels and chemicals. In the case where methane is the starting point for the production of synthesis gas, cobalt as a catalyst is of importance due to its low water-gas-shift activity.

Cobalt was chosen due to its interesting properties as a CO hydrogenation catalyst, for reasons mentioned in this section and Chapter 2.1. In addition, cobalt is also one of the classical catalysts in the Fischer-Tropsch synthesis /3/.

It was decided at an early stage of this work to use γ-Al_2O_3 and SiO_2 as support materials. Silica and alumina are of interest because of their industrial applications, i.e. Shell's SMDS process utilitizes a bimetallic Co-Zr/SiO_2 catalyst, Gulf Co-Ru/Al_2O_3 and Statoil's GMD process applies a Co-Re/Al_2O_3 catalyst /8/.

Also, the inherent properties of the support materials differ. Interaction between cobalt oxide and especially the alumina support is well established in the literature. The extent of interaction depends on the applied support, metal loading, preparation and pretreatment /9,10/. For silica, on the other hand, metal-support interactions are believed to be of a less severe character.

The present study aims to investigate the influence of metal loading and support in the CO hydrogenation reaction.

In this context, the following subjects can be considered:

- elucidation of the effect of the support on the reduction properties of cobalt, i.e. metal-support interactions, extent of reduction and phase composition.
- whether calcination is a necessary prerequisite for the formation of compounds by interaction between cobalt and the alumina support (cobalt aluminates).
- effect of reaction temperature, pressure and H_2 /CO ratio on the type, distribution and behaviour of adsorbed CO species during CO hydrogenation at reaction conditions.

- exploration of the influence of carbon or carbonaceous deposits at different reaction conditions.
- effect of metal loading on CO hydrogenation activity and selectivity, assessed in terms of the nature of the CO species.
- detection of reaction intermediates in the Fischer-Tropsch synthesis

The experimental approach chosen to address some of these questions is concerned with four techniques:

1. Fourier Transform Infrared Spectroscopy (FTIR)
2. Temperature Programmed Reduction (TPR)
3. Measurements of activity and selectivity
4. High pressure/high temperature gravimetric studies

Particular attention is paid in the current work to infrared investigations of the supported cobalt catalysts. This is due to the fact that few *in situ* IR studies carried out at high temperature and pressure have been published. The majority of the previous investigations have been concerned with the adsorption of carbon monoxide at low pressure and temperature.

Thus, a major goal of this work was to probe CO adsorption and hydrocarbon formation as a function of time, temperature, H_2/CO ratio and total reaction pressure. Using FTIR spectroscopy, the nature and behaviour of adsorbed species on the catalyst surface during CO hydrogenation at realistic reaction conditions were studied.

Parts of the results obtained in the IR investigations and related work on Ru and iron have been reported in Ber. Bunsenges. Phys. Chem. **97**, 308 (1993), Catal. Today **9**, 69 (1991), and as posters at the following conferences and meetings:

- 4th Nordic Symposium of Catalysis in Trondheim, October 3-4, 1991
- "In situ-Investigations of Physico-Chemical Processes at Interfaces", Lahnstein, Germany, October 5-6, 1992
- SPUNG Seminar, Trondheim, 1993

2. LITERATURF REVIEW

2.1. COBALT; CHEMICAL PROPERTIES AND CATALYTIC USES

Cobalt, a group VIII A transition element is located between iron and nickel in the periodic system, thus having several characteristics and properties in common with its neighbouring metals. The transition metal elements are distinguished from other metals not by their physical properties, but by their electronic structure. Their valence electrons are located in more than one shell, as illustrated in Table 2.1-1, which lists some of the features of the three metals in terms of the *d* and *s* orbital occupancy, the atomic radii and the metal crystal structure /11/.

Table 2.1-1: Basic data on iron, cobalt and nickel /11/.

Metal	*Lattice type*[a]	*Radius*[b]*/Å*	*Electronic structure*
Fe	b.c.c	1.24	$3d^6 4s^2$
Co	f.c.c.	1.25	$3d^7 4s^2$
Ni	f.c.c.	1.24	$3d^8 4s^2$

[a] : f.c.c.; face centered cubic, b.c.c.; body centered cubic.
[b] : the metallic interatomic distance is twice this value.

The oxidation state of Co is +2 or +3, as deduced from the electronic configuration of the *d* shells, d^7 and d^6, respectively. The lattice structure of bulk metal cobalt is of the closed-packed face-centered cubic (f.c.c.) type, exhibiting (111), (100) and (110) low index faces. The arrangement of the surface atoms on such planes are shown in Fig. 2.1-1.

Cobalt is widely utilized as catalyst in both homogeneous and heterogeneous reactions.
In homogeneous catalysis, unmodified cobalt carbonyl complexes [$CoH(CO)_3$] is the active catalytic species in the Ruhrchemie/BASF process for hydroformylation of propene to *n*-butanal (and *i*-butanal), *n*- and *i*-butanol. The SHELL hydroformylation process employs tertiary phosphine modified cobalt catalysts in order to shift the selectivity towards alcohols

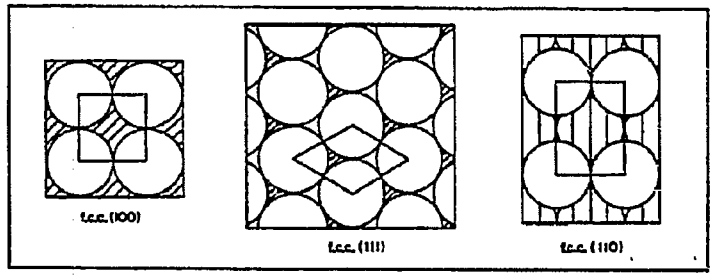

Fig. 2.1-1: Schematic view of surface atoms on (100), (111) and (110) planes of a f.c.c. metal lattice /11/.

and minimize aldehyde production /12/.

Liquid phase homolytic oxidation (autoxidation) of *p*-xylene to terephthalic acid (used in the production of synthetic fibres) by bromine promoted cobalt salts in acetic acid is another example of the applicability of cobalt.

In heterogeneous catalysis, supported cobalt catalysts find widespread use in a number of important reactions. The physical and chemical properties of cobalt catalysts active in hydrotreating /13-15/, selective hydrogenation /16-18/, hydrodesulfurization (HDS) /13,19,20/, oxidation /21,22/ and Fischer-Tropsch synthesis /23-28/ have been extensively studied.

The catalyst used in the above processes is frequently a multi-component system, consisting of cobalt and an additional metal dispersed on the oxidic support. Depending on the type of metals present on the surface, either cobalt or the second metal may act as a promoter, for example by enhancing the overall activity or by shifting the selectivity towards more desirable products. The complexity arising because of the presence of the two metals and the possible interplay or influence they may exert on each other, the nature and by which reaction mechanisms this may proceed, is far from completely understood.

An example of such a system is the bimetallic catalyst $CoO\text{-}MoO_3/Al_2O_3$ utilized in the removal of sulphur from petroleum feedstocks, hydrodesulfurization (HDS). The catalyst of choice ($CoO\text{-}MoO_3/Al_2O_3$) for this reaction has an order of magnitude higher activity compared to the CoO/Al_2O_3 or MoO_3/Al_2O_3 catalysts /19,20/. Different models have been proposed to account for the enhanced activity upon addition of cobalt, the synergism model

/29/, the pseudointercalation model /30,31/, and others /13/. The role of cobalt may be that of a promoter, increasing the activity of the molybdenum phase or, on the other hand, molybdenum may be considered a promoter in terms of dispersing the cobalt component on the catalyst surface /32/. Thus, the nature of the interaction between cobalt and molybdenum still remains uncertain.

In the Fischer-Tropsch synthesis, Fe, Ru, Co and Ni are in principle applicable, each showing different characteristic properties. Ni has a high selectivity to methane. Iron has a high specific Fischer-Tropsch and water-gas shift activity. Its ability to convert synthesis gas with low H_2/CO ratios to hydrocarbons makes iron suitable for indirect liquification of coal. Cobalt appears as the most promising alternative in replacing the iron catalysts due to higher yields of oil and waxes and lower yields of olefins and oxygenated compunds compared to iron catalysts at typical reaction conditions. The low water-gas shift activity and CO_2 selectivity of cobalt means that operation near the stoichiometry of the Fischer-Tropsch reaction is necessary. The price of the metal catalysts increase in the order Fe > Co > Ni. In order to compete with iron as a Fischer-Tropsch catalyst, the amount of cobalt must be low and the average lifetime in the reactor must be much longer than that of iron. Further extensive studies of cobalt as a potential replacement for the iron-based catalysts presently applied in commercial operation is needed.

2.2. THE NATURE AND ROLE OF CARBON IN CO HYDROGENATION OVER SUPPORTED COBALT CATALYSTS

There is a general consensus that the dissociation of carbon monoxide and the surface carbon thus formed plays an important role in the hydrogenation of CO over transition metal catalysts /33-36/. The dual role of carbon is that of being an reaction intermediate in the formation of products or being a precursor to the deposition of coke and graphite. The nature of the surface carbon is crucial in the determination of the subsequent reactivity.

On metal surfaces, two modifications of carbon which do not contain hydrogen have been identified, carbidic and graphitic carbon. Elemental or carbidic carbon (α-carbon), is the result of carbon monoxide dissociation where this occurs. It consists of carbon atoms coordinated to the metal surface but not involved in carbon-carbon bonding /37/. Amorphous or graphitic carbon can be formed by polymerization of elemental carbon. The structure of the graphitic carbon consists of one or several sheets of carbon with the carbon atoms in a sp^2 coordination /38/. Migration of carbon atoms into the lattice of the metal results in the formation of metal carbides. It has been suggested that cobalt forms two types of carbides, Co_2C and Co_3C /39/, and that bulk cobalt carbide can decompose to graphitic carbon above 700K /40/.

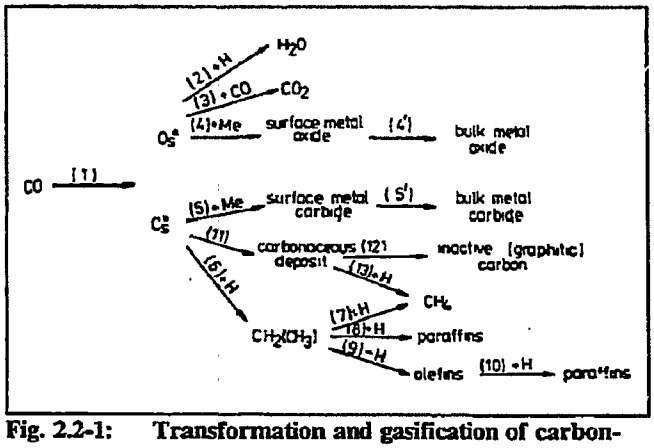

Fig. 2.2-1: Transformation and gasification of carbon-containing species on a metal surface /41/.

The reactivity of the carbon containing species towards hydrogen, as deduced for example from TPSR analysis, decreases from elemental carbon to graphitic carbon, which appears essentially unreactive under hydrogenation conditions. With carbidic carbon as a starting point, Fig. 2.2-1 illustrates the principal pathways for the formation of carbon-containing species /41/. CO is assumed to adsorb dissociatively (1), although possibly preceded by a molecularly adsorbed intermediate. Oxygen can be removed in the form of H_2O (2) or CO_2 (3) by hydrogen and

carbon monoxide, respectively. Surface oxygen may also participate in the formation of metal oxides (4 and 4'). Surface carbon atoms (C_s^*) can interact with the metal to form surface and bulk carbides (5 and 5'), while they are also susceptible to hydrogenation (6), resulting in methylene and methyl structures, the latter a necessary prerequisite for initiation of chain polymerization. Methane can be produced via pathway (7), that is, by hydrogenation of methyl species not participating in the polymerization. It could also be formed from partially hydrogenated carbonaceous deposits (13). The surface carbonaceous deposits may under certain reaction conditions interconvert to a less active or total inactive (graphitic) form (12).

Nakamura et al. /42/ demonstrated the existence of three types of carbonaceous species on a 6% Co/Al_2O_3 surface; CH and/or CH_2, carbidic and graphitic carbon.
Carbidic carbon was predominantly deposited at low temperature (503K), while graphitic carbon was the major component when the CO disproportionation reaction was carried out at 703K. The amount of CH_4 formed during pulsing with H_2 depended on the deposition temperature (503 or 703K). The activation energy for the CH_4 formation remained nearly constant, while the reactivity of the deposited species towards hydrogen decreased (upon heating of carbon deposited at 503K to 703K). This was found to correlate with the hydrogenation of carbidic carbon, the amount of which depended on the deposition temperature. Depositing carbon at 503K followed by heating to 703K resulted in decomposition of carbidic carbon to graphitic carbon, but a limited amount of carbidic carbon remained on the surface. A reversible conversion between graphitic and carbidic carbon was suggested to occur by thermodynamical equilibration at high temperature (703K). Graphitic carbon was found to be inactive towards H_2 between 353K and 703K.

In agreement with the findings of Nakamura et al. /42/, the TPSR results from the study by Lee et al. /43,25/ revealed two forms of carbon, atomic carbon (α-carbon) and polymeric carbon (C_β) with TPSR peaks at about 463K and 703K, respectively. With increasing CO disproportionation temperature (523-673K), an increase in the total amount of deposited carbon was observed on the surface of 10% Co/γ-Al_2O_3. The fraction of the active carbon form ($C_\alpha/C_\alpha+C_\beta$) decreased while the amount of carbon unreactive towards hydrogen [(C_t-($C_\alpha+C_\beta$))/C_t] increased with temperature. This was explained by configurational transformations of the α-carbon into polymeric carbon, crystalline graphitic carbon and bulk

metal carbide. AES (Auger Electron Spectra) confirmed the presence of carbon with different morphologies prevailing at different CO disproportionation temperatures, see Fig. 2.2-2.

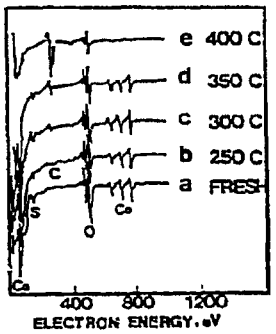

Fig. 2.2-2: **AES spectra of 10%-Co/Al_2O_3 /43/.**

At the lowest temperature investigated, 523K, C_α predominated, while at 673K, graphitic carbon which hardly reacted with hydrogen was predominant. The type of carbon present at the intermediate temperatures, 573 and 623K, was suggested to be of the polymeric and/or graphitic form. The AES spectra did not indicate the formation of cobalt bulk carbide at the intermediate temperatures.

The CO hydrogenation activity (mol/g cobalt-s) depended on the deposition temperature; decreasing activity with increasing temperature was observed. The decline in activity was believed to be caused by blockage of active sites due to accumulation of less active polymeric and/or graphitic carbon species. The decrease in catalytic activity was more pronounced for the catalysts with lower cobalt loadings, suggesting that carbon formation is favoured on small cobalt metal particles. The observed increase in the olefin fraction with increasing carbon deposition temperature was explained by reduced capabilities of the carbon covered catalyst to hydrogenate primary olefins to the corresponding paraffins.

In a later investigation, Nakamura et al. /44/ studied carbon deposition on polycrystalline Co-foils using XPS. The deposition of carbon on the cobalt surface was achieved either by dissociation of adsorbed CO or by the Boudouard reaction ($2CO_{(g)} \rightarrow C_{(s)} + CO_{2(g)}$).

Adsorption of CO at 77K followed by heating to 473K during which XPS spectra were recorded simultaneously identified three temperature regions of interest. Between 123 and 300K, desorption of carbon monoxide took place as indicated by the decrease in the $CO_{(s)}$ XPS peak at 285.3 eV. In the second region, 300-373K, new XPS peaks at 283.1 eV (C 1s) and 530.2 eV (O 1s) was believed to correspond to adsorbed carbon (carbidic carbon) and oxygen as a consequence of CO dissociation. The XPS spectra of the cobalt surface obtained between 373 and 473K revealed no peaks attributable to adsorbed CO at 285.3 eV (C 1s) and 531.8 eV (O 1s). In this temperature range, the XPS peak due to carbidic carbon (283.1 eV) remained relatively constant, indicating the absence of any carbon penetrating into the bulk

of cobalt. The fixed amount of carbidic carbon, θ_C, formed as a result of the dissociation of CO, was reported to 0.4. The sample was then cooled to 77K and CO introduced followed by heating to 473K. CO adsorption took place on the carbon covered surface at 77K, but CO desorbed upon heating.

When the Boudouard reaction was conducted at 500 and 700K, two forms of carbon were identified based on their characteristic XPS binding energies, carbidic carbon (283.1 eV) and graphitic carbon (284.8 eV). The amount of the surface carbon deposited at 700K was approximately equal to that deposited in the temperature range 373-473K during CO dissociation. Deposition at 500K resulted in a θ_C value for carbidic carbon of 1. The thermal decomposition of carbidic carbon to graphitic carbon in the absence of hydrogen is believed to occur above 700K. The transformation is illustrated in Fig. 2.2-3. Carbidic and graphitic carbon were deposited on the cobalt surface in a 1:0.2 ratio at 500K followed by heating to 700K. As can be seen, a limited part of the carbidic carbon (θ_C=0.4) remains stable at 700K and is not converted to graphitic carbon.

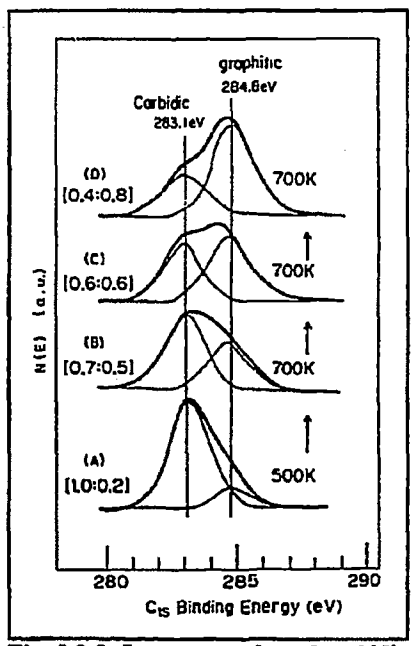

Fig. 2.2-3: Interconversion of carbidic carbon to graphitic carbon on Co-foils.
(A) after carbon deposition at 500K
(B) heating at 700K
(C) after 20 min.
(D) after 40-60 min. /44/.

It can be inferred from the above results that CO dissociation can not occur on a surface covered with carbidic carbon, while the disproportionation of CO still proceeds on a surface containing α-carbon. This may imply that the dissociation of CO require certain sites or planes. In the literature, CO dissociation have been reported to be provided by ensembles consisting of atoms located on different crystal planes. Examples of such planes are Co(1012), Co(1120), Co(001) and Co(1010) /39,45-47/. The formation of carbidic carbon are believed to take place on Co(1012) and Co(1120) crystal planes.

Carbon-containing deposits were observed in a thermogravimetric study of silica supported iron-cobalt catalysts during CO hydrogenation /41/. For the bimetallic catalysts, an initial rapid weight increase was caused by the formation of bulk metal carbides. The higher the iron content of the catalysts, the quicker the weight increase. The further increase in the masses of the bimetallic catalysts was regarded to be due to the build up of carbonaceous deposits. The 15% Co/SiO_2 catalyst, however, lacked the rapid weight increase in the initial stage of the CO hydrogenation reaction, see Fig. 2.2-4. This led the author to propose that bulk cobalt carbide was formed after an induction period, during which the formation of stable carbide nucleus was assumed. XRD analysis of the cobalt catalyst after 50 hours of CO hydrogenation reaction indicated the presence of Co_2C or possibly a carbide of smaller carbon-to-cobalt ratio. The carbonaceous deposits affected both the catalytic activity and hydrocarbon distribution. The initial rapid decrease in the conversion of CO to hydrocarbons was believed to be due to small amounts of carbonaceous deposits remaining on the surface of the metal or its carbide, thus blocking sites active in the hydrogenation reaction.

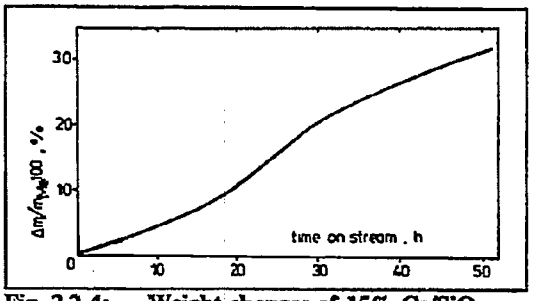

Fig. 2.2-4: Weight changes of 15% Co/SiO_2 during CO hydrogenation at 548K, H_2:CO=1.1:1 and 1 bar /41/.

The influence of the deposited carbonaceous species on the distribution of the hydrocarbons can be summarized by the following points:

1. A continuous increase in the methane fraction of the hydrocarbons with time during CO hydrogenation.
2. The fraction of the C_2 hydrocarbons increased while those of C_3 and C_4 decreased, regardless of the catalyst composition.
3. An initial rapid increase in the content of alkenes due to inhibition of reaction pathway (10) in addition to decreased hydrogenation of the hydrocarbon precursors (8).

In the study by Barcicki et al. /48/, 15% Co/SiO_2 was exposed to a puls of CO in the temperature range 298-623K followed by subsequent H_2 pulses at reaction temperature. Carbon deposited by Boudouard's reaction was not observed below 373K. The fraction of carbon deposited by the disproportionation reaction increased between 373 and 573K. Above 573K mainly all the carbon hydrogenated was found to originate from the Boudouard reaction, since no oxygen atoms were detected in the deposited layer. From the reaction with hydrogen, two modifications of carbon was assumed to be present, one easily hydrogenated (probably carbidic carbon), the other inactive towards hydrogen at 573K. At 473K, 96.1% of the deposited amount of carbon could be removed by 5 hydrogen pulses. Increasing the hydrogenation temperature resulted in decreasing degree of gasification. At approximately the same temperature (473K) the transformation of the reactive surface carbon into graphite-like structures occured. The relatively low temperature of carbon interconversion was explained by the low content of oxygen atoms in the deposited layer, which could dilute the surface layer of carbon and block surface area.

The surface properties of a fresh and carbon deposited 5% $Co/\gamma\text{-}Al_2O_3$ catalyst was compared using TPD and FTIR-spectroscopy /49/. Carbon was deposited at 523K by the Boudouard reaction. The CO TPD spectra of a fresh catalyst reduced at 798K for different periods of time (7-24 h.) showed peaks at 353K (α-band), 403K (β-band), 453K (γ-band) and 603K (δ-band). Their intensity varied with time of reduction. After carburization of the surface for 2 hours, the intensity of the δ-band was higher than on the fresh catalyst and slightly shifted to lower temperature. The β-band was absent in the TPD spectra of the carbon covered surface, while the α- and γ-bands were only slightly affected by carbon deposition. The assignment of the different peaks was as follows:

α-band:	either due to CO species adsorbed on cobalt aluminate or on the cobalt carbide surface (Co-C-CO).
β-band:	CO desorbed from a unreduced, oxygen contaminated Co-surface (cobalt oxide).
γ-band:	CO desorbed from a reduced Co-surface.
δ-band:	deposited carbon reacting with oxygen supplied from CO or CO_2, cobalt oxide or the Al_2O_3 support.

2.3. TEMPERATURE PROGRAMMED REDUCTION (TPR)

2.3.1. Introduction

The catalysts used throughout this study are uncalcined silica and alumina supported cobalt catalysts. Thus, the following literature review is mainly focused on earlier studies describing the characterization of similar catalysts, either using TPR or XPS alone, or a combination of the two techniques. Despite the fact that the chemical nature of cobalt species on the catalyst surface has not been investigated by XPS in the present study, studies applying this technique are still included in this review, since TPR and XPS are techniques that complement one another. Results from investigations using additional characterization techniques, like XRD and SIMS, will be refered to when applicable.

2.3.2. Reductive decomposition of $Co(NO_3)_2 \cdot 6H_2O$

The majority of the cobalt-TPR investigations have been performed on catalysts calcined prior to TPR analysis. Investigations concerning TPR studies of uncalcined (impregnated and dried) catalysts are scarce. Only a limited number of studies report the use of relatively mild pretreatment conditions before TPR analysis /50-52/. In this respect, it is of interest to establish the position of the peak(s) resulting from the reductive decomposition of nitrate ions in the applied metal precursor, $Co(NO_3)_2 \cdot 6H_2O$.

The TPR profile of unsupported cobalt nitrate has been reported to consist of two peaks located at 503K and 592K (β=24K/min.) /50/. Exothermic reductive decomposition of cobalt nitrate was believed to be responsible for the 503K peak, while the 592K peak was due to reduction of cobalt oxide formed during decomposition. TPR spectra of 10% Co supported on silica and alumina pretreated at 293K were similar to that of unsupported cobalt nitrate below ~600K. Increasing pretreatment temperature resulted in the disappearance of the peak assigned to nitrate reduction. A calcination temperature around 650K was found necessary to completely remove the peak near 500K, ascribed to hydrogen assisted decomposition of Co-nitrate /52/. Hoff et al. /10/ stated that a calcination temperature of about 673K was required to decompose virtually all of the cobalt nitrate. Rosynek et al. /51/ assigned a peak at 553K

(β=20K/min.) to the reductive decomposition of the nitrate ion in unsupported cobalt nitrate. The position of this peak shifted 30K to lower temperatures when cobalt nitrate was supported on silica.

2.3.3. The extreme situations, Co_3O_4 and $CoAl_2O_4$

Usually, but not necessarily, the applied metal precursor is cobalt nitrate hexahydrate, $Co(NO_3)_2 \cdot 6H_2O$. During calcination following impregnation of the actual support, decomposition of cobalt nitrate takes place and an oxide phase is formed, briefly discussed in the previous section (Chapter 2.3.2). The nature of the support can have considerable influence on these processes. Generally, the metal oxide and support can interact in three possible ways: (a) the support acts as a dispersing agent (weak interactions), (b) solid solution formation and (c) the formation of surface compounds (strong interactions).

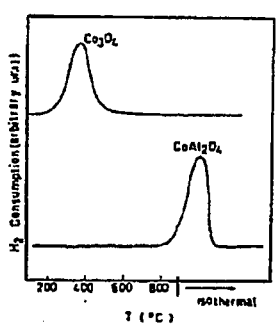

Fig. 2.3.3-1: TPR profiles of unsupported Co_3O_4 and $CoAl_2O_4$. β=10K/min., 10% H_2/Ar /56/.

Investigations /50,53-55/ indicate that cobalt oxide supported on alumina was incompletely reduced to the metallic state due to strong interactions between the metal and the support. Explanations which have been proposed to account for this are; the formation of cobalt aluminate spinel, cobalt ions positioned primarily at tetrahedral or octahedral lattice sites of Al_2O_3 (depending on the calcination temperature and metal loading) or a modification of the electronic properties of the cobalt oxide /56/. On alumina supported cobalt catalysts, at least two cobalt phases are reported, a crystalline phase as Co_3O_4 and a dispersed phase as a stoichiometric and non-stoichiometric cobalt aluminate /53,54/, probably with a spinel-type structure.

The TPR spectrum of unsupported Co_3O_4 has frequently been found to consist of a single, asymmetric peak located between 525K and 770K /50-52,56-60/, while others /54,61-65/, report a main high-temperature peak accompanied by a partial resolved low-temperature peak. The position of the peaks (singlet or doublet) depends on the applied experimental conditions. The temperature at which the single Co_3O_4 peak appears was almost identical to the temperature where the CoO reduction peak was observed /52,65/. The observation of only one

peak may be explained as a result of overlap between the two stages of reduction as an consequence of different TPR reaction conditions (gas flow rate of H_2/inert gas-mixture, H_2/inert gas ratio, the heating rate or the catalyst sample mass) /50/.

However, whether one single or two resolved peaks are observed, there exists a general agreement that the reduction of Co_3O_4 takes place in two stages via CoO. Hence, the reduction scheme can be written:

$$Co_3O_4 + H_2 \rightarrow 3CoO + H_2O \qquad 2.1$$

$$3CoO + 3H_2 \rightarrow 3Co + 3H_2O \qquad 2.2$$

$$Co_3O_4 + 4H_2O \rightarrow 3Co + 4\ H_2O \qquad 2.3$$

The asymmetry and broadness of the observed single peak was believed to encompass the two step reduction process for Co_3O_4 /50,56/. XRD-data obtained before and after the first stage indicated the presence of Co_3O_4 and CoO /61/.

The crystalline Co_3O_4 phase has been found rather easy to reduce, either in the bulk form or formed during the calcination step and consequently deposited on the catalyst surface, subjected to weak interactions with the support.

The opposite extreme situation; strong interactions between the cobalt and especially the alumina support results in the formation of compounds generally described as cobalt aluminates, $CoAl_2O_4$. The $CoAl_2O_4$-spinel has been found difficult to reduce. Studies have revealed that temperatures higher than 1120K are required to reduce the surface aluminate /50,52,56,58/. As mentioned earlier, interaction between dispersed metal ions and the γ-Al_2O_3 lattice provide the basis for the formation of the cobalt aluminate species. The crystal structure of γ-Al_2O_3 is that of an (imperfect) spinel with a deficit of cations, with Al^{3+} filling 2/3 of the tetrahedral sites in addition to the octahedral spinel cation positions. Two octahedral sites exist for each tetrahedral in γ-Al_2O_3 /53/. Co^{2+} may diffuse into the alumina during calcination where they can occupy octahedral and/or tetrahedral sites, forming a spinel type structure, believed to be quite resistent to reduction by hydrogen.

In addition to the cobalt phases described in the previous section (Chapter 2.3.3), the existence of intermediate phases of cobalt, their nature and distribution together with their

reduction behaviour have been given increased attention in the recent literature.
The influence of the cobalt loading, support and pretreatment conditions on these properties will be reviewed in the following section.

2.3.4. The effect of the cobalt loading

Several authors have examined the effect of the metal loading on the extent of interaction between the cobalt oxide and alumina, either by TPR /56/ or by employing ESCA, ISS, DRIFTS, XRD or SIMS as additional characterization techniques /53,54,57/.

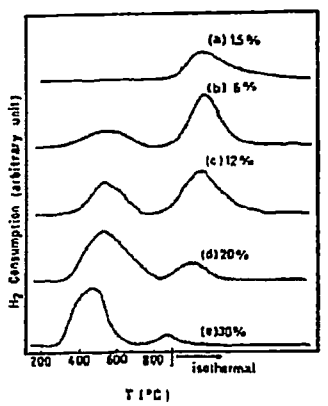

Fig. 2.3.4-1: TPR profiles of Co/γ-Al_2O_3 with different metal loading. β=10 K/min., 10% H_2/Ar /56/.

Wang et al. /56/ studied the reduction behaviour of alumina supported cobalt catalysts containing 1.5-30 wt-% Co. For cobalt catalysts with low metal loading (1.5 wt-% Co) a peak above 1173K was ascribed to the formation of amorphous surface cobalt aluminate. Catalysts with a cobalt content of 6% or higher showed the development of peaks centered around 773K. Both the low- and high-temperature peaks shifted to lower temperatures as the cobalt loading increased, Fig. 2.3.4-1. The peak areas for the peak above 1173K decreased with increasing metal loading, while the opposite was the case for the low-temperature peaks. It was suggested that the presence of reducible Co (easy-to-reduce) species enhanced the reduction of more strongly interacting cobalt species by facilitating nucleation of the cobalt oxide species. The low-temperature peaks were positioned at higher temperatures than the bulk Co_3O_4 reduction peak, which was explained by interactions between the cobalt oxide and cobalt aluminate requiring higher temperature for the reduction of cobalt oxide, or smaller particle size of supported Co_3O_4 compared to bulk Co_3O_4, making the reduction of them more difficult. Another proposed explanation was the existence of a phase different from Co_3O_4, possibly a Co^{3+} phase.
An amorphous, distorted overlayer Co_3O_4 phase consisting of Co^{2+} and Co^{3+} deposited over

the cobalt aluminate spinel structure was reported by Tung et al. /57/ in their EPR and DRS study of alumina supported catalysts containing up to 3% cobalt. TPR peaks at 620K and 875K were assigned to the reduction of Co^{3+} and Co^{2+} species, respectively, in the overlayer phase. Diffuse reflectance spectra (in the UV-VIS region) confirmed the assignment; the triplet (at 550, 580 and 620 nm) characteristic of cobalt aluminate was replaced by two separate peaks (at 400 and 700 nm) as the cobalt loading was increased from 0.3% to 1 and 3%. A further increase of the cobalt content (to 8% and 16%) resulted in XRD peaks corresponding to Co_3O_4 crystallites, which was suggested to be deposited on the distorted, amorphous overlayer. Additional features at 510K and 550K in the TPR profile of the catalyst containing 16% Co was ascribed to the reduction of bulk Co_3O_4.

Chin et al. /53/ characterized alumina supported Co catalysts with a metal concentration varying between 1% and 30%, employing ESCA, SIMS and ISS. For a given calcination temperature increasing metal loading resulted in decreasing XPS binding energies. Catalysts with low cobalt content (1% and 2%) had binding energies close to that of $CoAl_2O_4$, while the catalyst with high loading (30%) exhibited a binding energy equal to the one obtained for Co_3O_4. A linear correlation existed between the XPS peak area intensity ratio (Co $2p_{3/2}$/Al 2p) and the metal content up to ~10%, where a breakpoint was observed. Higher metal loadings yielded an enhancement of the intensity ratios. A similar situation with a breakpoint occurring at ~12% Co was observed when Co/Al ISS peak intensity ratios were plotted as a function of metal content. The indicated alterations in the surface composition was believed to be due to segregation of a Co_3O_4 phase (for Co concentrations ≥ 10%) on top of a surface saturated with Co-species (< 10% Co), that is, a surface where all γ-Al_2O_3 lattice positions are occupied. Reduction studies of Co/Al_2O_3 showed a linear increase in the reducibility of the catalysts with increasing metal content, but a change in the slope of the curve occured at about 12% cobalt, as shown in Fig. 2.3.4-2. This was found to be consistent with surface segregation of Co_3O_4. For catalysts with higher (than 12%) Co-

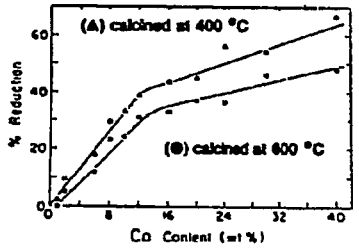

Fig. 2.3.4-2: Relationship between %-reduction and metal loading of Co/Al_2O_3 reduced at 673K for 4h. /53/.

content, the formation of larger Co_3O_4 crystallites led to a more moderate increase in the reducibility of the catalysts compared to those containing less than 12%. It was suggested that this could be due to the effect of the dispersion; the dispersion decreases with increasing metal loading, and a decrease in dispersion results in lower reducibility.

In their study of Co-catalysts with low metal loadings (1.1%-4.3%), Chung et al. /54/ verified the existence of two cobalt states, a reducible phase associated with bulk Co_3O_4 and a non-reducible state related to cobalt ions predominantly in tetrahedral lattice sites of the alumina support.

Diffuse reflectance spectra (DRS) of 1% Co/Al_2O_3 (batch-prepared; all Co added at once) showed an intense triplet (at 620, 580 and 545 nm) due to Co^{2+} located in tetrahedral lattice positions, while 3% Co/Al_2O_3 (batch) predominantly exhibited a broad band around 500 nm, assigned to octahedral Co^{2+}. Cobalt catalysts prepared by stepwise impregnation with 1 wt-% Co showed no reduction behaviour, while the reducibility of the batchwise catalysts (all cobalt added at once) increased with increasing amount of metal. XRD patterns of the batchwise catalysts (> 2% Co) indicated the existence of Co_3O_4, while no X-ray pattern indicative of Co_3O_4-phase was observed for Co-step catalysts containing up to 3.5 wt-% Co. These results may suggest a higher degree of dispersion of the cobalt ions into the γ-Al_2O_3 lattice for Co-step catalysts compared to the batchwise prepared catalysts.

TPR profiles (β=2.5K/min., 5% H_2/Ar) of CoO/γ-Al_2O_3 catalysts with metal loadings of 5-20 wt-% using cobalt nitrate as metal precursor /59/ exhibited reduction peaks attributable to cobalt species as discussed by Arnoldy et al. /52/ (see Table 2.3.6-1). Using a similar notation as the one introduced by Arnoldy et al. /52/, the reduction peaks are characterized by the reduction temperatures 400-450K (Co-I'), 503-553K (Co-I), 633-643K (Co-IIA), 693K (Co-IIB), 753-773 (Co-III), 853-873K (Co-IV) and >923K (Co-V).

The peaks observed at 400-450K (Co-I') and above 920K (Co-V) were ascribed to small particles of non-crystalline (amorphous) cobalt oxide akin to Co_3O_4 (Co-I) and Co^{2+}-species in subsurface and/or bulk phases, respectively. The Co-phase denoted Co-V detected higher than 923K probably corresponds to the Co-IVC and Co-IVD phases observed at 1150-1230K by Arnoldy et al. /52/. The Co-IIA and Co-IIB phases were believed to originate from surface Co^{3+} and a Co^{3+}-Al^{3+} mixed oxide bulk phase, respectively. Surface Co^{2+} was reduced in the temperature range 753-773K (Co-III). The authors /59/ further defined the Co-IV phase as

(sub)surface Co^{2+}-species. 3 wt-% CoO/γ-Al_2O_3 contained predominantly Co-IIA and Co-IV species, with a distinct peak for Co-IIA at 5 wt-% CoO. Co-IIB appeared at 5 wt-% CoO while small amounts of Co-I' were observed with a cobalt loading of 20 wt-%.

2.3.5. The effect of the support

The reducibility of cobalt (nominal loading 5-wt%) supported on SiO_2, γ-Al_2O_3 and TiO_2 was investigated by Castner et al. /58/. The TPR (β=4.5K/min., 2% H_2/Ar) and the Co 2p XPS spectra of Co/SiO_2 were found to be similar to those of unsupported Co_3O_4 with a TPR peak maximum near 623K. The major cobalt phase on SiO_2 was large (30Å), bulklike Co_3O_4 particles which were completely reduced to metallic cobalt below 723K, see Fig. 2.3.5-1.

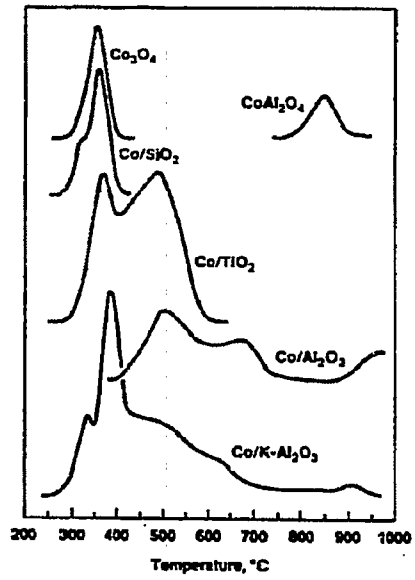

Fig. 2.3.5-1: TPR spectra of Co_3O_4, $CoAl_2O_4$and 5%Co supported on SiO_2, TiO_2 and Al_2O_3 /58/.

The TPR-spectrum of the Co/γ-Al_2O_3 catalyst featured three peaks (773K, 948K and 1173K) with no evidence of Co_3O_4. The high-temperature peak was associated with cobalt aluminate, while the two remaining peaks were tentatively ascribed to an intermediate cobalt phase (between Co_3O_4 and $CoAl_2O_4$) with a reducibility between that of cobalt oxide and cobalt aluminate, but of similar crystal structure. On the calcined TiO_2 supported Co-catalysts, reduction of Co_3O_4 occured at 648K, while the peak located at 753K represented the reduction of Co^{2+} to Co^0. XPS-analysis showed decreasing amounts of Co on TiO_2 (reduced at 753K in H_2) and γ-Al_2O_3 (reduced at 973K in H_2), which could be due to sintering of cobalt particles, diffusion into the support lattice or decoration of Co with Ti oxide species.

Interactions between Co_3O_4 and Al_2O_3 were stronger than that of Co_3O_4-SiO_2, as deduced from TPR spectra (β=10K/min., 8% H_2/Ar) in the study of Paryjczak et al. /64/. The reduction of

10% Co_3O_4/SiO_2 resulted in a maximum at 693K and was completed at 873K, while the 10% Co_3O_4/Al_2O_3 was incompletely reduced at 923K. 1% Co_3O_4/SiO_2 exhibited a maximum at *ca.* 643K ($Co_3O_4 \rightarrow CoO$), but was not fully reduced even at 873K.

Cobalt supported on kieselguhr (impure silica with low surface area) promoted with ThO_2 have been studied by Viswanathan et al. /61/, using H_2 and CO adsorption, XPS and TPR techniques. Catalysts with and without promoter addition had different percentage reduction, 75% and 39%, respectively. This was proposed to be due to the formation of a support adlayer encapsulating the cobalt oxide particles. ThO_2 probably restricted the migration of SiO_2 in the presence of water, hence a higher degree of reduction was achieved. XPS spectra showed surface segregation of thoria, which was believed to prevent the encapsulation of the cobalt oxide with kieselguhr. The results from H_2 and CO adsorption experiments gave a further indication of the assumed support-cobalt interaction. The H/Co and CO/Co ratios decreased with decreasing cobalt loading, indicating possible interaction between the cobalt metal and support in addition to cobalt-unreduced cobalt oxide (electronic) interaction.

2.3.6. The effect of different pretreatment conditions

A detailed characterization of cobalt species present in CoO/Al_2O_3 systems was conducted by Arnoldy et al. /52/. The majority of their study concerned the investigation of 9.1% Co/γ-Al_2O_3 calcined at different temperatures (575K-1290K), but the effect of different heating rates during TPR analysis and flow rates during calcination was also examined. Reduction of the Co-species was found to take place mainly in four temperature regions, around 600K (I), 750K (II), 900K (III) and 1150K (IV). Range II was subdivided into IIA and IIB, while reduction range IV could be separated into 4 distinguishable phases, IVA, IVB, IVC and IVD. The appearance and disappearance of these phases was strongly related to the calcination temperature, as shown in Fig. 2.3.6-1 The assignment of the various regions to different Co phases was also based upon XRD data as well as DRS in the UV-VIS range. Interpretations of the TPR peaks are summarized in Table 2.3.6-1. The 70K upward shift of the Co_3O_4 peak with increasing temperature was explained by a change in morphology; higher temperatures lead to less formation of metallic nuclei's facilitating the reduction of Co_3O_4, hence a shift to higher reduction temperature. The effect of the calcination temperature was explained by solid state diffusion of Co^{2+} and cobalt species in different oxidation states (Co^{2+}/Co^{3+}).

Table 2.3.6-1: **The assignment of observed TPR-peaks to different Co-phases according to Arnoldy et al. /52/.**
TPR conditions: β=10K/min., 67% H_2/Ar

REGION	*TPR-PEAKS (K)*	*CALCINATION TEMPERATURE (K)*	*COBALT-PHASE*
I	560, shifts 70K to higher temperature with increasing calcination tempeerature (575 → 875)	up to 900	Reduction of Co_3O_4 crystallites
IIA	~ 750	below 825	Reduction of dispersed surface Co^{2+}- species
IIB		below 1000	Mixed Co^{3+}-Al^{3+} oxidic crystallites, tentative formula $Al_{2/3}^{3+}(Co_2^{3+})O_4^{2-}$ or Co_3AlO_6
III	875	below ca. 950	Reduction of surface Co^{2+}
IVA	1100 - 1230	675 - 925	Reduction of surface Co^{2+}-ions with a high number of Al-O ligands
IVB		1035 - 1175	Reduction of (sub)surface Co^{2+}-ions in a not well-defined Co^{2+}-Al^{3+} spinel (Co^{2+} in a diluted form)
IVC	1230	1175	Reduction of Co^{2+} in a spinel of composition $Co_xAl_{(8/3-2/3x)}O_4$, $0 < x < 1$ x=0.18
IVD	1150	1290	Stoichiometric $CoAl_2O_4$

Region I: Reduction of well-defined Co_3O_4 crystallites. No more than 25% of the cobalt existed as Co_3O_4. Higher calcination temperature (>875K) resulted in the disappearance of the reduction peak assigned to this phase, suggesting that Co^{2+} migrate into the upper layer of the alumina support.

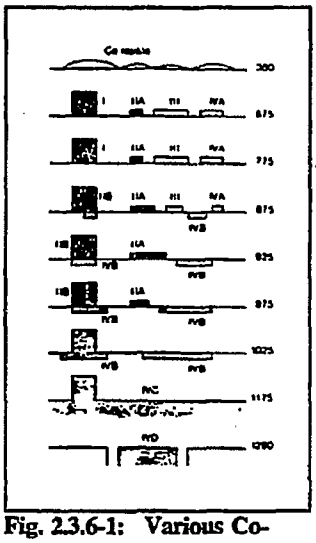

Fig. 2.3.6-1: Various Co-phases on 9.1% Co/γ-Al_2O_3 as a function of calcination temperature /52/.

Region IIA: Reduction of surface Co^{3+} ions. Co^{3+} can be formed from the conversion of phase III species into phase II (and phase IV) with increasing calcination temperature (775-925K).

Region IIB: At calcination temperatures in the range 875-925K, surface Co^{2+} and Co^{2+} in Co_3O_4 may become mobile. Diffusion of Co^{2+} into the γ-Al_2O_3 lattice and counter diffusion of Al^{3+} results in the formation of the mixed oxide Co^{3+}-Al^{3+}. Co^{3+} has a higher octahedral site preferency energy than Al^{3+} (105 kJ/mole versus 62 kJ/mole), thus Co^{3+} is expected to occupy octahedral and Al^{3+} tetrahedral lattice positions. The Co^{2+}-Al^{3+} exchange was suggested to occur via solid-state diffusion.

Region III: Observed for catalysts calcined below ca. 950K, and assigned to surface Co^{2+}. The presence of this phase was not detected using high calcination flow rates. High flowrate would have low effect on the oxidation of Co^{2+} to Co^{3+}, hence phase III and IV predominate. Low flowrate would result in oxidation of Co^{2+} and the presence of phase I and II.

Region IV: The amount of this phase increases with increasing calcination temperature, reflecting the diffusion of Co^{2+} into the alumina lattice. Similarly, the reduction temperature increases with increasing calcination temperature, implying increasing lattice stabilization of Co^{2+} with advancing solid state diffusion. Around 1000K, reduction of Co^{3+} to Co^{2+} and solid state diffusion of Co^{2+} results in the disappearance of phase I, II and III and the formation of species reduced in region IV. Calcination at 1290K gives stoichiometric $CoAl_2O_4$.

Different surface techniques (XPS, XRPD and XRD) in addition to TPR were used to characterize the reduction properties of alumina /59/ and silica /51/ supported catalysts prepared from various metal precursors. Cobalt nitrate (N) and acetate (A) /59/ in addition to cobalt chloride (C) /51/ were used as starting materials.

XPS, XRD and TPR analysis showed that poorly dispersed Co^{3+}-species (Co-I, I', IIA and IIB) prevailed on CoO/Al_2O_3(N), in contrast to on CoO/Al_2O_3(A), where considerable amounts of Co-IIB, IV and Co-V were predominant /59/. The TPR-areas for the latter catalyst are smaller and the Co2p/Al2p XPS intensity ratio are higher than those of CoO/Al_2O_3(N) suggesting that cobalt species in CoO/Al_2O_3(A) was highly dispersed, despite interactions with the alumina resulting in (sub)surface Co^{2+}-species and/or bulk phases.

The Co2p/Al2p ratios for uncalcined CoO/Al_2O_3(A) was slightly higher than those of CoO/Al_2O_3(N), indicating a slightly higher dispersion of cobalt in the former catalyst. An oxidation state of 2+ for cobalt was suggested for both of the uncalcined catalysts. After calcination, the Co2p/Al2p ratio for CoO/Al_2O_3(A) was roughly the same as before calcination, while a significant decrease was observed for CoO/Al_2O_4(N) (> 2 wt-% CoO), which could not be explained by cobalt migration into γ-Al_2O_3. Oxidation of Co^{2+} to Co^{3+} by nitrate anions during calcination may promote the agglomeration of cobalt species, resulting in poorly dispersed CoO/Al_2O_3. Co^{2+}, on the other hand, would be more mobile and diffuse into the alumina support.

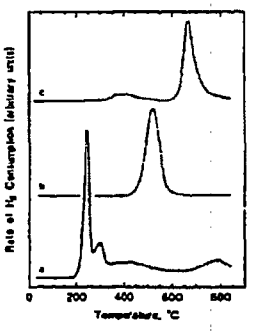

Fig. 2.3.6-2: TPR profiles of a) $Co(NO_3)_2/SiO_2$ b) $CoCl_2/SiO_2$ c)$Co(CH_3COO)_2/SiO_2$ /51/.

Uncalcined and calcined (at 773K) 6% Co/SiO_2 catalysts prepared from cobalt acetate, nitrate and chloride were examined by TPR (β=20K/min., 5% H_2/N_2), XPS and XRPD techniques /51/. The reduction of uncalcined Co/SiO_2(N) was found to occur in subsequent steps giving peaks at 573K, 703K and 1053K, as shown in Fig. 2.3.6-2. Species responsible for these three peaks was proposed to be various surface CoO_x-SiO_2 compounds. Co/SiO_2(C) exhibited a single peak (at 793K), which was nearly the same temperature as the one obtained from reduction of unsupported $CoCl_2 \cdot 6H_2O$ (808K). For Co/SiO_2(A), peaks were observed in the temperature range 573-773K, but the major peak occured at

933K. The TPR and XRPD-patterns of the calcined $Co/SiO_2(C)$ resembled closely those of unsupported Co_3O_4, while the calcined $Co/SiO_2(A)$ showed the absence of XRPD patterns characteristic of Co_3O_4. TPR-profiles of calcined $Co/SiO_2(N)$ showed two peaks at 603K and 983K in addition to a broad peak between 523K and 873K, possibly due to reduction of Co_3O_4. XRPD-measurements on this catalyst indicated the existence of small oxide particles (average size of 20 nm.). All the calcined catalysts had higher extents of reduction than their uncalcined counterparts, especially the nitrate derived catalysts showed marked improvements.

Cobalt catalysts (calcined at 673K for 5 h.) containing between 2 and 20 wt-% CoO prepared from different cobalt precursors (nitrate, acetate) and an ion-exchange method were characterized using TEM, DRS, XPS, XRD and TPR /60/. TEM micrographs and XRD patterns verified the existence of crystalline Co_3O_4 with a particle size of 5-8 nm (in aggregates of 80-100 nm) on the 2% $CoO/SiO_2(N)$ catalyst. As the cobalt loading increased, TEM micrographs revealed the presence of clusters of large cobalt oxide particles, 25 nm in size, probably formed by agglomeriation of smaller oxide particles. For the 2-10% $CoO/SiO_2(A)$ catalysts, no significant surface segregation or agglomeration of cobalt was observed, while small amounts of cobalt oxide particles of 5 nm (in aggregates of 20-25 nm) were detected for the 20% $CoO/SiO_2(A)$ catalyst. These findings indicate a better dispersion of cobalt oxide on the $Co/SiO_2(A)$ catalyst than on the nitrate based catalysts.

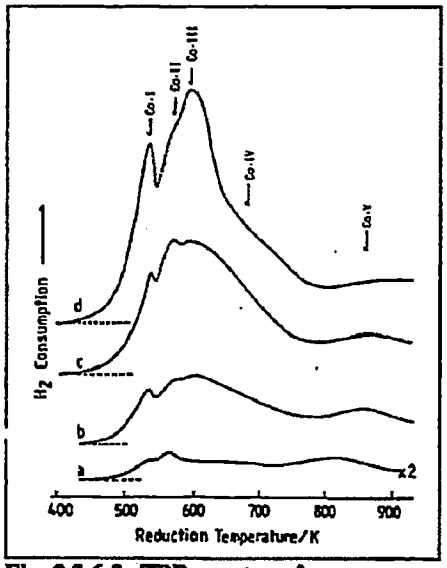

Fig. 2.3.6-3: TPR spectra of $CoO/SiO_2(N)$.
a) 2 wt-% b) 5 wt-% c) 10 wt-% and d) 20 wt-% CoO /60/.

The TPR profiles (β=2.5 K/min., 5% H_2/Ar) of the two catalysts reflected the already stated differences. Reduction peaks were observed at 538K (Co-I), 563K (Co-II), 593K (Co-III), 673K (Co-IV) and 800-860K (Co-V) for $CoO/SiO_2(N)$, see Fig. 2.3.6-3, while the $CoO/SiO_2(A)$ catalyst exhibited weak peaks due to Co-I (540K) and Co-IV. With a heating rate (β) of 10 K/min. and 64% H_2/Ar, 10%

CoO/SiO_2(A) and CoO/SiO_2(I) showed reduction peaks at 1030K (Co-VI) in addition to a high-temperature peak at 1081K (Co-VII) for the latter catalyst.

The Co-I and Co-II TPR peaks were assigned to Co_3O_4 phases with different particle size. 7 and 25 nm, respectively. Mixed oxides, $Si^{4+}_{x/2}Co^{2+}_{1-x}Co^{3+}_2O_4$ with spinel structures was believed to be responsible for the peak at 593K (Co-III). Co-IV was attributed to Co^{3+} species in octahedral symmetries interacting with the silica surface. A similar assignment was given for the Co-V species, viz. an interacting surface Co^{2+} species localized in octahedral interstices or surface silicate. The TPR peak at 1030K, observed for acetate derived catalysts and catalysts prepared by an ion-exchange technique, was also due to surface Co^{2+} species, but Co^{2+} in distorted tetrahedral symmetry positions. The TPR peak Co-VII was assigned to ion-exchanged Co^{2+} species.

2.4. FOURIER TRANSFORM INFRARED (FTIR) SPECTROSCOPY

2.4.1. Introduction

Due to extensive research concerning different aspects of the catalytic hydrogenation of carbon monoxide over supported Group VIII metals, a rather voluminous collection of literature has emerged, especially during the last two or three decades.
The scope of this literature review will, out of necessity, be limited to the adsorption of carbon monoxide or H_2 and CO on silica and alumina supported cobalt catalysts. However, relevant results from other catalyst systems will, where applicable, be included to some extent in order to point out differences or similarities in interpretations and/or elucidations of the experimental findings. Several additional surface analytical techniques (DRIFTS, LEED, EELS, HREEL) have been used to characterize the adsorption of CO on supported catalysts, and selected examples from the literature will be cited to illustrate important principles.

One should bear in mind, when reading the following sections, that oxides are rather ionic in character making them good infrared absorbers of their own. In the mid-infrared range (4000-500 cm^{-1}) silica becomes progressively opaque below 1300 cm^{-1}, while alumina has little transparency below 1100 cm^{-1}. Regarding CO adsorption, this means that the metal-carbon stretching frequencies (~500 cm^{-1}) and the metal-carbon monoxide angle bending frequencies (~600 cm^{-1}) are not accessible.

2.4.2. Carbon monoxide as a molecular probe

Carbon monoxide has attracted considerable interest as a molecular probe for infrared investigations largely due to the availability of information derived from spectroscopic studies of metal carbonyl complexes. Infrared spectroscopy combined with reaction studies-under either dynamic or static conditions-involving CO or for example CO and H_2, has proven particularly useful, since CO is a reactant and has a relatively high sticking coefficient (0.5-1) exhibiting a high infrared absorptivity, which makes it easy detecting rather small quantities.

The adsorption of carbon monoxide on transition metals results in the formation of adspecies

having structures closely related to those of the metal carbonyl compounds. Consequently, analogies are to be drawn between the type of bonding of the carbon monoxide that is believed to exist in metal carbonyl complexes and in the adsorbed state.

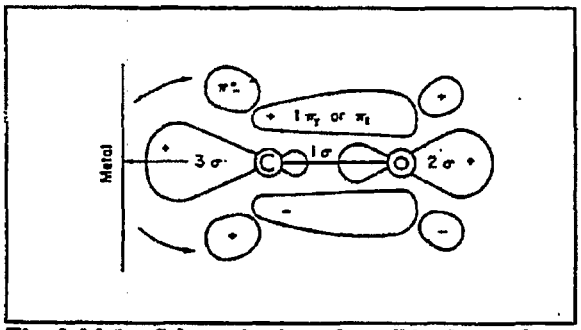

Fig. 2.4.2-1: Schematic view of possible electronic interactions upon adsorption of CO on a metal surface /68/.

Blyholder et al. /66,67/ have proposed a molecular orbital view of CO chemisorbed on metals. This generally accepted model for adsorption of CO on a zero valent metal involves two mechanisms which will tend to enhance each other in a synergic manner (Fig. 2.4.2-1). The mechanisms can be visualized as electron transfer from the 5σ orbital of the carbon atom into the vacant metal *d* orbitals coupled with the backdonating of electrons from a partly filled metal *d* orbital into the empty $2\pi^*$ antibonding orbital of CO. Since the 5σ is virtually non-bonding and the 2π strongly antibonding, the increased electron density in the antibonding orbital upon chemisorption increases the metal-carbon bond strength and decreases the C-O bond strength. Hence, the CO stretching frequency is observed to shift to a lower frequency in comparison with the central frequency for gaseous CO at 2143 cm^{-1}.

The presence of electron-donating or electron-withdrawing entities, such as for example H_2 or O_2, respectively, will each in their own way influence the electronic density of the metal particle, either by inducing a shift to higher frequency (reduced backbonding, O_2) or lower frequency (increased backbonding, H_2). Also, the vibrational frequency of CO is believed to reflect the nature of the different sites to which CO can be bonded, which is affected by particle size, nature of the support, sample preparation and pretreatment conditions.

Thus, it seems reasonable to assume that carbon monoxide will be a sensitive probe molecule showing characteristic frequency shifts depending on the electronic and geometric conditions governing its coordination to the metal surface.

2.4.3. Assignment of vibrational bands for CO on supported cobalt catalysts

Numerous studies devoted to the adsorption of carbon monoxide on alumina and silica supported cobalt catalysts have appeared in the literature during the last three decades. Most of these investigations are listed in Table 2.4.3-1. From this table, some generalizations can be made. The majority of the studies reveal that CO vibrations occur in three main frequency regions: 2180-2140 cm^{-1} (CO_C), 2070-2000 cm^{-1} (CO_B) and between 2000 and 1800 cm^{-1} (CO_A).

Infrared band(s) for CO in the 2070-2000 cm^{-1} spectral range.

IR-bands belonging to CO_B-species appear in the spectral range where the CO stretching vibrations of linear M-C≡O groups of metal carbonyls absorb, and have been ascribed to comparable adsorbed structures. This species is commonly designated linear CO, a terminal CO or "on top" CO, see Fig. 2.4.3-1.

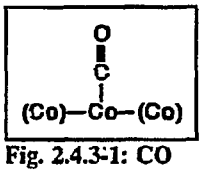

Fig. 2.4.3-1: CO adsorbed in a linear mode.

The vibrational frequency of linearly adsorbed CO shifts to lower wavenumber upon evacuation, either at room temperature /49,69,70-72/ or with increasing evacuation temperature /50,70,73/.
The observed shift in the CO frequency has been explained to be due to static factors (nonuniformity of the adsorption sites) and dynamic factors (vibrational and dipole-dipole interaction between CO molecules) /50,73/.

The effect of varying the CO pressure on the spectra resulted in a shift to higher wavenumbers with increasing pressure of CO for the absorption bands in the 2060-2020 cm^{-1} frequency range /69/. This was explained in terms of the number of CO ligands attached to single cobalt atoms [M(CO)n, n=x,y,z and z>y>x≥1]. The same interpretation was given /74/ for the 2070 cm^{-1} band found at higher coverage, which was attributed to two, three or four ligands chemisorbed at single sites. Similar trends of increasing frequency with increasing coverage of adsorbed CO were observed by Sato et al. /70/, where an indirect effect via the metal electrons was suggested to be the most important coverage-dependent factor.

Table 2.4.3-1: **Vibrational wavenumbers/cm^{-1}* for different modes of adsorbed CO on silica and alumina supported Co-catalysts.**

REFERENCE	*CATALYSTS*	*REACTION CONDITIONS*	*CO_C [Co^{2+}-$CO^{(\delta+)}$]*	*CO_B [Co^0-CO]*	*CO_A [$(Co^0)_3$-CO]*
49	5% Co/γ-Al_2O_3[2]	RT[1], P_{CO}=0.35-10 Torr	2164	2054,2023	
50,73	10% Co/γ-Al_2O_3[2]	300K,453-493K P_{CO}=50 Torr P_{CO+2H2}=760 Torr	2160	2075-2070 (2050)	1980,1880
55	5% Co/γ-Al_2O_3[2] 12% Co/γ-Al_2O_3[2]	RT P_{CO}<10^{-5} Torr	2176	2056-2030 2045-2028	
69	5% Co/SiO_2[2]	RT-600K P_{CO}=10-50 Torr	2181	2062-2055 2037-2032	
70	3.35% Co/SiO_2[2] 7.5% Co/SiO_2[2]	300-573K P_{CO}=0-3 Torr H_2/CO=1	2180 2180	2040-2000	
72	2% Co/SiO_2[4]	RT, P_{CO}=40 Torr		2050	
74	5% Co/SiO_2[2]	RT P_{CO}>0.5 Torr	2180,2130	2100-2090 2073-2060	2040-1800 2000-1700
77	10% Co/SiO_2[2]	RT-518K 3% CO/He	2101,2072	2050,2018	1865(?)
78	5% Co(N)/SiO_2[2] 5% Co(Ac)/SiO_2[3]	293K, P_{Tot}=760 Torr, H_2/CO=2	2177	2057	1848
85	1.3-1.5% Co/γ-Al_2O_3[4]	300K P_{CO}=10 Torr	2160	2060	1990,1950
86	5%,10%,20% Co/SiO_2[2]	RT, P_{CO}=10 Torr P_{H2}=100 Torr		2075-2050 2030-2020	1930
87	Co/Al_2O_3[7]	78K,195K,293K P_{CO}=10^{-5} - 1.3 Torr	2140	2070	1950,1820
109	1.66% Co/Al_2O_3[2]	298-673K P_{CO}=17.25 Torr	2180		
112	Polycrystalline cobalt[6]	RT P_{CO}=20 Torr		1990	1800
113	5% Co/Al_2O_3[5]	300K	2180 (2080)	1990	
114	Co/SiO_2[7]	RT	2179[8]		

* Wavenumbers given *before* evacuation
[1] Room Temperature
[2] Cobalt precursor : $Co(NO_3)_2 \cdot 6H_2O$
[3] Cobalt precursor : $Co(CH_3COO)_2 \cdot 4H_2O$
[4] Cobalt precursor : $Co_2(CO)_8$
[5] Oxidized in O_2 at 670K
[6] Reduction of Co_3O_4 in H_2 at 573K for 48 hr.
[7] Cobalt loading not given
[8] Bands also reported at 2160 and 2091 cm^{-1}

Generally, a number of explanations have been given for the frequency dependence of the CO absorption band upon the coverage, such as dipole-dipole interactions, indirect interaction *via* the metal or changes in the bonding to the metal, as illustrated in Fig. 2.4.3-2.

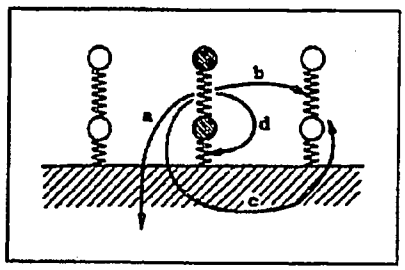

Fig. 2.4.3-2: Different types of interactions :
a).interaction with the substrate
b) direct molecule-molecule interaction
c) molecule-molecule interaction mediated via the substrate
d) interaction with thermally excited low frequency modes /75/.

All these kinds of interactions may, in principle, contribute to the observed frequency shift with increasing coverage of carbon monoxide.

Blyholder et al. /66,67/ suggested that as the number of adsorbed CO molecules increased, the competition for the surface metal *d* electrons would increase, leading to lesser extent (or suppression) of backbonding from *d* into the $2\pi^*$-orbitals. On the other hand, dynamic dipole interactions of adsorbed CO molecules was thought to constitute the main component of the CO-CO interaction, resulting in an increase in γ_{CO} with θ_{CO} /76/.

Several authors have reported that adsorbed CO in a linear mode constitute a structure exhibiting several distinguishable peak maxima /49,50,55,69,73,77/, while others /70,77,78/ report only a single band structure. Sato et al. /70/ argued that their single band for linearly adsorbed CO was a result of the low CO pressure, since Heal et al. /69/ applied higher pressure ($10<P_{CO}/Torr<50$) in their investigations. It has been suggested that the low frequency shoulder of the doublet (~2050 cm^{-1}) is related to adsorbed CO molecules on metallic cobalt having a slight positive charge /73/, that is, centres showing less marked electron donor properties ($Co^{\delta+}$) /50/. The position of the absorption band was found to be almost independent of the surface coverage of CO.

Upon adsorption of carbon monoxide on kieselguhr and ThO_2:kieselguhr supported Co-catalysts, an absorption band located at 1987 cm^{-1} was assigned to a linear type CO surface species /79/.

Infrared bands for CO in the 2000-1800 cm^{-1} spectral range.

The vibrational bands belonging to adsorbed CO designated as CO_A are in the literature preferentially ascribed to CO attached to two metal sites analogous to the binding which occur in the metallic carbonyls, as shown in Fig. 2.4.3-3.

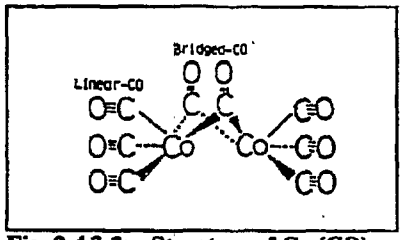

Fig. 2.4.3-3: Structure of $Co_2(CO)_8$ complex indicating linear- and bridgebonded CO /78/.

However, the assignment of CO_A-structures to bridgebonded carbon monoxide has been a subject for a longstanding controversy /11/.

Eischens and co-workers /80,81,82/ made their well known distinction between linear and bridged-bonded CO based on the small literature then available of infrared spectra of metal carbonyls.

While not denying the existence of bridged groups, Blyholder et al. /66,83/ preferred to ascribe these low-frequency absorption bands to adsorbed CO in a linear form in which the π-bonding to the metal was unusually strong, due to less competition for the $d\pi$ electrons from other ligands. Such a situation would occur, for example, at a corner or edge of the metal crystallites, since these sites would allow a greater backbonding by the $d\pi$-$p\pi^*$ mechanism. However, in a later paper, Blyholder /84/ concluded that the strongest CO adsorption and the weakest CO bond-order (hence the lowest γ_{CO} frequency) could possibly be associated with multi-bridged species. Of the two possibilities, most workers seem to favour the bridge-bonded complex, although experimental data excluding one mechanism on the expense of the other is not available /88/.

A conclusive assignment of the bands below 2000 cm^{-1} to bridge-bonded CO must be supported by the observation of the metal-carbon stretching vibrations in the lower frequency range (<1000 cm^{-1}).

Absorption bands attributable to multi-coordinated carbon monoxide has been reported in a number of papers /50,73,74,78,85-87/. Frequently, they extend over a broader frequency range and show weaker intensity compared to bands caused by linearly adsorbed carbon monoxide. The bands are almost unaffected by evacuation at (elevated) temperatures, suggesting that CO

was coordinated to the strongest adsorption sites of metallic cobalt /73/. The bands ascribed to bridge-bonded CO in the study by Ferreira et al. /74/ was related to the coverage of adsorbed CO in the sense that they appeared first at very low coverage. Increasing the CO pressure (>0.5 Torr) resulted in decreasing intensity of the bands, suggesting that linear (terminal) CO structures displaced the bridge mode adsorbed CO.

Adsorption of carbon monoxide at increasing coverage over Pd/SiO_2 was found by Eischens et al. /80/ to result in the development of absorption bands below 2000 cm^{-1}. At higher coverages, a band appeared at 2060 cm^{-1}, increasing with increasing doses of CO. Desorption was found to occur in the reverse order of the band appearance. An explanation which accounted for the observed changes as a function of θ_{CO} was suggested to be surface heterogeneity /80,88/, i.e. the presence of sites with different energies causing the different adsorption bands. It was suggested that CO adsorbed in a bridge-bonded mode at low coverage, and in a linear mode (2060 cm^{-1}) when all the double metal sites were occupied. LEED studies /89,90/ of CO adsorption on the Ni(100) and Pd(110) faces demonstrated the existence of different modes of carbon monoxide adsorption. Ni(100) exposed to CO at room temperature gave initially a structure (2×2) consistent with one CO molecule for every two surface metal atoms /89/, while analogous structures were observed on Pd(110) faces /90/.

Considering the study of Blyholder /66/, the above observed spectral changes could also be explained in terms of different degrees of back-bonding. Metal atoms at edge or corner sites was proposed to have more *d* electrons to coordinate with carbon monoxide (due to fewer CO neighbours), leading to a stronger metal-carbon bond and a weaker, polarized carbon-oxygen bond, which in turn results in absorption at lower frequencies. Adsorption occuring on planar sites would lead to more CO molecules competing for $d\pi$-electrons, reduced back-bonding and a shift to higher frequencies.

Infrared bands for CO in the 2200-2130 cm^{-1} spectral range.

The CO_c structures causing the high frequency bands appearing in the spectral range 2200-2130 cm^{-1} have been given various assignments, as discussed by Little /91,92/.

Gardner et al. /93/ correlated the vibrational frequency of carbon monoxide with the number of valence electrons in the adsorbate; a hyperbolic relationship was assumed. The partly ionized CO^+ would have nine valence electrons and a frequency of 2184 cm^{-1}.

Sato et al. /70/ ascribed their high wavenumber band to $CO^{\delta+}$ coordinated in a linear mode to cationic sites. They argued that this assignment was justified by the close correlation of the band frequency with that of CO^+ (2184 cm^{-1}).

Heal et al. /69/ found a single, sharp absorption band located at 2181 cm^{-1}, which was attributed to weakly held chemisorbed CO, may be with some physisorbed CO. The adsorption of these CO species was believed to take place on an oxidized surface, in accordance with the data of Voroshilov et al. /94/.
A distinct absorption band, observed at 2140 cm^{-1}, was believed to be characteristic of reversibly chemisorbed CO in a linear form /87/.

Ferreira et al. /74/ assigned the high frequency bands positioned at 2130 cm^{-1} and 2180 cm^{-1} to CO ligands attached to lattice cobalt ion and oxygen ion sites, respectively, on a partially oxidized cobalt metal sample.
Absorption bands located above the frequency for $CO_{(g)}$ (2143 cm^{-1}) were proposed to originate from CO species physically adsorbed on the unreduced Co-surface /49,55/.

Increasing the CO pressure has been reported to result in an increased intensity of the band, unaccompanied by a shift in frequency /49,69,70/. This, in addition to the position of the bands and the generally easy removal of the bands upon evacuation at rather low temperatures, indicate weak adsorption of the CO_C species. The adsorption can then be envisaged to occur only via δ-donation of the lone pair electrons of the carbon atom. The contribution via π-back-donation is small or negligible, possibly because of the low *d*-electron density available on these surface sites /70/.

The presence of these bands in the spectra may indicate that it is difficult to reduce the cobalt catalysts completely /49,50,55,73,78,85/. Alternatively, it has been suggested that adsorbed carbon monoxide is partly dissociated leading to reoxidation of the surface /11/. Nevertheless,

the bands are often well-defined and easy to discern.

The incomplete reduction of Co catalysts, especially those of low metal loading supported on Al_2O_3, may be explained by strong interactions between the dispersed cobalt oxide particles and the alumina support. Incorporation of Co^{2+} to some extent within the bulk structure of γ-Al_2O_3 upon impregnation or calcination results in the formation of a structure similar to that of the spinel $Co(Al_2O_4)$.
Adsorption of CO on spinel-type Co aluminates at low temperatures (170K) has been reported to give a main absorption band at 2170 cm^{-1}, a shoulder at 2140 cm^{-1} and a very weak band near 2210 cm^{-1} /95/. The 2140 cm^{-1} band, corresponding to CO on Co^{2+} and the 2170 cm^{-1} due to CO on octahedrally coordinated Al^{3+} ions, exhibited the same behaviour upon evacuation at elevated temperatures. The weak band at 2210 cm^{-1} may be assigned to CO on tetrahedral Al^{3+}.
The existence of the different phases of cobalt was discussed in Chapter 2.3.

2.4.4. Infrared bands for CO on Co_3O_4

In addition to the previous reported investigations dealing with alumina and silica supported Co catalysts, IR-spectroscopy has also been used-although to a limited extent-in identifying the nature of adsorbed CO on cobalt oxide, Co_3O_4.
Adsorption of CO (at 298K) on Co_3O_4 degassed at 823K resulted in a weak band at 2070 cm^{-1} in addition to several bands below 1700 cm^{-1} (associated with monodentate and bidentate carbonate species) /96/. The 2070 cm^{-1} band was ascribed to weakly adsorbed CO without any further mentioning of the type of coordination.

When cobalt oxide exposed to CO was heated between 313 and 423K, no absorption bands in the 2500-2000 cm^{-1} range were observed /97/. However, after heating at 493K in 500 Torr CO, a band appeared at 2185 cm^{-1}, ascribed to a terminal carbonyl group, possibly $Co\text{-}CO^+$.

Busca et al. /98/ investigated the adsorption of CO on Co_3O_4 after two different pretreatments of cobalt oxide; evacuation at 790K or exposure to hydrogen at 523K.

Adsorption of carbon monoxide at room temperature following vacuum treatment at high temperature (790K) resulted in absorption bands located at 2180, 2120, 2070 and ~2000 cm^{-1}. Prolonged exposure to CO resulted in the progressive disappearance of these bands accompanied by the appearance of bands at 2060, 1980 and 1950 cm^{-1}.
The different absorption bands were interpreted as follows. The 2180 cm^{-1} band was assigned to CO on unsaturated Co^{3+} ions. The 2120 cm^{-1} band was suggested to be due to CO coordinated to Co^{2+}, while the 2070 cm^{-1} band could be due to CO on Co^{2+} having a different coordination or to CO on Co^{+}. The bands at 2060, 1980 and 1950 cm^{-1} were assigned to different stretching modes of CO in complexes such as $Co(CO)_3^{n+}$, where n was 0 or 1.

After reduction at 523K, CO adsorption gave rise to a band at 2140 cm^{-1} (CO on Co^{2+}), a complex band in the 2080-2020 cm^{-1} range and several maxima in the spectral region 2000-1750 cm^{-1}. The band previously observed at 2180 cm^{-1} was absent. The absorption bands appearing between 2000 and 1750 cm^{-1} could be ascribed to μ_2- and μ_3 bridging carbonyls in complexes such as $Co_4(CO)_{12}$ or $Co_2(CO)_8$, and $Co_6(CO)_{16}$, respectively. Bands in the range 2080 to 2020 cm^{-1} were suggested to be due to linear carbonyl species in the above complexes.

2.4.5. Assignment of vibrational bands for CO on evaporated cobalt films

Infrared spectra of carbon monoxide adsorbed on evaporated films of cobalt have been studied by a number of authors /99-103/, and a summary of the results from these investigations are given in Table 2.4.5-1.

There exists a general similarity between the infrared spectra of supported and evaporated cobalt, and the scheme of interpretation used earlier (Chapter 2.4.3) will also be applicable to evaporated cobalt films.

Examination of Table 2.4.5-1 indicates the appearance of absorption bands due to linearly and bridgebonded CO in the frequency range 2040-1900 cm^{-1} and below 1900 cm^{-1}, respectively, but the linear CO-groups do tend to have a lower stretching frequency than those observed for supported cobalt catalysts. A suggested explanation has been that evaporation of films

in the presence of gaseous CO may lead to contamination from carbon monoxide /11/, since occlusion and disproportionation of CO on hot metal filaments are possible under such conditions /104/.

Comparing Table 2.4.3-1 and Table 2.4.5-1 reveals, however, a significant difference in the infrared spectra of evaporated and supported cobalt, the latter giving rise to high frequency absorption bands above 2100 cm^{-1}. The difference in the spectral features between the evaporated metal films and supported metal particles can be due to a combination of several effects; the degree of reduction of the metal particles, different metal particle size and different degree of crystallinity, and epitaxial or electronic effects, in which the supporting substrate affects the formation of crystallites or specific planes on crystallite surfaces /11/.

Table 2.4.5-1: Vibrational wavenumbers/cm^{-1} for different modes of CO on evaporated films of cobalt.

REFERENCE	*SUBSTRATE OR SUPPORT*	*REACTION CONDITIONS*	*CO_B (Co^0-CO)*	*CO_A [$(Co^0)_2$-CO]*
99	NaCl[1]	RT[2] P_{CO}=0.1 Torr	1980	1880
100	CaF_2[3]	170K, RT $P_{CO}=10^{-3}$ Torr	1990 (170K) 1970 (RT)	
101	NaCl[4]	113K, 308K P_{CO}=	2040 (113K) 1975 (308K)	
102	---[5]		2032 2016	1856
103	NaCl[6]	RT P_{CO}=700 Torr	1960 A) [7]	1815 A) [7]

(1) Evaporated on NaCl windows in the presence of CO
(2) No temperature range given, assumed room temperature
(3) Evaporated on CaF_2 windows under vacuum conditions
(4) Evaporated on NaCl windows under UHV conditions
(5) Evaporated in the presence of CO
(6) Evaporated in the presence of A) 0.1 Torr CO or B) 0.1 Torr H_2
(7) No infrared bands due to chemisorbed CO were detected on cobalt films evaporated in 0.1 Torr H_2 after addition of olefins followed by admission of 700 Torr CO.

2.4.6. The effect of metal loading on the infrared spectra of supported cobalt catalysts

Some investigations have reported the influence of different cobalt content on the infrared bands appearing in the region normally expected for molecularly adsorbed carbon monoxide.

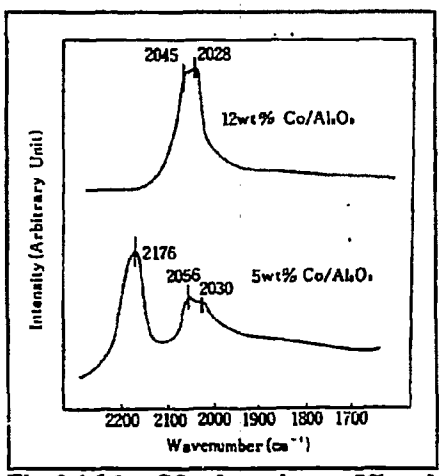

Fig. 2.4.6-1: CO adsorption on 5% and 12% Co/Al_2O_3. Reduction conditions: 823K for 17 hr /55/.

The absence of the high frequency band (2176 cm^{-1}) in the spectra of the 12% Co/Al_2O_3 catalyst, see Fig. 2.4.6-1, was believed to be due to a more complete reduction of the high metal loading catalyst /55/. A lower activation energy for reduction for the 12% Co/Al_2O_3 catalyst than for 5% Co/Al_2O_3 was reported, indicating that the extent of reduction increases with increasing metal loading.

In the study conducted by Sato et al. /70/, both CO_C and CO_B structures were reported for cobalt (7.5 wt-%) supported on silica. The IR spectra of the low loading catalyst, 3.35% Co/SiO_2 in the CO region featured only the high frequency band due to CO_C species. XPS studies showed the presence of Co^{2+} and metallic cobalt on the catalyst with the highest cobalt loading, but mainly Co^{2+} for the 3.35% Co/SiO_2 catalyst. It was suggested that the cobalt ions could be coordinated to the silica surface in two different ways, strongly or more loosely bound. Co^{2+} coordinated more weakly was believed to be present in higher amounts and easier to reduce, and it was proposed that this form of Co^{2+} was absent in the case of the 3.35% Co/SiO_2.

Kuznetsov et al. /105/ reported minor changes in the positions of the absorption bands in the 2075-1900 cm^{-1} region upon introduction of CO over 5% and 10% Co/SiO_2 (prepared by using cobalt nitrate as the metal precursor). A downscale shift in frequency of the most intense peak was observed with increasing cobalt loading (5% Co/SiO_2:2050-2075 cm^{-1}, 10% Co/SiO_2:2035 cm^{-1}).

2.4.7. The effect of hydrogen on adsorbed CO

The effect of introducing an additional gas on the spectrum of CO has been shown to result in a shift in either frequency direction for the CO stretching bands, depending on the particular metal and the added gas /88/. Amongst others (NO,O_2), H_2 has frequently been used. The reaction between H_2 and CO giving rise to several proposed reaction intermediates is of considerable interest from the point of view of the Fischer-Tropsch synthesis. Therefore, the following brief section surveys only investigations utilizing hydrogen as coadsorbate.

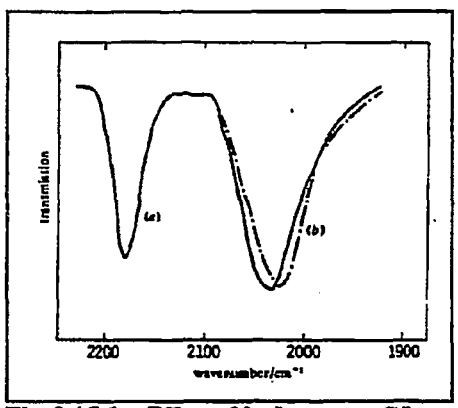

Fig. 2.4.7-1: Effect of hydrogen on CO adsorption on 7.5 wt-% Co/SiO_2 /70/:
(a) CO alone
(b) $H_2/CO=1$

The effect of hydrogen on adsorbed CO is believed to result in a displacement of the CO stretching frequency to lower wavenumbers /66,91/. It is likely that the presence of hydrogen, acting as an electron donor, may increase the availability of *d*-electrons for backbonding from the metal to the adsorbed CO via π-bonding. This would indicate a strengthening of the metal-carbon bond and a subsequent weakening of the carbon-oxygen bond in CO, hence a downscale shift in frequency.

Fig. 2.4.7-1 illustrates the effect of hydrogen on the adsorption of CO /70/.

Heal et al. /69/, however, reported lower intensity and a high frequency shoulder on their 2022 cm^{-1} band after H_2 addition. They argued that the high frequency shoulder indicated chemisorption of several ligands on the same metal site, suggesting the formation of $H_YM(CO)_X$, $Y \geq 1$. In such a complex, hydrogen would compete for the available *d*-electron density, the M-C bond would be weakened, the C-O bond would be stronger, hence a shift to higher CO frequencies would occur. The magnitude of the shift would depend on the ability of hydrogen to accept *d*-electrons (forming a M-H species) and the relative proportions of the *d*-electron density distributed between the M-H and M-C bonds within the proposed complex /69/.

Eischens et al. /80/ stated that adding a gas to chemisorbed CO influences the electronic nature of the metal rather than leading to structural changes of the adsorbed CO.

Coadsorption of carbon monoxide and hydrogen over supported cobalt catalysts has been reported to result in a shift to lower wavenumbers for the CO stretching band compared to a hydrogen free system /50,70,73,78/. The reduction in frequency was thought to be caused by an electronic modification of the surface metallic sites, probably by reagents or products formed during the hydrocarbon synthesis /50,73/, while others /70/ interpreted the observed shift in terms of a weakening of the C-O bond due to an increased electron density available for backbonding, in line with the previous explanation.

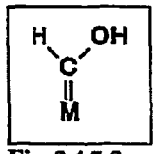

Fig. 2.4.7-2: Structure of hydroxy-carbene.

The question is, whether the observed displacement in frequency is consistent with the formation of a hydroxycarbene (see Fig. 2.4.7-2) or "enolic" species /80/. Justification for the "enolic" complex has been based on coadsorption experiments involving H_2 and CO resulting in surface species in which 1:1 stoichiometry of each adsorbate was reported /106,107/. On the other hand, no interaction was observed /50,70,73/ between hydrogen and chemisorbed CO indicative of the formation of a Fischer-Tropsch type intermediate like the above mentioned complex.

Generally, one would expect that the formation of a complex of an "enolic" structure should be accompanied by the disappearance of the CO stretching absorption band together with the formation of a hydroxyl band /80/. The possibility exists that the OH-groups may be hidden under the OH-stretches belonging to the support (Al-OH or Si-OH). However, the C-H stretch of an carbon-containing species should cause a distinct, high frequency band. In addition, under the conditions where the 1:1 H_2/CO complex has been observed, the CO band is still intact.

With this in mind, the infrared results indicate that if oxygenated building blocks like hydroxycarbene exist, they probably exhibit a rather transient character and/or that appreciable quantities of this complex is not formed under the specific reaction conditions.

2.4.8. Infrared bands of adsorbed species in the frequency region 3050-2700 and 1800-1200 cm^{-1}

In addition to the frequency range normally expected for the adsorption of different modes of carbon monoxide (2200-1800 cm^{-1}), other spectral regions also investigated includes the 3050-2700 cm^{-1} and 1800-1200 cm^{-1} spectral range.

Bands observed between 3050 and 2700 cm^{-1}.

Infrared absorption bands appearing in the 3050-2700 cm^{-1} range have generally been ascribed to C-H stretching vibrations in CH_2- and CH_3-groups.
Few studies have reported the presence of bands in this frequency range during CO hydrogenation over alumina and silica supported cobalt catalysts.
Arakawa et al. /78/ ascribed bands located at 2927 cm^{-1} and 2856 cm^{-1} to asymmetric and symmetric stretches of CH_2-groups, respectively.
Heal et al. /69/ reported methane (Q-branch at 3017.5 cm^{-1}) as the main product detected in the temperature range 468 to 488K during heating of 5% Co/Al_2O_3 in an atmosphere of hydrogen and carbon monoxide.
In the study by Ansorge et al. /108/, absorption bands due to the formation of hydrocarbons were reported in the following positions: 2970 and 2930 cm^{-1} (asymmetric CH_3 and CH_2-stretch) and 2890 and 2860 cm^{-1} (symmetric CH_3 and CH_2-stretch).

Bands observed between 1800-1200 cm^{-1}.

Bands observed in this frequency region can be ascribed to C-H deformations, symmetric or asymmetric (correlating with the asymmetric and symmetric C-H stretching bands in CH_2/CH_3-groups). O-C-O or C=O in oxygen-containing species like surface formates or carbonates /91/.

Savel'eva et al. /109/ reported several bands in the frequency range 1690-1230 cm^{-1} and assigned them to a number of carbonato-carboxylate complexes formed upon the interaction between CO and the support (Al_2O_3). The bands disappeared upon vacuum treatment at 573K.

Arakawa et al. /78/ observed a absorption band at ca. 1460 cm^{-1} (depending on the reaction conditions) which was related to the CH_2-groups observed in the 3050-2700 cm^{-1} range.

The formation of carbonate groups (1525 cm^{-1} and 1345 cm^{-1}) and formate groups (1580 cm^{-1} and 1385 cm^{-1}) were detected during CO treatment of a 5% Co/Al_2O_3 catalyst at high temperature /86/.

CO adsorption and/or coadsorption of CO and H_2 over ZrO_2 has been found to result in the appearance of absorption bands attributable to bidentate carbonate (1550 cm^{-1} and 1330 cm^{-1}) and formate groups (2877 cm^{-1}, 1358 cm^{-1} and 1365 cm^{-1}) /110/.

Adsorption of formic acid on 5% Co/SiO_2 at 303K revealed the presence of physically adsorbed HCOOH (on the silica support) giving absorption bands located at 2960 cm^{-1}, 1725 cm^{-1} and 1410 cm^{-1} as well as formate ion (adsorbed on the cobalt metal) showing characteristic absorption at 2945, 1580 and 1380 cm^{-1} /111/. Increasing the temperature lead to a rapid decrease in the 1725 cm^{-1} band intensity, while the 1580 cm^{-1} band was essentially unaffected by the desorption temperature.

2.5. CO HYDROGENATION ACTIVITY AND SELECTIVITY

2.5.1. Introduction

This brief literature review is confined to studies reporting the effect of cobalt loading and support on the CO hydrogenation activity and selectivity. The influence of dispersion and extent of reduction is not treated in any specific detail in the following chapter. Several papers and review articles gives a thorough discussion of these and other topics, for example Bartholomew /6/, Iglesia et al. /115/, Che et al. /116/, Moon et al. /117/ and Johnson et al. /118/.

2.5.2. Effect of metal loading and support on CO hydrogenation activity and selectivity

Several studies provide evidence that the support can affect the activity and selectivity properties of Co for CO hydrogenation.

Castner et al. /58/ investigated the influence of different support materials on CO hydrogenation activity for a 5% Co-catalyst. They found that the activity (based on total catalyst weight) decreased in the order Co/silica > Co/titania > Co/alumina > Co/K-alumina. Variations in activity was explained by the amount, type and reducibility of the cobalt species present on each catalyst. For example, Co/SiO_2 had the highest concentration of reduced surface cobalt (presumably due to the easy reducable Co_3O_4-phase), while cobalt-aluminate species on the Co/Al_2O_3 catalyst, showing evidence of being hard to reduce (from TPR measurements), probably caused the low activity of this catalyst. Thus, a relationship seemed to exist between the reduction properties of the cobalt species on the different supports and the CO hydrogenation activity.

These findings were in accordance with the conclusions from the work of Reuel et al. /119/, in the sense that the alumina supported Co-catalyst was reported to be less active than Co/SiO_2, viz. decreasing specific activity in the order Co/titania > Co/silica > Co/alumina for cobalt loadings of 3 wt-%. The initial activity varied three orders of magnitude between the

different Co-supported catalysts. Increasing the Co-loading of the alumina supported catalysts from 3 to 15 wt-% resulted in a 20-fold increase in the specific activity. In fact, a linear increase in specific activity with decreasing dispersion was observed. This was suggested to be due to changes in surface structures with decreasing particle size, or electronic modifications because of the intimate contact between the small metal particles and the support.

The hydrocarbon selectivity could also be correlated with dispersion and the extent of reduction. Higher dispersions and lower extents of reduction resulted in the observation of lower molecular weight hydrocarbon products. This could be related to the presence of stable surface oxides, e.g. cobalt aluminate, catalyzing the water-gas-shift reaction thereby increasing the ratio of H_2/CO at the surface.

Vannice /120/ reported the order of specific activity of supported Co-catalysts to Co/silica > Co/alumina > Co/titania for cobalt loadings between 1.5 and 4 wt-%. The observed higher activity for Co/SiO_2 compared to Co/Al_2O_3 was suggested to be due to a more complete reduction of the dispersed Co on SiO_2.

Fu et al. /121/ also observed variations in activity and selectivity of Co/Al_2O_3 with metal loading, reduction temperature and catalyst preparation. Increasing the cobalt loading from 3 to 25% (decline in dispersion from 15 to 6.7%) resulted in increasing specific activity or turnover number, that is, increasing activity with decreasing dispersion in accordance with the observations of Reuel et al. /119/. The variation in specific activity was suggested to be due to variations in the distribution of low and high coordination sites (depending on the metal particle size), and by changes in the nature of adsorbed CO species. Linear and bridge bonded CO was suggested to dominate on the poorly dispersed catalysts, while subcarbonyls (more than one CO molecule adsorbed per metal surface atom) were prevalent on well-dispersed cobalt. The low activity of the well-dispersed cobalt catalysts was explained in terms of the different modes of adsorbed CO, since subcarbonyls was considered to adsorb on sites of low activity.

The above results may suggest that CO hydrogenation is a structure sensitive reaction. Such a conclusion however, must be considered in view of the recent studies of CO hydrogenation

over well-dispersed iron on alumina /122/ and on overlayers of Co on W(100) and W(110) /123/. Keeping the extent of reduction constant, the specific activity was independent of the dispersion, suggesting that the reaction is structure insensitive. A similar relationship has been observed in investigations of single crystal Ni /124/ and Ru /125/.

In the Temperature Programmed Surface Reaction (TPSR) study by Lee et al. /77,126/, two different reaction pathways for CO adsorption and hydrogenation was proposed:

1) Dissociation of carbon monoxide on the metal followed by hydrogenation of the atomic (α-) carbon (Reaction A)
   and
2) Spillover of hydrogen and carbon monoxide to the support were a CH_xO complex was formed, followed by diffusion of the complex to metal crystallites, where it decomposed (Reaction B).

Reaction A was associated with large, 3D Co metal crystallites, pathway B with sites of both large and small crystallites. The authors stated that the observed variations in activity could be explained by the distribution of A and B states (reactions), which was related to the metal loading and reduction temperature. Mechanism A dominates on catalysts with high cobalt content and extent of reduction, while the influence of Reaction B increases with increasing metal loading.

Varying the metal content appears to be one of the major factors influencing the selectivity. Longer hydrocarbon chains and less formation of CO_2 are characteristic when the metal loading is increased. The C_{5+} hydrocarbon fraction increases, the selectivity to C_1 and C_2 decreases and the olefin/paraffin ratio decreases with increasing cobalt content /121,127/.

Fu et al. /121/ observed a shift in the product distribution for Co/alumina catalysts towards heavier hydrocarbons as the metal loading was increased; α increased from 0.7 to 0.9 as the wt-% Co increased from 3% to 15%. The increase in the hydrocarbon chain length with decreasing dispersion over cobalt alumina catalysts with varying cobalt loading was suggested to be due to changes in the strength of adsorption of carbon containing intermediates with

loading and dispersion. This can be interpreted in terms of different CO adsorption stoichiometry, as discussed previously. It was assumed that the metal-carbon bond strengths for adsorbed hydrocarbons would show similar behaviour, thus leading to higher residence times and lower termination rates with increasing metal loading, which would give longer hydrocarbon chains.

Keeping the metal loading constant (10 wt-% Co/γ-Al_2O_3) and varying the reduction time and temperature resulted in decreasing dispersion with decreasing extents of reduction when the catalysts were reduced at 598 or 648K (for different periods of time) /128/. It was suggested that the presence of unreduced cobalt oxide modified the electronic properties of the reduced cobalt metal, causing suppression of hydrogen adsorption. This would mean that the dispersion based on chemisorption of hydrogen will be underestimated at low extents of reduction. H_2 suppression was also believed to be the reason for the enhanced production of olefins on the partially reduced Co-catalysts.

3. PRINCIPLES

3.1. THE FISCHER-TROPSCH SYNTHESIS

The catalyzed hydrogenation of carbon monoxide constitutes an important class of reactions over Group VIII metals. Among these catalytic processes, e.g. methanation, alcohol synthesis and Fischer-Tropsch synthesis, the industrial interest has focused on oxygenate production, while extensive research related to the Fischer-Tropsch process has been carried out since its discovery by Sabatier et al. /1/.

The products obtained from the reaction between hydrogen and carbon monoxide depends on the type of catalyst applied, as illustrated in Fig. 3.1-1.

3. CH_3OH	Route 3: $Cu/ZnO/Al_2O_3$
↑	
H_2/CO → 1. Hydrocarbons	Route 1: Fe, Ru or Co catalysts
↓	
2. Higher alcohols ($C_{2+}OH$) accompanied by other oxygenates	Route 2: Nitridized Fe, or alkalized Fe or Co, promoted Rh-catalysts

Fig. 3.1-1: Process routes to liquid energy carriers from synthesis gas /129/.

The stoichiometry describing the conversion of synthesis gas to typical methanation and Fischer-Tropsch products can be represented by the following equations /130/:

$$n\mathrm{CO} + 2n\mathrm{H_2} \rightarrow \mathrm{C}_n\mathrm{H}_{2n} + n\mathrm{H_2O} \qquad (n=2,3,....) \qquad 3.1$$

$$m\mathrm{CO} + (2m+1)\mathrm{H_2} \rightarrow \mathrm{C}_m\mathrm{H}_{2m+2} + m\mathrm{H_2O} \qquad (m=1,2,3,....) \qquad 3.2$$

$$p\mathrm{CO} + 2p\mathrm{H_2} \rightarrow \mathrm{C}_{p-1}\mathrm{H}_{2p-1}\mathrm{CH_2OH} + (p-1)\mathrm{H_2O} \qquad (p=1,2,3,....) \qquad 3.3$$

$$2\mathrm{CO} \rightarrow \mathrm{C} + \mathrm{CO_2} \qquad 3.4$$

$$\mathrm{CO} + \mathrm{H_2O} \rightarrow \mathrm{CO_2} + \mathrm{H_2} \qquad 3.5$$

Typical products from the Fischer-Tropsch reaction are predominantly linear alkanes and alkenes. Alcohols, if produced, are mostly primary *n*-alcohols. The Boudouard reaction (3.4) results in the deposition of carbon, and is favoured by decreasing H_2/CO ratios. The secondary water-gas-shift reaction (3.5) produces hydrogen, and is useful when the H_2/CO ratio of the feed differs from that required by the stoichiometry of the desired products /130/.
The Fischer-Tropsch synthesis over traditional catalysts like Fe, Co and Ru, results in a range of products, from CH_4 to long chained hydrocarbon waxes. It is generally agreed that the formation of the hydrocarbons is governed by a stepwise growth mechanism, involving one carbon entity at a time being added to the growing chain:

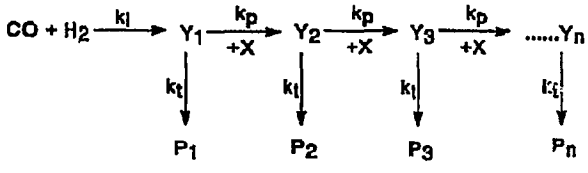

3.6

$CO + H_2 \rightarrow Y_1$ is the initialization step, and Y_n the growing chain (surface intermediate). X is the monomer and P_n is the product containing n carbon atoms. k_p and k_t are the rate constants for chain propagation and termination, respectively.

The probability of chain growth, α, can be defined as follows :

$$\alpha = \frac{r_p}{r_p + r_t} \qquad 3.7$$

where r_p= chain propagation rate
r_t= chain termination rate

If it is assumed that α is independent of chain length, and that chain growth occurs only in one direction, the distribution of the hydrocarbon products can be described by the chain polymerization kinetics model of Anderson-Schulz-Flory (ASF) /28/. The ASF polymerization equation is written as /6/:

$$\frac{W_n}{n} = (1-\alpha)^2 \cdot \alpha^{n-1} \qquad 3.8$$

where n = number of carbon atoms in the product

W_n = weight fraction of product containing n carbon atoms

α = chain growth probability

α is obtained by a least-squares linear regression of the logarithmic form of equation (3.8);

$$\ln\left(\frac{W_n}{n}\right) = \ln(1-\alpha)^2 + (n-1)\cdot\ln\alpha \qquad 3.9$$

If the product distribution among the carbon numbers follows the polymerization equation, one would expect a linear relation between $\ln(W_n/n)$ and n, with slope $\ln \alpha$.

The theoretical product distributions can be calculated as a function of the chain growth probability. Fig. 3.1-2 shows the results obtained for hydrocarbon fractions in the range C_1-C_{120} /131/. The figure indicates that high yields are only possible for the extreme ends of the hydrocarbon product spectrum, CH_4 and waxes. With the exceptions of C_1 and/or C_2, the theoretical results in Fig. 3.1-2 agrees well with the experimentally determined product spectra /26/. Deviations from equation 3.9 can be explained by /26/:

* secondary reactions on the support
* further chain growth after readsorption of desorbed products
* incorporation of C_2-C_4 into growing chains
* additional production of methane by different pathways
* change in α with chain length

The selectivity limitations arise from the polymerization kinetics governing the chain growth and can not be circumvented unless other factors are brought into play, for example by the use of shape selective zeolite containing catalysts, unsteady state operation or interception of intermediates /6/.

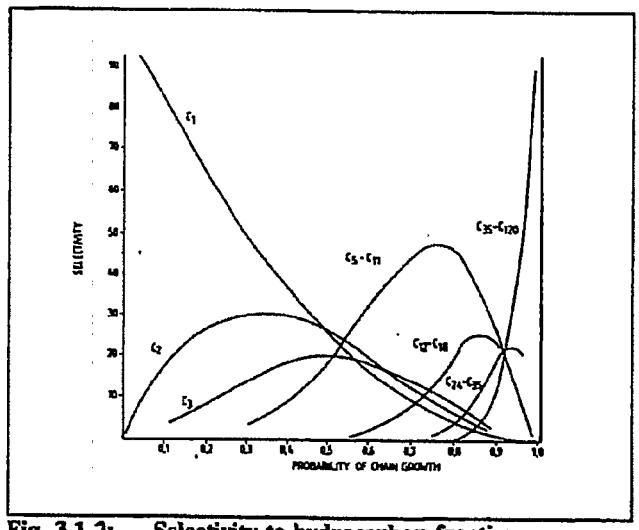

Fig. 3.1-2: Selectivity to hydrocarbon fractions as a function of chain growth probability, α /131/.

Since the discovery of the process there has been an ongoing controversy over the perceived mechanism of the reaction on the catalyst surface. Discussions concerning the mechanism of the Fischer-Tropsch reaction has focused on mainly three reaction pathways:

- surface carbide mechanism [dissociative adsorption of carbon monoxide]
- hydroxycarbene mechanism [hydrogenation of associated adsorbed CO to M=C(OH)H]
- carbonyl mechanism [insertion of CO in growing chains]

The different pathways propose the formation of different intermediate complexes and their nature and extent of participation in the chain growth leading to the observed product distributions. The carbide mechanism, originally proposed by Fischer et al. /132,133/, has gained credibility through extensive research the last two decades, and is now generally considered to be a plausible explanation for describing the interaction between hydrogen and

carbon monoxide with the catalytic surface and subsequent synthesis of hydrocarbons. Ample evidence has shown that this is the prevalent mode of CO activation at higher temperatures over Fe, Co and Ni. The various steps may be visualized as follows:

CO dissociation:

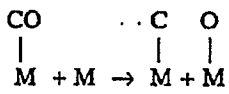

M represents a catalytic site on the metal surface

3.10

Hydrogenation:

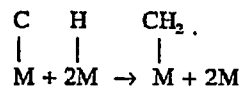

3.11

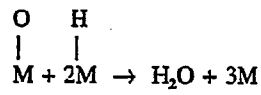

3.12

Chain growth:

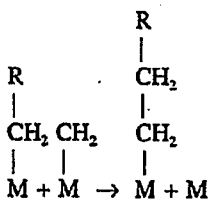

3.13

Termination:

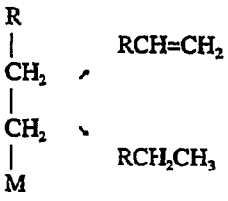

3.14

3.15

Carbon monoxide is dissociatively adsorbed, and the carbon atoms are hydrogenated to CH_x species. Adsorbed oxygen is removed by CO (as CO_2) or by hydrogen (as H_2O). Methane is formed via hydrogenation of surface methyl groups:

$$\begin{array}{l} CH_3\ H \\ |\quad| \\ M + M \rightarrow CH_4 + 2M \end{array} \qquad 3.16$$

while propagation proceeds by insertion of CH_2-groups into a metal-alkyl bond. Termination of the chain growth may occur by β-H abstraction resulting in α-olefines or by hydrogenation yielding paraffines.

One of the key objections to the carbide mechanism is its failure to account for the formation of large amounts of oxygenated products, e.g. alcohols. While the two mechanisms, hydroxycarbene and carbonyl, explains the formation of oxygenates, it has been proposed that methanation occurs via the carbide route and chain growth by CO insertion. Attempts have been made to present a general mechanism which includes the features of alkane, alcohol, acid and aldehyde formation /26/. According to the scheme in Fig. 3.1-3, this mechanism is essentially a combination of the carbide and CO insertion mechanism. Chemisorption of CO results in a complex with C and O associated with either one another or with the metal site. Dissociation gives atomic C and O. Carbon atoms can be hydrogenated to CH_2 or bulk carbon (graphite) can be formed by agglomeration. Alternatively, the C-O complex can be hydrogenated to a CH_2O complex (A), which in turn forms either CH_3OH or CH_2 or water by hydrogenation. Chain growth occurs by insertion of the C-O complex followed by hydrogenation. Termination resulting in the desired organic products can occur by desorption or hydrogenation of the surface complex (B). The combined mechanism also provides an explanation for the often observed high CH_4 selectivity compared to the other carbon number cuts. CH_4 can be formed via hydrogenation of C atoms or via hydrogenation of the HCOH complex (A) and of the resultant methanol.

The reaction kinetics of CO hydrogenation on supported cobalt catalysts have been reported in a number of papers /27,119-121,134-137/. The hydrogen reaction order is typically about 0.5 to 1.0, while that of CO is either negative or near zero. Therefore, the rate of reaction is

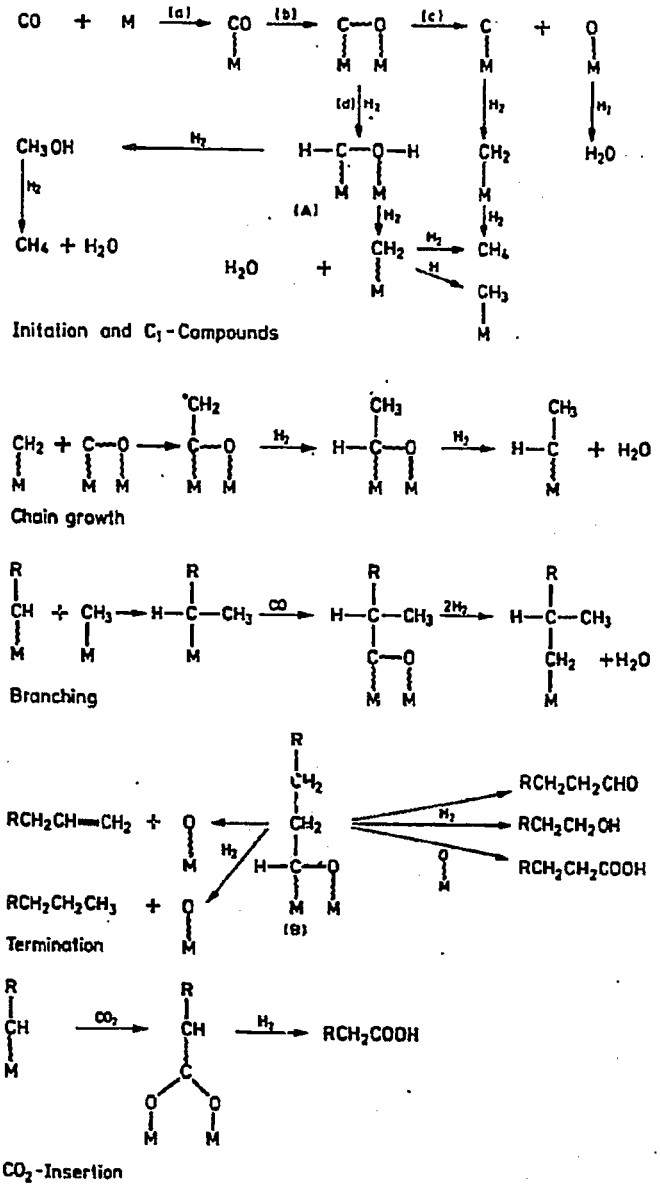

Fig. 3.1-3: **A general reaction mechanism scheme incorporating the features of both the CO insertion and the carbide mechanism /26/.**

generally proportional to the concentration of hydrogen in the gas phase. By considering the elementary reaction steps, rate expression of the Langmuir-Hinschelwood type can be obtained. Derivation of the rate expression based on the surface carbide mechanism assuming hydrogenation of surface carbon to be the rate-determining step gives:

$$-r_{CO} = \frac{K_1 \cdot P_{CO}^{1/2} \cdot P_{H_2}^{1/2}}{(1 + K_2 \cdot P_{H_2}^{1/2} + K_3 \cdot P_{CO}^{1/2})^2} \qquad 3.17$$

Derivations of rate expressions based on the carbonyl and hydroxycarbene mechanisms have been given elsewhere /138/.

A brief summary of kinetic parameters for CO hydrogenation on supported Co catalysts is given in Table 3.1-1.

Table 3.1-1: Fischer-Tropsch reaction kinetics of cobalt catalysts.

$-r_{CO} = A \cdot e^{-Ea_{CO}/RT} \cdot (P_{CO})^X \cdot (P_{H_2})^Y$

CATALYSTS	X^A	Y^B	$Ea_{CO}{}^C$ *(kJ/mol)*	*REFERENCES*
2% Co/Al_2O_3	-0.48	1.22	112	27
3-15% Co/Al_2O_3	---	---	96 to 146	119
3% Co/SiO_2	---	---	67	
10% Co/SiO_2	---	---	69	
4% Co/SiO_2	---	---	95.4	120
3-25% Co/Al_2O_3	---	---	87 to 130	121
14% Co-1% La_2O_3/Al_2O_3	-0.33	0.55	---	134
6.2% Co/Al_2O_3	-1.5 to 0.5	-0.5 to 1.0	---	135
3% Co/Al_2O_3	-0.43	1.24	100	136
3% Co/Al_2O_3	-0.20	1.10	105	137
10% Co/Al_2O_3	-0.90	0.83	100	

A = reaction order, P_{CO} B = reaction order, P_{H2}
C = activation energy for CO conversion

3.2. TEMPERATURE PROGRAMMED REDUCTION (TPR)

The reduction of a metal oxide (MO) by hydrogen to form the metal (M) and water vapour may be described by the general equation /139/:

$$MO_{(s)} + H_{2(g)} \rightarrow M_{(s)} + H_2O_{(g)} \qquad 3.18$$

Oxides, which reduction are associated with a negative standard free energy change, and CoO is one of them, are thermodynamically feasible. The TPR profiles are obtained by passing a mixture of hydrogen and inert gas over the metal oxide while increasing the temperature at a linear programmed rate. Since the gas flow is kept constant, the changes in hydrogen concentration is proportional to the rate of reduction. The peak maxima occuring at a certain temperature corresponds to a maxima in the rate of reduction. The positions of the peaks appearing in the TPR spectrum are determined by the chemical nature and the environment of the reducible species /140/, i.e. the strength of the bonding between metal and the support, between the metal and metal oxide and the particle size of the metal precursor. The peak area reflects the amount of hydrogen consumed, thus making it possible to estimate quantitatively the extent of reduction by using a suitable calibration compound, such as CuO or Ag_2O.

Several experimental parameters will affect the spectra, the most important being the heating rate and the gas flow rate. Increasing the heating rate induce in general sharper peaks and also a shift to higher temperatures but lower resolution is obtained /139,140/. A lowering of the heating rate results in spectra with higher resolution, less intense and broad peaks.
A decreasing flow rate has the same effect on the shape of the reduction peaks as increasing heating rate. The opposite, an increase in the flowrate results in a lowering of the degree of conversion, thus increasing the concentration of the reactant. Hence, the peak maxima are expected to be shifted to lower temperatures.
The effect of increasing the mass of the catalyst is reduced resolution, which may lead to to difficulties in separating two reduction processes. The temperatures at which the composite reduction occurs can then be higher than those of the separate processes /139/.
Furthermore, in too large catalyst beds temperature gradients may exist, in addition to significant hydrogen concentration gradients, resulting in non-homogeneous reduction.

In summary, care must be exercised when direct comparison of the reduction peaks are performed on the results obtained in different laboratories due to the above mentioned effects.

3.3. INFRARED SPECTROSCOPY

3.3.1. Theory

The interaction between the dipolar motions of molecules or groups of atoms within molecules and the electric component of the electromagnetic field is the basis for rotational, vibrational and electronic spectroscopy. Electronic spectra are observed in the ultraviolet/ visible region due to transitions between electronic levels, while resonances associated with molecular vibrational frequencies occur in the 4000-200 cm^{-1} portion of the infrared spectrum.

The expression for the vibrational frequency of a molecule can be derived using the classical approach based on Hooke's law ($f=-kx$) in combination with Newton's second law of motion ($f=ma$). In the case of a diatomic molecule (A-B), the equation of harmonic motion is given by

$$\mu_m\left(\frac{d^2x}{dt^2}\right)=-k\cdot x \qquad 3.19$$

where k=force constant of the bond, μ_m is the reduced mass $m_A \cdot m_B/m_A+m_B$ and $x=r-r_e$, the displacement of the atoms from the equilibrium separation r_e to a distance r, see Fig. 3.3.1-1. f will be a function of the potential energy, and integration of the right hand side of equation 3.19 gives the change in the potential energy of the system:

$$U=0.5k\cdot x^2 \qquad 3.20$$

Assuming small values for x, the solution of equation 3.19 is:

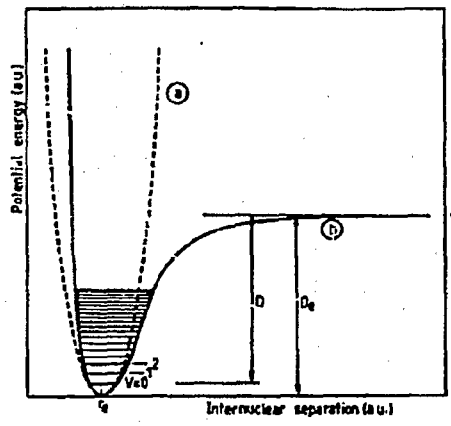

Fig. 3.3.1-1: Potential-energy function for a real diatomic molecule with a dissociation energy and equilibrium bond length r_e(b). The dashed (a) is the potential energy function for the harmonic oscillator that approximates the potential at small displacements from r_e. The lines parallel to the abscissa axis represents allowed energy levels /141/.

$$x = A\sin(2\pi\gamma t) \qquad 3.21$$

where

$$\gamma_e = \frac{1}{2\pi}\sqrt{\frac{k}{\mu_m}} \qquad 3.22$$

A small displacement of one of the masses relative to the other will result in simple harmonic vibrations, and γ_e is the frequency at which the system vibrates and denoted the equilibrum frequency. If the frequency γ of the incoming light corresponds to γ_e, a coupling with the dipole moment of the diatomic molecule (A-B) occurs, causing vibration of the molecule /141/. If the diatomic molecule is of the type A-A (symmetric), no coupling occurs, hence the molecule will not absorb infrared radiation.

For more complex molecules than the diatomic, equations can in principle be derived which expresses the potential and kinetic energy in terms of the displacement x of the atoms.

Solving under the constraint that the total energy is constant, the number of solutions (or vibrational degrees of freedom) will be 3N-6 for a polyatomic molecule and 3N-5 for a linear molecule, N being the number of atoms. That is, N atoms require 3N Cartesian coordinates to describe their motion. Three coordinates are associated with translational degrees of freedom (movements of the entire molecule through space while the positions of the atoms relative to each other remain fixed) : three more coordinates (two for a linear molecule) associated with the rotational degrees of freedom (the interatomic distances remains constant but the entire molecule rotates with respect to three mutually perpendicular axes that passes through its center of mass). All other movements of the atoms in a molecule are known as vibrations and are determined by the condition that the average position and orientation of the molecule remain fixed while the relative positions of the atoms change.

The classical model approach provides considerable information on the existence of vibrational frequencies of atoms within molecules, but, on the other hand, it does not explain the existence of rotational frequencies, unless electronic motion occurs at the same frequencies /141/.

Quantum-mechanical considerations involving the solution of the Schrödinger equation assuming the harmonic oscillator energy potential function results in allowed, equally spaced energy levels defined by:

$$\varepsilon = (n + 0.5)h\gamma \qquad 3.23$$

where h is Planck's constant. When the quantum number (n) is zero, that is, the oscillator is in the ground state, the system still retains ½hγ of energy. This is known as the *zero point* energy, and is of importance in thermodynamic and kinetic studies /142/. One of its consequences is that the dissociation energy (D_e) of isotopic species will be different, since $D=D_e-0.5h\gamma$ and γ will be different because of the different masses, cfr. Eq. 3.22.

From the quantum-mechanical approach the probability of inducing transitions between different energy levels can be predicted. The *selection rule* $\Delta n=\pm 1$ is valid for the harmonic oscillator, which means that n must change by ±1 for the transition to be active in the infrared. Usually, these transitions occur between the ground state (n=0) and the first excited

level (n=1). This is due to the fact that the number of molecules not in the ground state is negligibly small at room temperature, i.e. hγ is generally large compared to kT /143/. Such a conclusion is based on the use of the energy of a molecule vibration in addition to the Maxwell-Boltzmann distribution expression:

$$\frac{N_i/g_i}{N_f/g_f} = e^{-(\varepsilon_i-\varepsilon_f)/kT} \qquad 3.24$$

which defines the ratio of the relative population of molecules at the discrete energy levels ε_i and ε_f. g_i and g_f are the numbers of allowed quantized levels with these energies. N_i and N_f is the number of molecules with energies ε_i and ε_f. If the population of the states is referred to that of the lowest energy, denoted f=0, equation 3.24 becomes:

$$\frac{N_i/g_i}{N_0/g_0} = e^{-(\varepsilon_i-\varepsilon_0)/kT} = e^{-(\Delta\varepsilon_i)/kT} \qquad 3.25$$

where $\Delta\varepsilon_i=\varepsilon_i-\varepsilon_0$. Thus, if $\Delta\varepsilon_i$ is large compared with kT, the ratio $(N_i/g_i)/(N_0/g_0)$ will be very small. Vibrational transitions from the ground state to the first state is usually observed in the 4000 - 200 cm^{-1} spectral range.

An important selection rule for infrared activity is that a molecule will only absorb radiation if the change in the vibrational energy transitions is associated with a change in the dipole moment of the molecule. In terms of adsorption of probe molecules on dispersed metal surfaces, the "metal surface selection rule" states that only molecular vibrations giving rise to a change in the dipole moment perpendicular to the metal surface are infrared active /143/.

The rotation of a molecule creates a centrifugal force that couples with the vibration resulting in spectral absorption due to the combined rotation-vibration. This is often observed in high resolution spectra as fine detailed structures around the fundamental absorption bands. The frequency conditions of such a combination rotation-vibration can be derived from the basis

of the Born-Oppenheimer approximation and the Schrödinger equation solved for anharmonic oscillators, and have been found to be /141/:

$$\gamma = \frac{\Delta\varepsilon}{h} = \gamma_0 + \frac{2h}{8\pi^2 I}m \qquad 3.26$$

$$\gamma = \gamma_0 + 2Bm \quad \text{and} \quad B = \frac{h}{8\pi^2 I} \qquad 3.27$$

where I = the moment of inertia of the molecule.

B = the rotational constant

m = molecular quantum number that can have values ±1, ±2, ±3 etc.

The value of γ_0 defines the position of the center of the fundamental vibration-rotation band while the second term, 2Bm, determines the rotational fine structure. When m is positive, lines are observed on the high-frequency side of γ_0, when m is negative lines are observed on the low-frequency side of γ_0. These series of lines are known as the P and R branch, respectively, and their absorption maxima are-in the case of gas phase CO-located at approximately 2181 cm^{-1} and 2112 cm^{-1}.

Group frequencies:

As the number of atoms in a molecule increases, the physical interpretation of all the vibrational movements becomes a difficult and complicated task. However, the concept of *group frequencies* implies that it is not necessary to identify every single observable vibration in a complex molecule in order to unambigously determine the molecular structure.
Group frequencies are frequencies characteristic of a group of atoms relatively unaffected by the constitution or structure of the rest of the molecule. Characteristic frequencies occur when /144,145/:

1) the masses of end atoms are small compared to the rest of the molecule

2) there is a considerable difference in either the force constants of two atoms of like mass or in the masses of the internal atoms.

It can be said that chemisorbed CO exhibit two group frequencies, one due to CO bonded to a single metal atom, the second as a result of the bonding to two or more metal atoms. Upon adsorption of CO on a catalyst surface, the rotational fine structures of the bands disappear since the rotational freedom is lost or at least severly restricted. Furthermore, due to the bonding mechanisms, a weakening of the CO bond would be expected. The decrease in the force constant results in a lowering of the carbon monoxide frequency in comparison with gaseous CO (at about 2143 cm^{-1}). In addition, the CO frequency is changed when the surface coverage changes, when other molecules are coadsorbed and when the size of the metal particle varies, etc.
Other examples of important group frequencies are the asymmetric and symmetric stretch of CH_2-and CH_3-groups, and the OH stretching vibration.

Band intensity:

The intensity of an infrared band is proportional to the square of the derivative of the dipole moment with respect to a distance along the normal coordinate, and is quantitatively given by /91/:

$$A = \frac{N}{3C^2} \left(\frac{\delta\mu}{\delta Q}\right)^2 \qquad 3.28$$

where N = is a constant
C = the velocity of light
μ = the dipole moment
Q = normal coordinate associated with the particular vibrational mode.

For the stretching vibration of a diatomic molecule, Q is proportional to $r-r_e$, where r_e is the internuclear equilibrium distance and r the distance of displacement during the stretching vibration.
The intensity can be used as a quantitative measure of the coverage of adsorbed molecules,

or qualitatively either as a measure of either the interaction between the adsorbate and the surface or between adsorbed molecules /143/.

Experimentally, the integrated intensity can be estimated from the expression /91/:

$$A = \frac{1}{c \cdot l} \int \ln\left(\frac{I_0}{I}\right) d\gamma = \frac{a}{c \cdot l} \qquad 3.29$$

where A = integrated absorption intensity (cm/mol)

c = concentration of the absorbing species (mol/cm^3)

l = pathlength through the sample (cm)

$a = \int \ln (I_O/I)\, d\gamma$ = area under the absorption band (cm^{-1})

The integrated absorption intensity represents the integral of the extinction coefficient, ε_γ, for a given frequency, over the frequency range γ_1 to γ_2 of the infrared band caused by a particular species /146/:

$$A = \int_{\gamma_1}^{\gamma_2} \varepsilon_\gamma \, d\gamma \qquad 3.30$$

3.3.2. Optical principles

The theory and principles behind Fourier Transform infrared spectroscopy measurements have been described thoroughly in several excellent books and review articles /147-150/. This, the primary purpose with this chapter is to give a brief introduction to the topic, outlining the most important and fundamental aspects necessary to achieve a basic understanding of the means by which continous polychromatic radiation is resolved into its spectral elements.

The interferometer constitutes by far the most important and central part of any commercial FTIR instrument. Although there are subtle, but significant differences in the construction of the present available interferometers, the principle theory behind all scanning interferometers are basically similar, and can be related back to the early work by Michelson /151,152/, who in 1891 laid the foundation for and designed the first interferometer. Fig. 3.3.2-1 and 3.3.2-2 show the optical layout of the Michelson and the Genzel interferometer, respectively, the latter placed in the FTIR instrument used in the present study.

The incident, polychromatic radiation is split into two components by the beamsplitter, partly reflecting and partly transmitting the beam of radiation to the fixed and movable mirrors, respectively. The scanning mirror is either moved at a constant velocity or step scanned, that is, held at equally spaced points for fixed short periods of time and rapidly stepped between these points. Due to the difference in the optical pathlength, δ (introduced by the movable mirror) between the beams reflected from the fixed and movable mirror, the beams interfere either constructively or destructively after recombination at the beamsplitter. The intensity of the radiation is then detected as a function of the difference in the optical path length between the two components, thus yielding the interferogram, see Fig. 3.3.2-3:

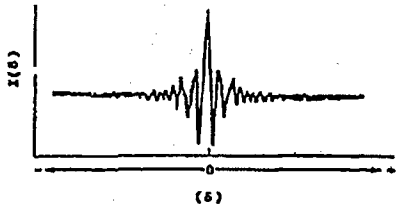

Fig. 3.3.2-3: Interferogram using a polychromatic infrared source /153/.

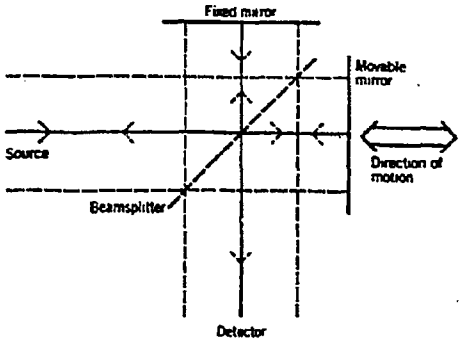

Fig. 3.3.2-1: Schematic drawing of a Michelson interferometer /149/.

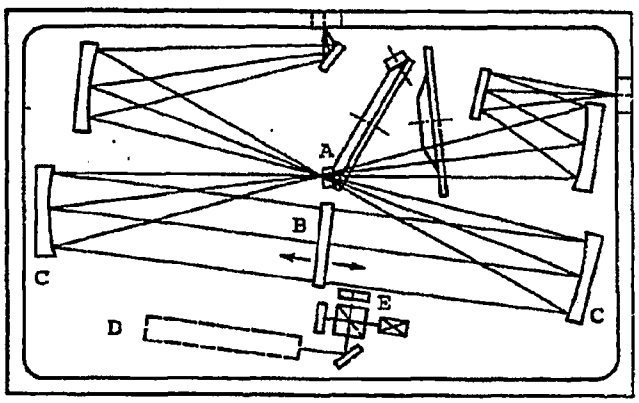

Fig. 3.3.2-2: Optical design of the Genzel interferometer /149/.

A: Beamsplitter (KBr)

B: Movable mirror (double sided)

C: Spherical collimating mirror

D: He-Ne laser

E: Reference interferometer

The real difference between the Michelson and the Genzel interferometers is the size of the beam at the beamsplitter. In the Genzel interferometer the beamsplitter is located at the focal plane, that is, the beam is *focused* at the beamsplitter. The transmitted and reflected beams are then collimated by two spherical mirrors so that the two beams travel collinearly into a *double-sided* mirror. Hence, twice the optical path difference of the Michelson interferometer is generated in the Genzel interferometer for the same physical mirror travel distance. In other words, the same resolution is obtained by only half of the mirror distance. Furthermore, the modulation frequency is twice of what it would be using a standard Michelson interferometer for a given mirror velocity.

If the scanning mirror is moved at a constant velocity, the signal intensity recognized by the detector will vary sinusoidally with time between zero (destructive interference) and maximum (constructive interference).
The quantity measured at the detector is the intensity $I(\sigma)$ of the combined IR beams as a function of the moving mirror displacement σ, the interferogram. The interferogram can mathematically be represented by the integral (using a continuum source)

$$I(\sigma) = \int_0^{\infty} B(\bar{\gamma}) \cos 2\pi \bar{\gamma}\sigma \cdot d\bar{\gamma} \qquad 3.31$$

which is one-half of a cosine Fourier transform pair, the other being the parameter $B(\gamma)$, which gives the intensity of the radiation at a frequency γ cm^{-1} /149/:

$$B(\bar{\gamma}) = \int_{-\infty}^{\infty} I(\sigma) \cos 2\pi \bar{\gamma}\sigma \cdot d\sigma \qquad 3.32$$

These equations define the relationship between the interferogram and the frequency spectrum.

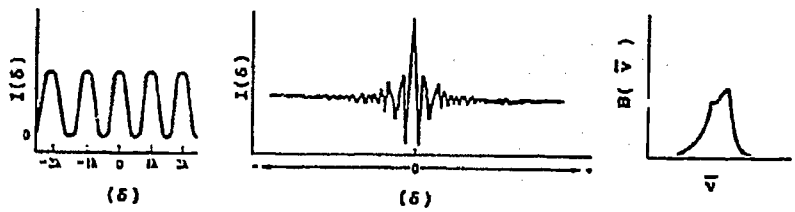

Fig. 3.3.2-4: Interferogram and resulting spectrum /153/.

The advantages of a Fourier Transform infrared spectrometer are best realized by comparison with dispersive grating instruments. In these spectrometers, the recombined beams following passage through sample and reference enters the monochromator through slits, and is dispersed into its spectral elements by a grating /148/. Parts of the intensity is lost due to the use of prisms and gratings. This is to a greater extent avoided in a FTIR instrument (although depending on the size of the chosen aperture, which may cause loss of intensity if selected small) where filtering or dispersion of the beam is not required, thus eliminating the energy wasting slits. This can be examplified by considering a grating spectrometer, operating between 4000 and 1000 cm^{-1} at a resolution of 4 cm^{-1}. The energy reaching the detector will be (4/3000) 0.13%, or the energy proportion lost is 99.87%. Increasing the resolution worsens the situation. The greater throughput (the product of the solid angle and area of the beam from the source) of the interferometric instruments is known as *Jacquinot's advantage*. The effect stems from the use of circular apertures in FTIR instruments which have larger surface areas than the linear slits of the dispersive spectrometers. The spectral signal to noise ratio also benefits from the increased signal reaching the detector.

The principle and fundamental advantage of interferometry, also called *Fellgett's advantage*, is due to the fact that data from all of the wavenumbers (spectral resolution elements) are detected simultaneously during a complete scan. The advantage can be expressed in two ways:

1. With equal signal to noise ratio, spectra will theoretically be recorded X times faster with a Fourier Transform infrared spectrometer than with a dispersive instrument, where X is given by $\gamma_R/\Delta\gamma$, γ_R is the frequency domain of interest and $\Delta\gamma$ the resolution.

2. With equal measurement time, the theoretical signal to noise ratio in the spectra recorded with a FTIR spectrometer will be improved by a factor of $X^{0.5}$ compared with the corresponding measured using conventional IR spectrometers.

The underlying assumption for the quantitative assessment of the Fellgett's advantage is that the optical conditions are identical, that is the source, throughput and detectors should be comparable. In practice, the real benefit of Fellgett's advantage has been found to be smaller

than theoretically predicted, the X dependency has been suggested to be $(X/8)^{0.5}$ instead of $X^{0.5}$ /154/.

Furthermore, the accuracy in the determination of the position of the moving mirror is coupled to the accuracy of each wavenumber. By the use of an auxiliary laser, usually He-Ne lasers, the position of the scanner can be determined to better than 0.005 μm. This, in return, results in near absolute frequency accuracy, better than 0.01 cm^{-1} over the range 4800 - 400 cm^{-1}. This advantage of the Fourier Transform technique is known as *Connes advantage*.

4. EXPERIMENTAL AND PROCEDURES

4.1. PREPARATION OF CATALYSTS

The supported Co-catalysts used in the present study are listed in Table 4.1-1. The cobalt content of the catalysts were determined by the use of atomic absorption spectroscopy (Appendix A1).

Table 4.1-1: List of the investigated cobalt catalysts

Co-CONTENT (weight-%)	*SUPPORT*	*BET AREA OF SUPPORT* (m^2/g)
0.82	SiO_2 (Ventron)	400
4.7	SiO_2 (Ventron)	400
1	γ-Al_2O_3 (Alon C, Degussa)	100
4.6	γ-Al_2O_3 (Akzo Chemie)	186

Apart from the γ-Al_2O_3 from Akzo Chemie, the supports were used as received. The Akzo Chemie alumina support was received as pellets, which were crushed and sieved to fractions less than 400 mesh size. Before impregnation, the supports were dried in air at 400K for 12-24 hours.

The metal precursor was in all cases $Co(NO_3)_2$-$6H_2O$, distilled water was used as solvent. The appropriate amount of support was impregnated with an aqueous solution of the cobalt salt. The amount of the aqueous solution depended on the wettability of the support. The ratio cobalt-nitrate solution/support was approximately 2.1 ml/g and 0.85 ml/g for the silica and alumia supported catalysts, respectively. The resulting suspension was dried overnight in air at 373-393K. Following drying, the catalysts were crushed and sieved to fractions less than 400 mesh. None of the catalysts were subjected to further pretreatment, i.e. calcination. This was mainly due to the fact that previous investigations showed it difficult to achieve pressed disks with acceptable strength and transparency after calcination at elevated temperatures /138/.

4.2. TEMPERATURE PROGRAMMED REDUCTION (TPR)

4.2.1. Apparatus

The reduction behaviour of the silica and alumina supported Co catalysts was studied by the continuous flow technique using an in-house built apparatus /155/. A schematic drawing of the TPR apparatus is shown in Fig. 4.2.1-1.

The H_2/Ar carrier gas is purified by passing it through a Alltech oxytrap and a 5A molsieve in order to remove trace amounts of water and oxygen. The gas stream is then split in two, one path leading to the reference side of the TC detector in the Shimadzu GC-8A gas chromatograph, while the other directs the carrier gas stream through the reactor before reaching the detector. Hydrogen in the effluent stream was analysed on the TCD after the removal of water by a cold trap at dry ice-acetone temperature.

The reactor is made of quartz, consisting of a inner and outer tube, where the inlet gas is preheated by the gas leaving the reactor in the outer quartz tube. The catalyst is placed on a sinter at the bottom of the inner quartz tube. The actual catalyst temperature was monitored by a thermocouple inserted on top of the inner quartz tube, extending down into the sample bed. The reactor was heated by a Kanthal type furnace, regulated by a programmable Eurotherm 818P temperature controller connected to a thermoelement located outside of the sample holder.

4.2.2. Procedure

Approximately 200 mg of the impregnated and dried catalyst (particle size < 400 mesh) was transferred to the reactor, which in turn was connected to the TPR apparatus by feed gas tubes and thermoelements. After pressure testing the reactor, ample time was allowed for the system to stabilize, thus achieving a non-fluctuating and stable baseline. The applied reducing gas was 7% H_2 in Ar at a flow rate of 30 Nml/min. The temperature was ramped at a linear rate of 10K/min. from room temperature to a setpoint of 1223K, which generally resulted in an actual bed temperature 25-35K lower than the set point value. Subsequently, the sample was held at 1223K (set point value) for various periods of time, usually between 10 and 40 minutes.

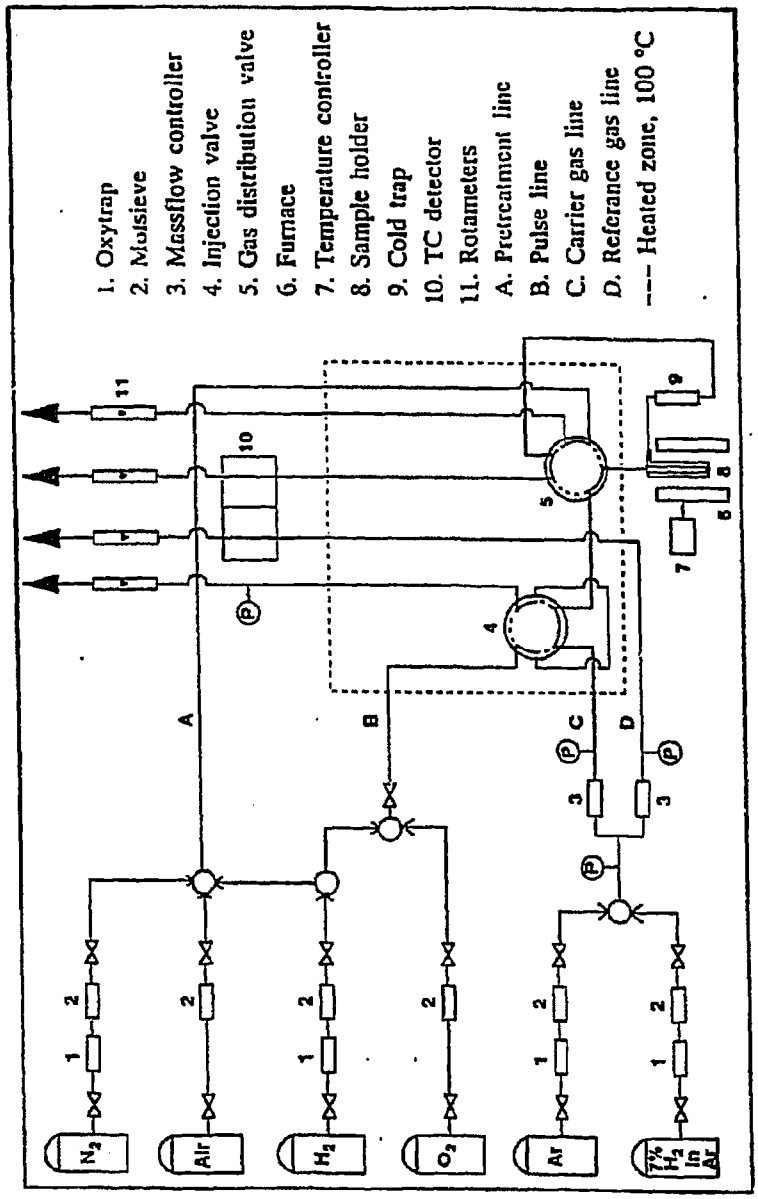

Fig. 4.2.1-1: Schematic view of the apparatus used in the TPR investigations /155/.

Hydrogen consumption during the TPR analysis manifested itself as peaks appearing in the spectrum. In order to obtain a quantitative estimate of the hydrogen consumption, TPR profiles of Ag_2O was recorded under identical conditions. 100% reduction of the calibration sample Ag_2O is assumed to occur.

4.3. FOURIER TRANSFORM INFRARED (FTIR) SPECTROSCOPY

4.3.1. Preparation of pressed disks for IR measurements

Self-supporting wafers, 13 mm. in diameter and weighing 10-25 mg. were prepared by pressing the finely ground, uncalcined catalysts (particle size less than 400 mesh) in an evacuable KBr die and a hydraulic press.

Several methods of loading the catalyst powder into the KBr die were tried with various degrees of success. A further description of the different methods are given in detail in Appendix A2. In short, the generally applied method depended on the type of support, silica or alumina. When the silica supported catalysts were used, the catalyst was distributed randomly on the surface of the optical pellet and the die was knocked two or three times against the table to achieve an even distribution of the catalyst powder. In the case of the alumina supported catalysts, the die plunger was placed on top of the catalyst located in the center of the optical pellet and rotated an appropriate number of times to distribute the catalyst powder over the complete pellet surface. The die was then assembled and transferred to the hydraulic press. Generally, it was found that the alumina-supported catalysts required higher pressure (2000-3000 kg/cm^2) and longer pressing times (5-12 minutes) than silica supported catalysts (60-100 kg/cm^2, ~10 sec.). This was also the case for pure silica and alumina. Descriptions of the various combinations of pressure and pressing times investigated are given elsewhere (Appendix A2). The pressing conditions cited above resulted in wafers with acceptable mechanical strength and transparency. Typically, silica supported Co-catalysts transmitted 4-19% of the incident radiation compared with 4-11% in the case of alumina supported catalysts. The pure silica support gave the highest throughput, 20-70%, while the figures for pure alumina were approximately in the same range as those for the alumina-supported catalysts.

This illustrates the most serious problem encountered in examination of supported catalysts by the transmission method, namely the severe loss of energy because of scattering and absorption by the metal oxide support material. For all catalysts, the signal to noise ratio was lower at the extreme wavenumbers compared to the regions of main interest, probably as a result of the MCT-detector's response characteristics and the energy profile of the applied source. The silica support was opaque to infrared radiation below 1300 cm^{-1}, while alumina in this respect was somewhat better, as it began to lose transparency at about 1100 cm^{-1}.

4.3.2. High-pressure infrared cells

The design of the two infrared cells used in these experiments was similar to that of Hicks et al. /156/ and to the one used in a previous FTIR investigation of iron Fischer-Tropsch catalysts /138/. However, certain minor modifications were implemented in relation to the original design. Fig. 4.3.2-1 shows a picture of one of the applied infrared cells.

The entire cell was made of stainless steel, as was the pellet holders. Sealing between the CaF_2-windows (6.1-6.16 mm. thickness, 25 mm. diameter, Specac, England) and the cell flanges was ensured by the use of Statotherm graphite profile rings (21 mm. o.d., 17 mm .i.d., 2 mm. thickness, Burgmann, Germany) with a reported maximum temperature of 823K. Polycrystalline CaF_2 instead of single crystal CaF_2 was used due to greater thermal shock resistance. The combination of polycrystalline CaF_2-windows and graphite seals resulted in low leakage and enabled the cells to be operated at relatively high temperature and pressure. Slow heating and cooling rates (2K/min.) were applied to avoid cracking of the windows. Nichrome wires (Elektrothermal) were used as heating elements. The wires were wound around the exterior of the cells and covered with heat insulating glass tape (Vidatape C, 50 mm.). Eurotherm 815P temperature controllers (one for each cell) and a thermocouple (type K) placed in close proximity with the catalyst wafer were used to regulate the temperature in the infrared reactors. In addition, a second thermocouple (type K) was used to monitor the temperature between the nichrome heating wires and the cell itself.

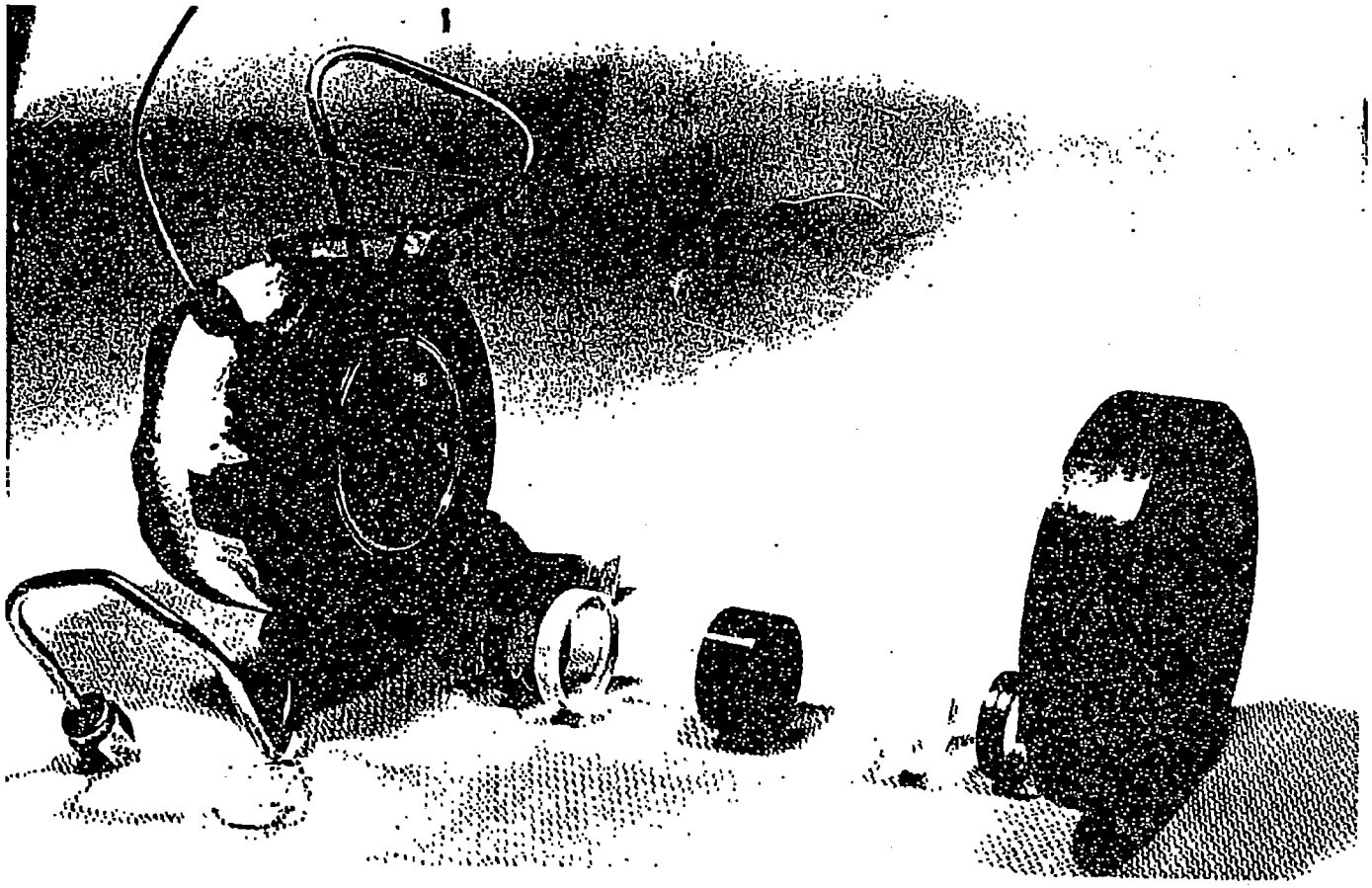

Fig. 4.3.2-1: Picture of the high-pressure high-temperature infrared cell.

4.3.3. Gas flow system

Fig. 4.3.3-1 shows a schematic diagram of the gas handling system associated with the high-pressure high-temperature infrared reactors.
The flow system consisted of four identically built feed gas lines. The separate feed lines are connected to a 5-way ball valve, whose position determines the desired type of reactant gas. Further specifications concerning type, purity and composition of the applied gases are given in Appendix A3.

4.3.4. Data acquisition

Infrared spectral data were recorded using a Bruker IFS 113v FTIR spectrometer. The instrument was equipped with a Genzel interferometer, KBr beamsplitter, Globar lamp and a liquid nitrogen cooled mercury-cadmium-telluride (MCT) detector. The section containing the optics and the sample compartments was maintained under vacuum. Transmission infrared spectra were obtained using the Bruker ATS software package, which provided several options for processing of the recorded infrared spectra, such as baseline correction, peak picking and subtraction of spectra. In the present work, a subtraction factor of 1 was used when subtracting the reference absorbance spectra from the sample absorbance spectra.
The majority of the infrared spectra presented in this work were obtained by coadding 32 to 100 interferograms to improve the signal-to-noise ratio. All spectra were obtained using a resolution of 4 cm^{-1}. Higher resolution was not required since the narrowest band observed was 8 cm^{-1}. None of the spectra are smoothed or enhanced in any other way unless otherwise noted. The spectral parameters applied during data collection and data processing are given in Appendix A4.

4.3.5. FTIR-procedure

The pellet holders with pressed discs of either the supported catalyst or the pure support were placed in their respective cells, which in turn were assembled and leak tested with N_2. After wrapping the cells in heating wires and insulating tapes, the cells were mounted on separate plates, to which electrical wiring and stainless steel tubes for the feed gas supply were

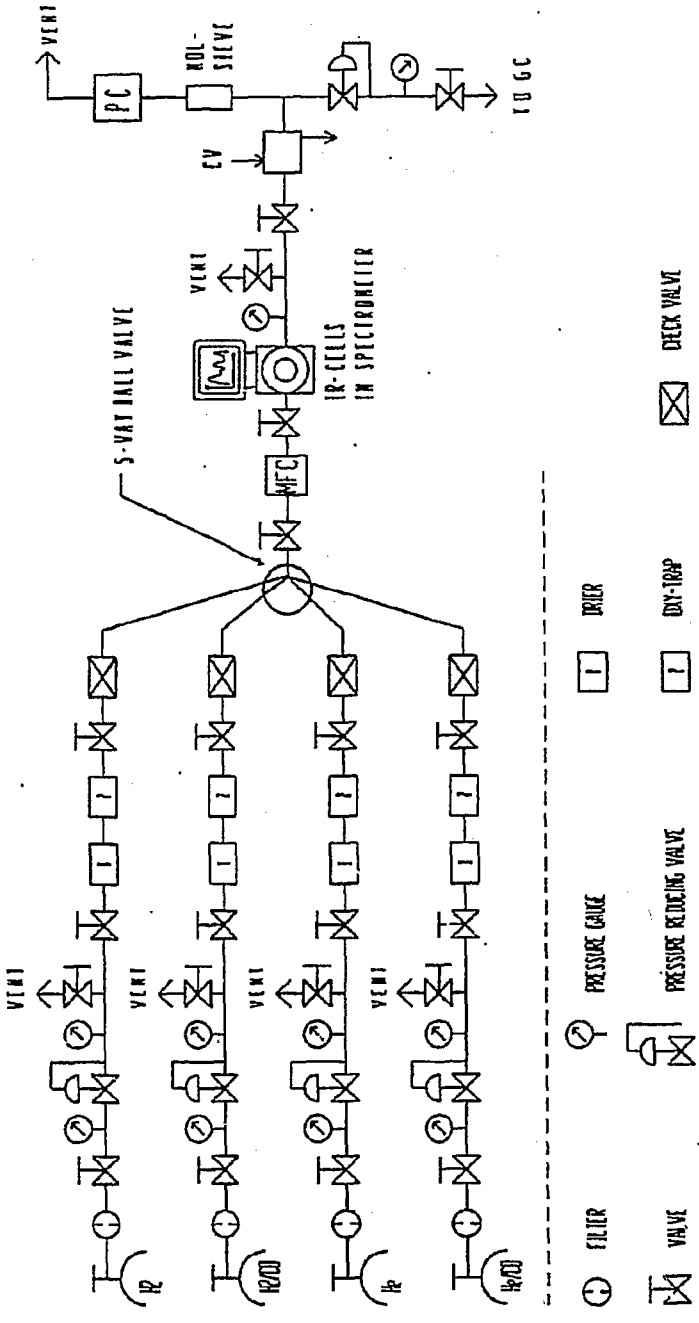

Fig. 4.3.3-1: Experimental apparatus used in the FTIR investigations.

connected. The cell containing a pressed disc of the pure support was placed downstream from the cell containing the supported catalyst disc. Vertical and horizontal alignments of the cells with respect to the focus of the infrared beam were then done in order to achieve optimal energy throughput.

Hydrogen was introduced and the temperature was raised at a rate of 2K/min. to the reduction temperature, 673K. The heating programme included holding for 30 min. at 373K (removal of water) and 523K (decomposition of nitrate). The catalysts were reduced in hydrogen *in situ* (673K, P_{Tot}=2.5-11 bar, 100 Nml H_2/min.) for 16-20 hours. The pretreatment procedure for the pure support was similar to that of the supported catalysts.

Following reduction, the catalysts were either cooled in H_2 to the desired reaction temperature for CO hydrogenation experiments, or to room temperature in He for CO adsorption experiments. When CO hydrogenation was studied, the experiments were carried out at the following reaction conditions: P_{Tot}=2.5-11 bar, T=473-573K and a H_2/CO ratio of 2 or 3. CO adsorption experiments were performed by introducing He:CO (9:1, P_{Tot}=2.5-6 bar) at room temperature followed by He flushing.

Spectra of the catalysts in H_2 or He after reduction, but before introduction of reactant gases at the actual reaction temperature, were used as reference spectra.

At an early stage of the experimental work, back diffusion of oil from the vacuum pump connected to the optics bench deposited on the mirrors located before and after the sample compartments. After installation of a filter (zeolite type) and a liquid nitrogen trap, the problem was considerably reduced and almost non-existing. Nevertheless, actions were taken before and after an experiment was conducted in order to ensure negligible influence of oil on the mirrors. The mirrors were cleaned, and single beam spectra were recorded with an open beam path and with the infrared reactors mounted in the sample compartments before startup of an experiment. Following the reduction procedure, another single beam spectrum was recorded after the temperature was stabilized on the desired reaction temperature and after additional cleaning of the mirrors. After the experiment was completed, yet another single beam spectrum was obtained and compared with the spectrum recorded at the beginning of the experiment.

4.4. CATALYTIC ACTIVITY MEASUREMENTS

4.4.1. Apparatus and analytical equipment

The activity and selectivity measurements were performed in two apparatus; the one described in this section and the microbalance/microreactor apparatus described in Chapter 4.5.

A schematic drawing of the kinetic apparatus is shown in Fig. 4.4.1-1. The reactant gases, hydrogen and premixed CO/N_2 (7.5% N_2) were purified by a Alltech oxytrap and a Linde 5A molecular sieve for water and iron-carbonyl removal. The flowrate of these gases was regulated with Hitech F100/200 mass flow controllers.

The high pressure, fixed bed microreactor was made of stainless steel, 45 cm long with an inner diameter of 1.12 cm. The catalyst was placed on a stainless steel frit located 11 cm from the bottom of the reactor. Heating of the reactor was provided by a Kanthal type furnace. The temperature was measured at two points: a thermocouple was extended downward into the catalyst bed, while the second thermocouple was located 0.5-1 cm below the catalyst bed. The latter thermoelement was used for regulation of the reaction temperature in connection with a programmable West 2050 temperature controller. The difference in temperature between the two measurement points did not exceed 3K.

Feed and product analysis were carried out using an online HP5890 gas chromatograph (GC) equipped with a HP 3393A integrator. N_2 (internal standard), CO, CO_2 and CH_4 were separated by a Carbosieve-SII 1/8" 110/120 (Supelco) column connected to a thermal conductivity detector (TCD). The hydrocarbons were separated by a Megabore 30 m GSQ (J&W Scientific) column connected to a flame ionization detector (FID). The carrier gas was He, purified by Chrompack oxygen and moisture filters. In order to avoid condensation of liquid products, all tubes and valves in the section downstream of the reactor involving FID analysis was heated to 423-473K.

Calculations of the degree of conversion of CO and the selectivity of CO_2 and CH_4 were based on the use of nitrogen as internal standard. Hydrogen and water were not analyzed quantitatively. The total CO conversion was always lower than 5% and usually between 1 and 2%. Low conversion of CO is required to ensure differential bed conditions with minimal effect of mass and heat transfer. Too low conversion of CO, on the other hand, lead to difficulties in obtaining an accurate carbon balance.

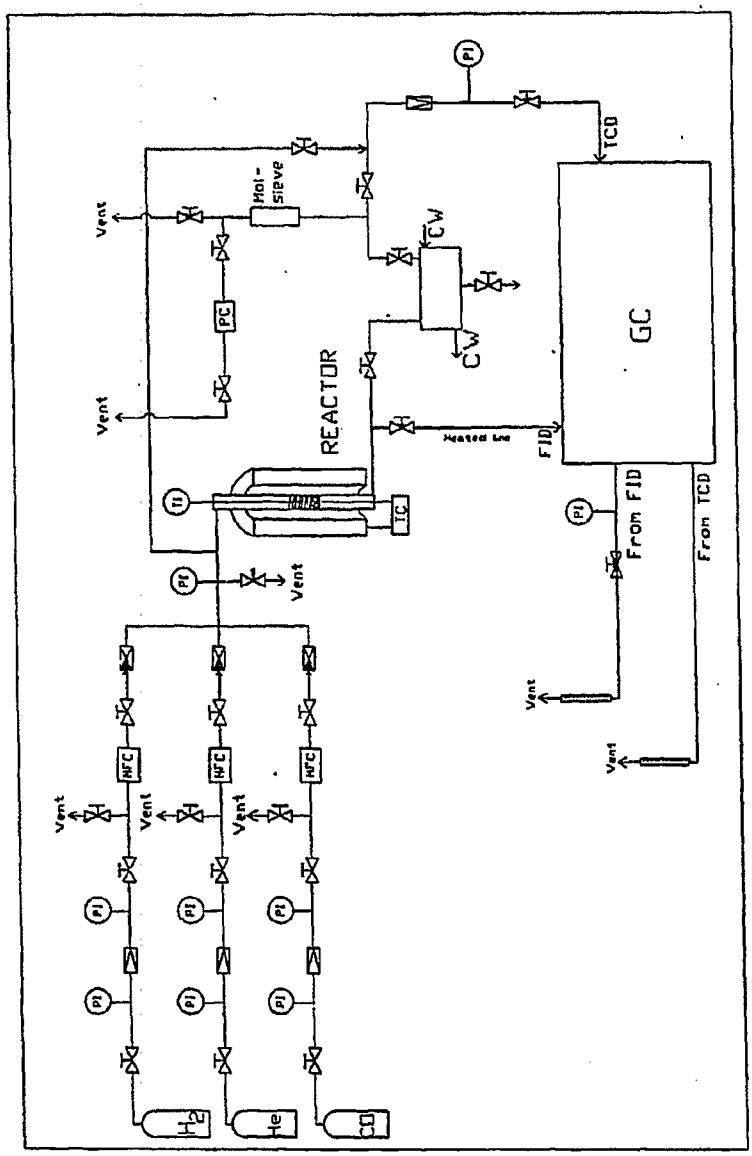

Fig. 4.4.1-1: Schematic view of the gas handling apparatus for the activity measurements /157/.

4.4.2. Procedure

0.7 g of the catalyst, particle size 52-200 mesh, was placed between two layers of glass wool in the reactor. After leak testing by pressurizing with He, the temperature was raised 2K/min. to 673K in flowing hydrogen at a total pressure of 6 bar. The catalyst was reduced at this temperature for 16 hours. Following reduction, the temperature was adjusted to the desired reaction temperature, and hydrogen was then replaced by synthesis gas. He was initially introduced together with synthesis gas in order to reduce the possibility of run-away due to the exothermic nature of the reaction. The flow of inert gas was gradually removed during a time period of 7-25 min. after introduction of H_2/CO. CO hydrogenation was carried out at 6 bar total pressure (H_2/CO=2) and 523K. The only experimental parameter varied from one experiment to another was space velocity, which was in the range 6900-23700 Ncm^3/g catalyst·h.

Feed and product TC analysis were taken at regular intervals; normally every 30 min. with the first analysis after 0.5-1 hour of reaction. The analysis system did not permit analysis with both detectors simultaneously. Therefore, TC product samples for analysis were first taken before obtaining a FID product analysis. Additional TC product samples were then taken followed by the second FID analysis. Analysis of the feed composition (by TCD) was obtained at the end of each experiment. Appendix A5 shows examples of TCD and FID chromatograms obtained during an experiment in the above described apparatus.

4.5. GRAVIMETRIC STUDIES

4.5.1. Gas handling system and analytical equipment

The gravimetric investigations were performed in the apparatus illustrated in Fig. 4.5.1-1 /138/. The basic features of the experimental setup consists of a gas handling system, the reactor and the analysis system. The reactor, shown in Fig. 4.5.1-2, is an integrated microbalance/ microreactor made of stainless steel with an outer diameter (O.D.) of 0.5 inches connected to the 3/8 inches O.D. tubing of the microbalance via two flanges bolted together and sealed with a gold ring. The microbalance is a Sartorius model 4436 with 0.1 μg sensitivity. If desirable, the system could be converted to a pure microreactor by

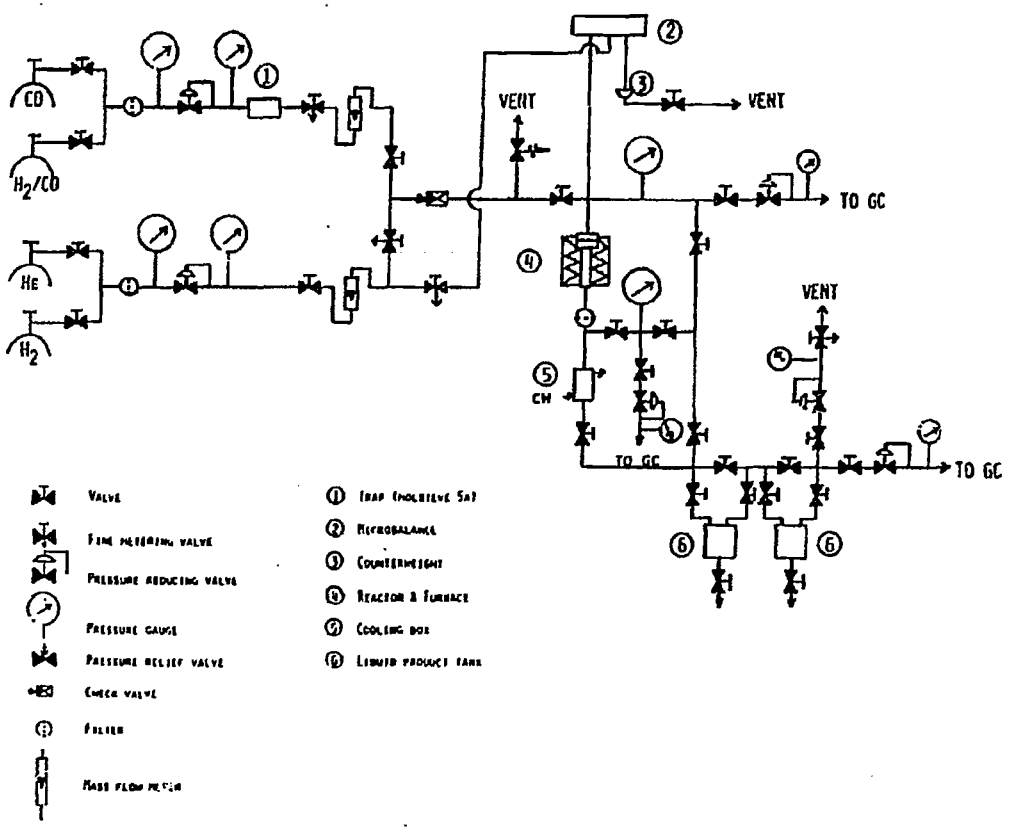

Fig. 4.5.1-1: Schematic diagram of the gas handling system for the microbalance studies /138/.

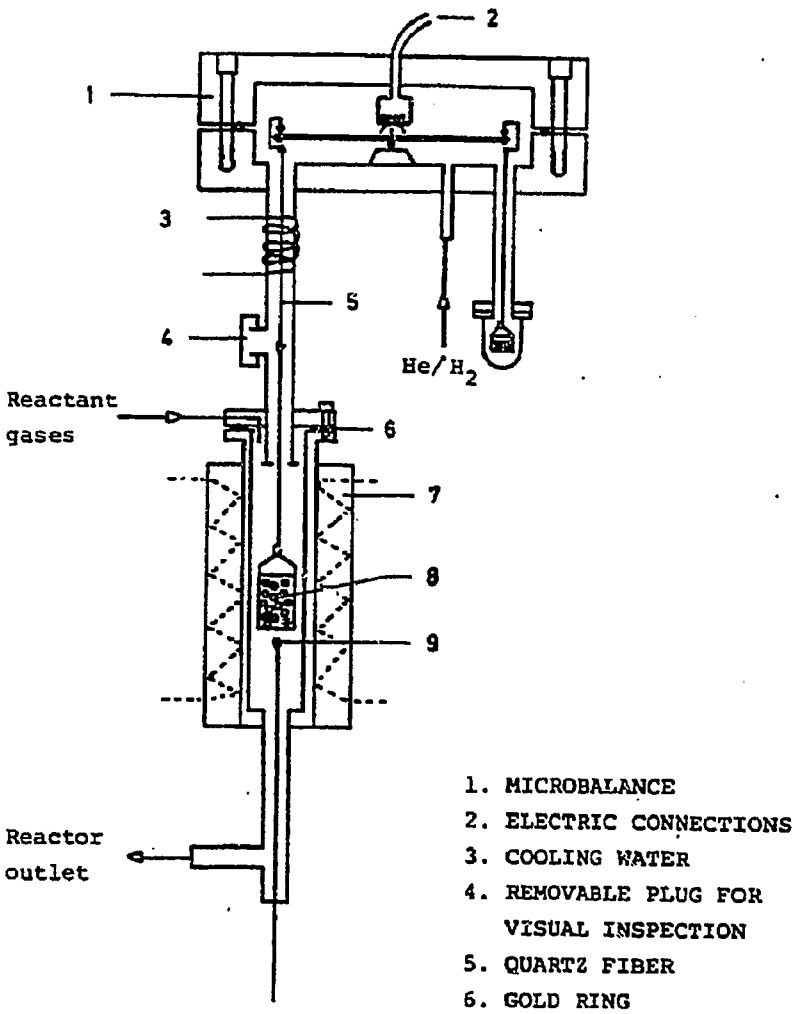

Fig. 4.5.1-2: Combined high-pressure microbalance/microreactor for gravimetric experiments /138/.

disconnecting the reactor from the microbalance, changing the top flange of the reactor and installing a stainless steel frit as support for the catalysts. Heating of the reactor was provided by an electrical furnace. The temperature was regulated by an Eurotherm temperature programmer/controller with a thermocouple located in close proximity of the catalyst basket. Analysis of gas samples from the feed and product streams were carried out by the use of a PYE Unicam 204 GC equipped with a thermal conductivity- and flame ionization detectors. CO, N_2, CH_4 and CO_2 were analyzed on an Alltech CTR-I packed column, while the hydrocarbon fractions were separated on a Supelco SP2100+0.1% Carbowax packed column.

4.5.2. Procedure

The stainless steel basket containing approximately 0.7 g catalyst (18-26 mesh) was hooked onto the quartz fiber connected to the microbalance. Fresh catalysts were used for each of the experiments in order to avoid the influence of historical effects. After leak testing the system with helium, the temperature was raised to 673K in flowing He and the catalyst was dried overnight at this temperature. The microbalance head was always purged with He in order to prevent condensation of reaction products and to maintain a constant gas density around the taring counter weight. If the weight curve after drying overnight tended to fluctuate, the temperature was increased to 723K for 3-5 hours in order to achieve a more stable weight curve. Next, the temperature was lowered to 473K, hydrogen was introduced and the temperature was increased 2K/min. to the reduction temperature, 673K. The catalysts were reduced in flowing hydrogen (P_{Tot}=6 bar, 200 Nml/min.) for 16-20 hours.

After reduction, the catalyst was cooled in hydrogen to the desired reaction temperature and the feed was switched to synthesis gas. The gravimetric studies were carried out in the temperature range 473-723K. at a total pressure of 6 bar with a H_2 to CO ratio of 2. The space velocity of the synthesis gas was in most cases kept constant within an experiment. This was mainly due to the fact that the flow of gas past the catalyst basket will exert a drag force, thus influencing on the weight curve. CO hydrogenation was usually continued for 3-5 hours with regular sampling and GC analysis of the product and feed streams. The analogue signal from the microbalance was transformed to a Toshiba T1000 portable computer running a BASIC data acquisition programme /158/. The sampling frequency was preset to every 15 second. Synthesis gas was either replaced by helium and then hydrogen or directly by

hydrogen at reaction conditions in order to study the reactivity of the deposited material. After 3-4 hours of exposure to hydrogen, the temperature was increased at a rate of 5K/min. to 673 or 723K for a further investigation of the nature and reactivity of the deposited material.

5. RESULTS AND DISCUSSION

5.1. TEMPERATURE PROGRAMMED REDUCTION OF SILICA AND ALUMINA SUPPORTED COBALT CATALYSTS

5.1.1. TPR-investigations of 0.82% Co/SiO_2 and 4.7% Co/SiO_2

The TPR-profiles of uncalcined Co/SiO_2 catalysts with different metal loadings are shown in Fig. 5.1.1-1, in which the TPR-spectrum of pure SiO_2 is also included. While no reduction peaks were observed in the temperature range from room temperature to 1223K for silica alone, low temperature peaks at 510K and 535K in addition to a broad high temperature peak around 1104K could be seen in the spectrum of 0.82% Co/SiO_2. Furthermore, a weakly resolved peak appears near 648K.

TPR-analysis of the 4.7% Co/SiO_2 catalyst revealed a significantly more complex reduction behaviour. Peaks were observed at 517, 564, 1050 and 1160K, with the 517K peak being clearly the most intense. A broad peak extending over the temperature range 590-873K is also discernible, showing evidence of having two relatively poorly resolved maxima at 687 and 757K. The high temperature tailing and the lack of any return to the baseline of this peak indicate difficulties in achieving complete reduction of the responsible cobalt species. The reduction process is not completed until a temperature of almost 1223K is attained.

The estimated total degree of reduction based on the hydrogen consumption of the peaks in the TPR-spectra of the silica supported catalysts is given in Table 5.1.1-1. Hydrogen consumption required for the reductive decomposition of the metal precursor is not included in the table. The overall extent of reduction increases with increasing cobalt content, in accordance with the findings of Bartholomew et al. /6,121/.

According to the literature, the distinct peaks at 510K and 517K correspond to the reductive decomposition of residual cobalt nitrate without the reduction of cobalt /50-52,157/. The increase in peak area (hydrogen consumption) with increasing cobalt loading is consistent with such an assignment. The much less intense peaks centered around 564K and 535K are

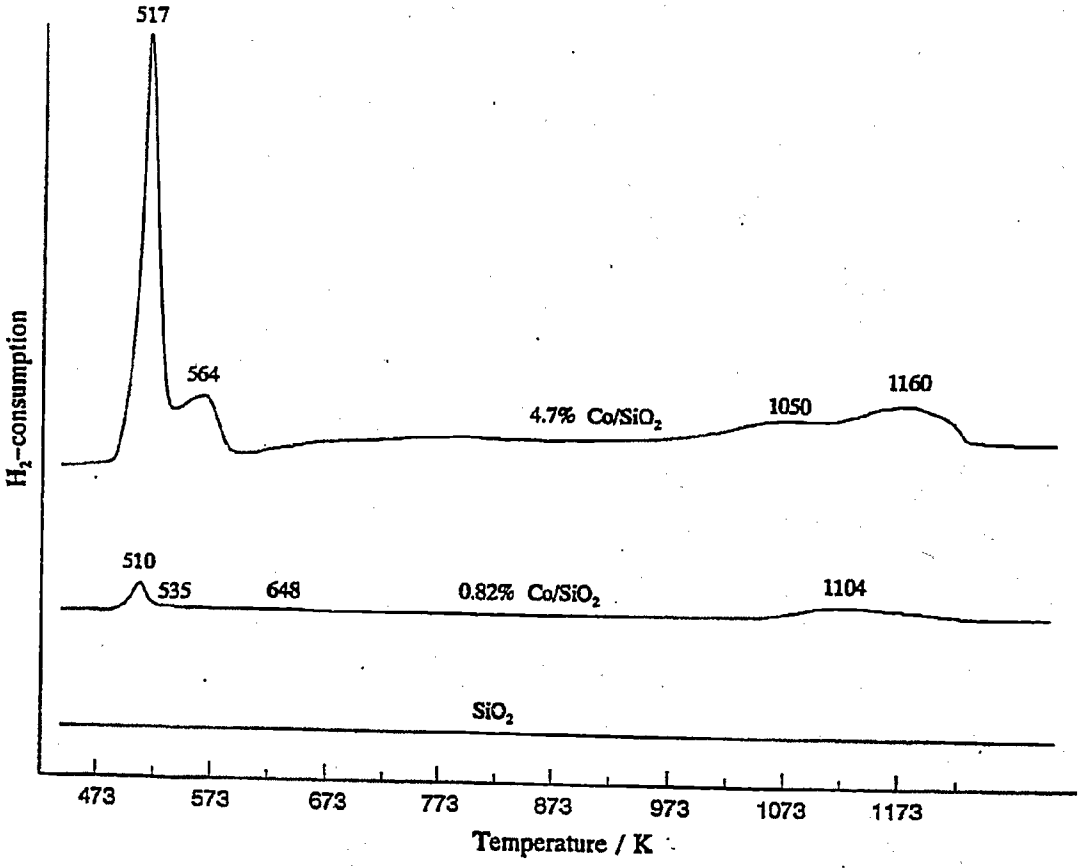

Fig. 5.1.1-1: **TPR-profiles of SiO_2, 0.82% Co/SiO_2 and 4.7% Co/SiO_2.**

Heating rate: 10 K/min.

Temperature interval:		
	SiO_2	**293-1223K**
	0.82% Co/SiO_2	**292-1223K**
	4.7% Co/SiO_2	**293-1223K**

Table 5.1.1-1: Estimated degree of reduction of 0.82% Co/SiO_2 and 4.7% Co/SiO_2.

	Extent of reduction (%)[1]							
Catalyst	535K	564K	687K	757K	1050K	1104K	1160K	Total
0.82% Co/SiO_2	12.9[2]					45.6		58.5
4.7% Co/SiO_2		15.3	9.2	14.4	24.8		27.4	91.1

[1]: Hydrogen consumption, expressed as degree of reduction, assuming all Co as Co_3O_4.
[2]: Peak area measured by cut and weigh.

probably due to reduction of crystalline cobalt oxide formed during the course of decomposition of the metal precursor, cobalt nitrate. The cobalt oxide reduced in this step is suggested to be Co_3O_4. Based on the present results, there is, however, an uncertainty in the determination of the type of the cobalt oxide formed during the decomposition step, that is, whether it is Co_3O_4 or CoO. Evidence for the formation of both types has been presented in the literature /51,52,58/. Generally, however, on catalysts with relatively high cobalt content, the major oxidic phase is believed to be Co_3O_4 /52,53,58,59/. This is also supported by the UV-VIS diffuse reflectance measurements in section 5.2.4.1, which showed absorption bands attributable to Co_3O_4.

Two explanations can be offered to elucidate the appearance of the reduction peaks at higher temperatures. One may suggest that the peaks at 535K and 564K represent the reduction of Co_3O_4 to cobalt metal (Co^0), and that the peaks in the temperature range 590K to 1160K are due to reduction of more resistant Co species, possibly formed upon interaction between cobalt and the support. Alternatively, the peaks at 535K and 564K can be due to the reduction of Co^{3+} to Co^{2+}, while the later steps represent reduction of Co^{2+} to the zero-valent state, or perhaps to Co^{2+} combining with the silica support.

TPR-spectra featuring one single peak for the reduction of unsupported Co_3O_4 have been reported /50-52,56-60,157/. The assignment of the 535/564K peaks to reduction of Co_3O_4 to

cobalt metal can be suggested, based on the correlation of these peak positions with those reported for Co_3O_4. The location of the reduction peaks in the present study is somewhat at the lower end of the temperature range often reported for Co_3O_4 reduction. 590-673K /51,52,58/, but this is probably a consequence of the different pretreatment and TPR conditions employed. Following this line of argumentation, it would seem that cobalt species on the SiO_2 is present as relatively large, bulk-like particles, reduced to the zero-valent state below approximately 600K.

Whether one single or two peaks appear in the TPR-spectrum of Co_3O_4, it is believed that the reduction of Co_3O_4 occurs in two stages, $Co_3O_4 \rightarrow CoO \rightarrow Co$ (see section 2.3.3). Thus, the 535/564K peaks can alternatively be interpreted as due to the reduction of Co^{3+} to Co^{2+}. The peaks appearing in the temperature range 550-773K (0.82% Co/SiO_2) and 590-873K (4.7% Co/SiO_2) can then be proposed to be caused by the consecutive reduction of CoO to cobalt metal. The observation of a two stage reduction ($Co^{3+} \rightarrow Co^{2+} \rightarrow Co^0$) can possibly be a consequence of support interactions, making the cobalt oxide harder to reduce. The reduction of Co_3O_4 on silica supported Co catalysts (calcined at 573K for 5 hours) have been reported to occur in two separate steps at 589K and 633K (β=24 K/min.), in contrast to the TPR-profile of the unsupported (bulk) Co_3O_4 /50/. Roe et al. /159/ observed a two stage Co_3O_4 reduction with peaks at approximately 623 and 690K (β=12 K/min.). Paryjczak et al. /64/ reported TPR-spectra of unsupported Co_3O_4, 1% and 10% Co_3O_4 supported on silica. The presence of the support decreased the reducibility of the cobalt oxide and a shift of 30-50K to higher temperatures was observed. It was also suggested that the peak occuring at 643K (1% Co_3O_4/SiO_2) could be ascribed to the reduction step $Co_3O_4 \rightarrow CoO$ /64/.

It is not believed, however, that the reduction peaks located at 535/564K and in the temperature range 550-773K (0.82% Co/SiO_2) and 590-873K (4.7% Co/SiO_2) correspond to such a successive reduction process of cobalt. This is mainly due to the relatively large peak separation and that the hydrogen consumption of these two peaks is not in accordance with the stoichiometry of the reaction (the area of the peak(s) in the 550-773K and 590-873K region should be three times larger than those at 535/564K).

Support interactions may be responsible for the reduction peaks appearing at higher temperatures (> 550/590K). Based on the view that the reduction of Co_3O_4 can be represented by the peak at 564K (and 535K), an explanation can be proposed which leads to the assignment of different high temperature peaks to different Co phases. It must be expected that Co^{2+} and Co^{3+} species are present on the surface. This is supported by the results of Rosynek et al. /51/, where XPS investigations of a reduced and uncalcined 6% Co/SiO_2 catalyst showed the presence of Co^{2+}. The XPS spectra of the uncalcined and reduced 6% Co/SiO_2 catalyst were indistinguishable from spectra of the uncalcined catalyst obtained before hydrogen treatment (at 673K for 16 hours). Okamoto et.al. /60/ stated that the dominant Co phase on impregnated and dried catalysts was Co^{2+}, as deduced from the Co $2p_{3/2}$ peak at 782 eV accompanied by a shake up satellite (3*d*-4*s*) at 787 eV /51,59/. The possibility of an interaction of divalent and/or trivalent Co species with the silica support must be considered, which may explain the appearance of multiple reduction peaks in the high temperature range. The most likely candidates being a result of such interactions are proposed to be (sub)surface compounds, possibly mixed oxides of the type Co-Si-O and/or cobalt silicates.

By regarding the broad peak in the temperature range 590K to 873K on 4.7% Co/SiO_2 as consisting of two individually peaks appearing at 687K and 757K, the reduction peaks at 648/687K can tentatively be assigned to Co^{3+} species, either existing as well dispersed (sub)surface particles or occupying octahedral sites in the mixed oxide $Si^{4+}_{x/2}Co^{2+}_{1-x}Co^{3+}_2O_4$. A mixed oxide consisting of Co^{3+}, that is, where Co^{2+} has been replaced by Si^{4+}, could be represented by the formula Co_4SiO_8 /60/.

Co^{2+} species, but in different surroundings can be suggested to be responsible for both the 757K peak and the high temperature peaks located above 1000K. Surface Co^{2+} cations and/or Co^{2+} in a mixed oxide like xCoO(-ySiO_2), may possibly be responsible for the former reduction peak, while the latter is suggested to arise from surface cobalt silicate, i.e. Co_2SiO_4 or $CoSiO_3$. Whether the two peaks (1050 and 1160K) indicates Co^{2+} in different lattice positions, i.e. tetrahedral or octahedral coordination, is not clear. Whether there is a splitting of the 1104K peak into two individual peaks (1050K and 1160K) at the higher metal loading, or an absence of the 1050K peak and a shift to lower temperatures (1104K) for the high temperature peak (1160K) occuring on the 0.82% Co/SiO_2 catalyst, is harder to judge. One

could tentatively speculate if the peak at 1104K (0.82% Co/SiO_2) represents reduction of Co^{2+} coordinated in tetrahedral positions in the surface cobalt silicate.

The high temperature peak(s) must be related to strong interactions between cobalt and the silica support due to their positions, which implies hard-to-reduce species.

The underlying assumption for the formation of the spinel structure is the solid state diffusion of Co-ions into the silica lattice. One can argue that at the applied temperatures the rate of such a reaction would be low. The solid state reaction between CoO and SiO_2 requires a reaction temperature of about 1173K /160/. However, it can be questioned whether the calcination step is a necessary prerequisite for the silicate (and for that matter, aluminate) formation. It is possible that this might occur during the reduction or even at earlier stages, for example during the impregnating step. Roe et al. /159/ showed that reduction (at 673K for 2 hr.) of impregnated and calcined 8.08% Co/SiO_2 followed by TPR-analysis revealed the presence of Co_2SiO_4, as a result of metal support interactions. On the other hand, Puskas et al. /161/ found no evidence for cobalt silicate formation in high metal loading catalysts prepared by the incipient wetness technique. The formation of cobalt silicates is often reported in studies where catalysts have been prepared by the pH-controlled precipitation technique (pH 8.0-8.4). Rosynek et al. /51/ stated that the appearance of reduction peaks (at 673, 703 and 1053K) was due to the formation of surface CoO_x and silicate compounds formed during and after the nitrate decomposition step.
In the case of alumina supported catalysts, direct TPR-analysis of impregnated and dried catalysts revealed the presence of cobalt aluminate, $CoAl_2O_4$ /65/.

An alternative explanation for the observation of high reduction temperature peaks can possibly be related to water, i.e. formed during reduction of the cobalt oxide. Migration of SiO_2 particles in a reducing atmosphere in the presence of water vapour may occur, resulting in an encapsulation of parts of the cobalt oxide and thus increasing its resistance towards reduction. Viswanathan et al. /61/ have indeed proposed such an explanation to account for the decrease in the extent of reduction of their kieselguhr supported Co catalysts. Lund et al. /162/ reported silica migration in the presence of water above 523K for several silica containing materials.

A second possible effect of water (vapour) may be that H_2O inhibits the reduction process, as suggested by Castner et al. /163/. It was proposed that peaks observed at high temperature were not necessarily due to the reduction of cobalt silicate, but could rather be related to the presence of small catalyst pores causing accumulation of water, being difficult to remove.

With increasing metal loading, the peaks assigned to the reduction of Co_3O_4 are shifted towards higher temperature, and the relative proportions of the peaks increase. Also, one should expect increasing dispersion with decreasing metal loading. Thus, the increase in the Co_3O_4 peak temperature can be due to different particle sizes of Co_3O_4 on the 0.82% and 4.7% Co/SiO_2 catalysts. Okamoto et al. /60/ reported a linear increase in the reduction temperature with increasing particle size, suggesting a limited diffusion rate of oxygen anions through the oxide particles during reduction. On the other hand, small particles are more susceptible to particle-support interactions, increasing their resistance towards reduction. Judging from the TPR-profiles in Fig. 5.1.1-1, the latter effect seems to be of minor importance.

5.1.2. TPR-investigations of 1% Co/γ-Al_2O_3 and 4.6% Co/γ-Al_2O_3

TPR-profiles of the alumina supported catalysts with different cobalt loading indicate that the reduction pattern of these catalysts are similar, though certain shifts in the positions of the individual peaks were found, as seen in Fig. 5.1.2-1.

TPR-analysis of the support γ-Al_2O_3 showed only a single reduction peak located at 1149K.

With 1% Co/γ-Al_2O_3, hydrogen consumption peaks were observed at 504 and 567K in addition to a high temperature peak located at 1127K. The two peaks appearing at low temperature (504 and 567K) exhibited comparable intensities.

The TPR-spectrum of the 4.6% Co/γ-Al_2O_3 catalyst revealed the existence of several peaks with varying intensities at 571, 573-643, 984 and 1173K. The intensity of the peaks above 1100K apparently increased with increasing metal loading.

The position and peak area of the major peak at 571K suggests that it is due to the decomposition of cobalt nitrate, as previously discussed and reported /50-52/. The observed increase in peak area (hydrogen consumption) with increasing cobalt content is in accordance with such an assignment.

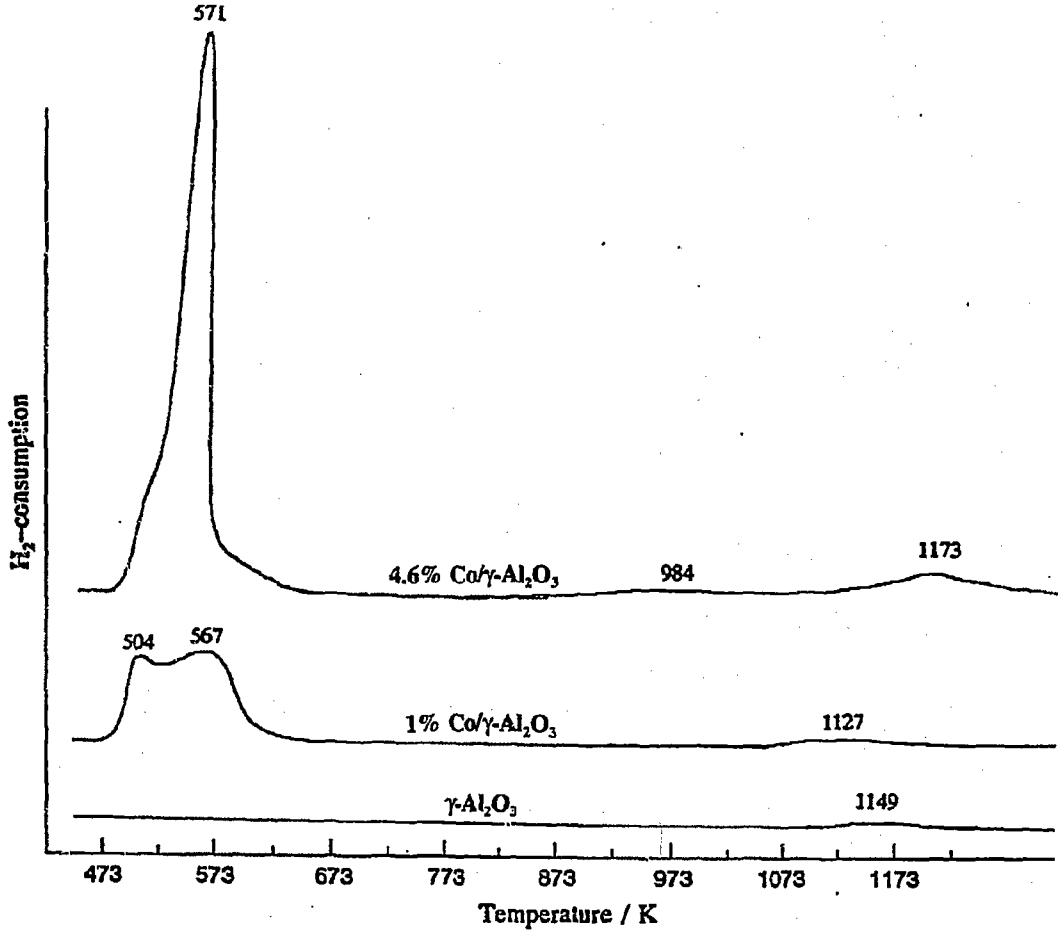

Fig. 5.1.2-1: TPR-profiles of γ-Al_2O_3, 1% Co/γ-Al_2O_3 and 4.6% Co/γ-Al_2O_3.

Heating rate: 10 K/min.

Temperature interval:		
	γ-Al_2O_3	**293-1223K**
	1% Co/γ-Al_2O_3	**294-1203K**
	4.6% Co/γ-Al_2O_3	**298-1203K**

By analogy with the earlier assignments, the weak high temperature shoulder on the nitrate peak in the range 573K to 643K on the 4.6% Co/γ-Al_2O_3 catalyst can be attributed to the reduction of cobalt oxide, Co_3O_4. No such shoulder was discernible on the nitrate peak at 567K in the case of the 1% Co/γ-Al_2O_3 catalyst, indicating the absence of any resolved reduction peak for cobalt oxide. This may seem reasonable if it is assumed that all available cobalt at an early stage of preparation, viz. during impregnation, has penetrated into the alumina lattice, and as a consequence, relatively high temperatures are necessary to achieve reduction of these species.
One may also speculate if the absence of any Co_3O_4 reduction peak is due to the fact that the decomposition and reduction stages perhaps occur almost simultaneously, and that these processes are enveloped in the 567K peak.

A weak, broad peak around 673-723K appears in the TPR-spectrum of 4.6% Co/γ-Al_2O_3. This peak is tentatively assigned to the reduction of either surface Co^{3+} or Co^{3+} in a mixed oxide overlayer phase like Co^{3+}-Al^{3+} /52,57,59/. The inherent weakness of the peak may indicate that the majority of the Co^{3+} is reduced in the temperature range 573-643K. Furthermore, it can be speculated whether the oxidation of Co^{2+} to Co^{3+} in the presence of nitrate anions occurs only to a limited extent, since the hydrogen consumption (expressed as the degree of reduction) is higher at higher temperatures (see Table 5.1.2-1).

For this catalyst, appreciable hydrogen consumption could also be registered around 984K. Similar peaks in this temperature range were not detected during analysis of 1% Co/γ-Al_2O_3 or the blank γ-Al_2O_3. Reduction peaks appearing in the vicinity of these temperatures have often been assigned to surface overlayer Co^{2+} species /52,58/, exhibiting high stability towards hydrogen reduction.
Strong interaction between the cobalt oxide and the alumina support has usually been described to result in the formation of a surface cobalt aluminate spinel phase.
Okamoto et al. /59/ assigned reduction peaks above 920K to subsurface and/or bulk Co^{2+} in an Al_2O_3 matrix.

Table 5.1.2-1 shows the calculated degree of reduction of the alumina supported catalysts with different metal loading. Hydrogen consumed in the reductive decomposition of cobalt nitrate

Table 5.1.2-1: **Estimated degree of reduction of 1% Co/γ-Al_2O_3 and 4.6% Co/γ-Al_2O_3.**

	Extent of reduction (%)				
Catalyst	573-643K	984K	1127K	1173K	Total
1.0% Co/γ-Al_2O_3			17.2		17.2
4.6% Co/γ-Al_2O_3	10.8[2]	6.7		24.6	42.1

[2]: Key as for Table 5.1.1-1.

is not included in the table.

Comparison of Table 5.1.1-1 and Table 5.1.2-1 suggest that the total extent of reduction increases with increasing metal loading, regardless of the applied support. The silica supported cobalt catalysts exhibit a higher total degree of reduction than their alumina supported counterparts.

The lower degree of reduction of the alumina supported cobalt catalysts may be attributed to interactions between the cobalt oxide and the alumina support. Co^{2+} can be incorporated in the defective alumina spinel structure, occupying tetrahedral and/or octahedral interstices. Generally, Co^{2+} in tetrahedral positions have been found more difficult to reduce than the octahedric Co^{2+} /50,53/. It is therefore believed that the high temperature peaks (1127K:1% Co/γ-Al_2O_3 and 1173K:4.6% Co/γ-Al_2O_3) can be represented by the reduction of Co^{2+} surrounded by several Al-O ligands, forming a surface cobalt aluminate spinel structure, with chemical and spectroscopic properties closely resembling those of bulk cobalt aluminate /53/. The TPR-spectra show that the surface Co^{2+} spinel phase is difficult to reduce, reflecting the stability of Co^{2+} in tetrahedral positions in the alumina lattice.

At low metal concentrations, cobalt ions would be located in tetrahedral lattice sites on the support, with XPS binding energies close to that of $CoAl_2O_4$ /53/. When all tetrahedral sites are filled, unoccupied octahedrally coordinated sites are progessively populated, as a result of the increased Co content. Eventually, one would expect the segregation of a bulk-like

cobalt oxide phase /53/ and a higher percentage of reducible cobalt with higher metal loadings, in accordance with the present results. Within the confines of the limited experimental data it is not possible to determine if there is a finite and eventually upper limited amount of Co species dispersed into the alumina lattice. The present results suggest that at least 1% Co is coordinated with the γ-Al_2O_3 matrix. It has been proposed that metal loadings less than 2% favours the formation of surface spinel structures /53,56,141,164/. Van't Blik et al. /65/ found that 1.55% Co was converted to $CoAl_2O_4$ upon reduction of an impregnated and dried 4.44% Co/γ-Al_2O_3 catalyst.

The TPR-spectrum of the support material, γ-Al_2O_3, consists of a single peak at 1149K. Peaks in a similar temperature range were also observed on both the 1% Co/γ-Al_2O_3 and 4.6% Co/γ-Al_2O_3 catalysts, as previously mentioned. The presence of the peak in the support spectrum implies that these peaks can not be solely due to cobalt-alumina interactions.
At this temperature level, phase transitions between different types of alumina occur, viz. γ-Al_2O_3 is converted to δ-Al_2O_3 around 1173-1273K. Further heating to > 1373K results in the transformation to α-Al_2O_3 /165/. Both of these alumina compounds could in principle be responsible for the observed high temperature peak, but the conversion of γ-Al_2O_3 to δ-Al_2O_3 seems most likely, based on the temperature of the phase transition. Hydrogen consumption is registered in the temperature range where the alumina phase transition is believed to occur. Whether this can be related to the reduction of Al^{3+} to aluminium (Al^0), is presently not known. δ-Al_2O_3 contains lower amounts of hydroxyl groups /165/, and the high temperature peaks may possibly be related to the hydrogen assisted removal of hydroxyl groups as water in connection with the phase transition.
Arnoldy et al. /52/ attributed a peak near 1120K to the reduction of impurities in their γ-Al_2O_3, i.e. iron, sulfite and sulfate.

The TPR-spectrum of 1% Co/γ-Al_2O_3 showed the appearance of two distinct peaks at 504K and 567K, while no hydrogen consumption was registered in the temperature range 600-1000K, supporting the previous suggestion that the available metal ions are stabilized by chemical interactions with the γ-Al_2O_3 lattice. In accordance with the previous interpretations, the 567K peak is attributed to the hydrogen assisted decomposition of the metal precursor, cobalt nitrate. The low temperature shoulders on the peaks (571 and 567K) designated to

decomposition of cobalt nitrate appeared at similar temperatures in the TPR-spectra of the 1% and 4.6% Co/γ-Al_2O_3 catalyst.

The assignment of these low temperature shoulders is an intriguing question, to which no satisfactory answer can be offered. The 504K peak was not resolved in the TPR-profile of the 1% Co/γ-Al_2O_3 when a different heating rate (2K/min.) was used; a relatively broad peak could be observed with maximum rate of reduction at 517K. A TPR run (β=2K/min.) with the 4.6% Co/γ-Al_2O_3 catalyst showed no indications of a low temperature shoulder. These peaks were not observed with silica alone or with 4.7% Co/SiO_2.

TPR-spectrum (β=10K/min.) recorded with an empty reactor showed no reduction peaks between room temperature and 1223K.

Its absence in the spectrum of the support material γ-Al_2O_3 means that it must be related to the metal precursor. Its location argues against any reduction of the cobalt oxides. Unsupported cobalt nitrate has been reported to be reduced in two steps, with peaks occuring at 503 and 592K (β=24K/min.) /50/, and at 553 and 643K (β=20K/min.) /51/. The first of these peaks is usually attributed to the reductive decomposition of cobalt nitrate, the second to reduction of cobalt oxide formed during the previous step.

The bands are observed only with the alumina supported cobalt catalysts, and one may speculate if they can be related to the reductive decomposition of the metal precursor, by which the nature of the support affects the progress of the reduction/decomposition process. In this context, reduction of NO_x-groups in the cobalt nitrate can be suggested, but the reaction (cobalt nitrate to cobalt nitrite):

$$Co(NO_3)_2 + 2H_2 \rightarrow Co(NO_2)_2 + 2H_2O \qquad 5.1$$

can only be regarded as speculative. In the study of Lapidus et al. /50/, the strong exothermic nature of the cobalt nitrate reduction was believed to lead to an overheating of 4.6% Co/γ-Al_2O_3, which could cause interactions between cobalt oxide and the support.

Another explanation for the low temperature peaks on the alumina supported cobalt catalysts could be dehydration, i.e. loss of water or crystal water from the cobalt nitrate. Water, either physically held on the alumina or chemical bound to the hydrated nitrate will be driven off at increasing temperatures, but an explanation which accounts for hydrogen consumption during these processes can not be given.

5.2. FOURIER TRANSFORM INFRARED (FTIR) INVESTIGATIONS

5.2.1. Introduction

The catalysts used in the FTIR spectroscopic investigations were 0.82% Co/SiO_2 and 4.7% Co/SiO_2 as well as 1% Co/γ-Al_2O_3 and 4.6% Co/γ-Al_2O_3.

The pretreatment of the catalysts and the experimental procedures have been described in Chapter 4.3.

With a few exceptions, the experiments were conducted using two similarly designed infrared cells. The cell containing a pressed disk of the pure support was placed downstream from the cell containing the supported cobalt catalyst disk. During the course of an experiment, spectra were recorded of both the catalyst sample and the support disk. In this way, contributions due to gas phase compounds and the support could be subtracted.

As previously mentioned, single beam spectra of the freshly reduced catalysts in H_2 (or He) at the actual reaction temperature before introduction of synthesis gas (or 10% CO in He), were used as reference spectra.

Infrared spectra obtained under reaction conditions covered the 4000-500 cm^{-1} (MID-IR) range. Within this frequency domain, three regions are of particular interest; 3050-2700 cm^{-1}, 2100-1800 cm^{-1} and 1800-1200 cm^{-1}. Spectra of adsorbed species in these frequency regions will be presented - unless otherwise stated - in two different ways:

1. Spectra of molecularly adsorbed CO, when observed, are presented as difference spectra. Post run, manual subtraction of the spectra of the support disk (denoted reference absorbance spectra) from the spectra of the catalyst disk (sample absorbance spectra) recorded under reaction conditions yielded the difference spectra. Consequently, infrared absorptions due to for example gas phase CO (the R and P branch) and, in principle, support effects, could be minimized or eliminated.
2. Spectra of adsorbed species in the C-H stretching region and the region below 1700 cm^{-1}, the frequency range generally attributable to C-H bending vibrations or O-C-O or C=O vibrations in surface species like formates or carbonates, are presented as standard absorbance spectra, $A=-\ln (I/I_0)$, where I_0 and I are the intensity of the incident and transmitted infrared beam, respectively.

Being aware of the inherent risk in quantitatively comparing the intensitites of the infrared bands from different samples, this is nevertheless done in order to at least extract useful information about possible trends in the experimental data. Thus, absolute values of the band intensities from different samples at different reaction conditions are usually not compared or used, except in the estimation of the heat of adsorption of carbon monoxide on 4.7% Co/SiO_2, and in the calculations of the amount of adsorbed CO and CH_2/CH_3 on the same catalyst. In those figures where the intensity appears along the y-axis, the absorbances are related to a common basis. The band intensities are corrected, taking into account the weight of the catalyst pellet and the cobalt content. In some cases, for example in the subtraction of reference absorbance spectra from the sample absorbance spectra, the effect of imperfect matching of the sample and the blank lead to artifacts which may be misinterpreted.

5.2.2. A brief study of SiO_2

The majority of the experiments in the present infrared study have been carried out using silica supported Co-catalysts. However, silica itself is known to have numerous absorption features in the mid-infrared region, thus making the interpretation of spectra recorded under reaction conditions not so straight forward as may be anticipated.

Infrared absorption spectra of silica obtained at different temperatures under pretreatment conditions are shown in Fig. 5.2.2-1. The spectra were obtained by referencing silica spectra at various temperatures to a silica spectrum taken at 373K. A number of temperature dependent features can be seen, especially in the high-and low frequency end of the spectra. The broad, inverted band extending over the 3800-3300 cm^{-1} range is attributed to O-H stretching vibrations mainly due to strongly hydrogen-bonded hydroxyl groups (peak maxima near 3500 cm^{-1}) and to free, unpertubed by hydrogen bonding (isolated, non-interacting) hydroxyl groups (silanol-groups; SiOH, strong inverted band around 3734 cm^{-1}). The lines appearing in the broad band centered around 3500 cm^{-1} can be ascribed to surface hydroxyl groups exhibiting different degree and strength of hydrogen bonding between adjacent groups. The inversion of these bands arises from different concentrations of hydroxyl groups on the surface at different temperatures. Increasing the temperature resulted in some depletion of the hydrogen bonded surface hydroxyl groups, while the silanol groups, in which hydrogen bonding to other surface hydroxyl do not occur, were rather unaffected by temperatures up

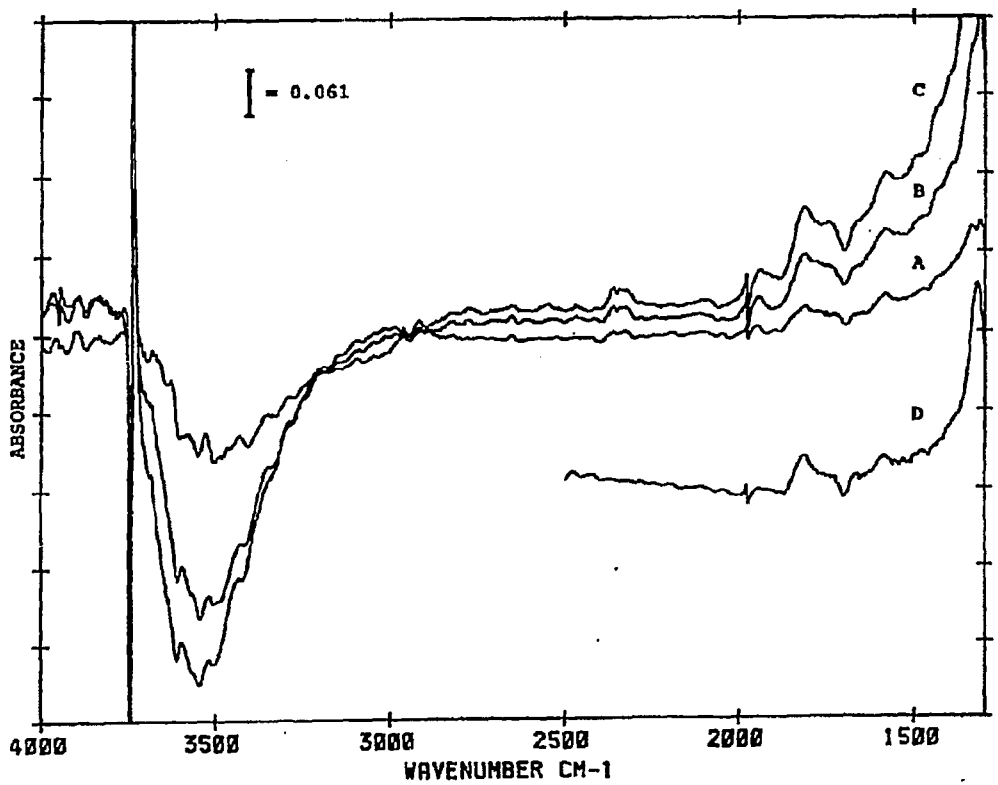

Fig. 5.2.2-1: **Infrared spectra of SiO_2 at different pretreatment temperatures.**
A : 473K, B : 573K, C : 673K, D : 523K (recorded after drying at 673K for 14 hours)
Pretreatment conditions:
P_{Tot} = 6 bar, 100 Nml H_2/min.

to 673K. The weaker the hydrogen bonding interaction, the higher is the temperature required for dehydroxylation of these species /166/.

The bands located at 1979/1940 cm^{-1}, 1813 cm^{-1} and 1580 cm^{-1} are due to silica lattice vibrations (overtone bands). The intensity of these bands increased with increasing temperature, yielding a temperature-dependent absorption spectrum. The absorption resulting from silica overtone bands as well as the fundamental transverse and longitudinal vibrations of the SiO_2-lattice (below 1500 cm^{-1}) must, to the greatest possible extent, be eliminated. This is especially important for the overtone bands, due to the fact that the weak absorption band ascribed to bridge-bonded CO may be superimposed on the relatively strong silica lattice vibration bands. Another point to be considered is the effect of the sample thickness on the absorbance-temperature relationship. Different Co-catalyst samples may exhibit a different absorbance dependency of the temperature than shown in Fig. 5.2.2-1 due to different amounts of silica. When the intensities (as peak heights) of the silica overtone bands are plotted as a function of temperature, a linear correlation is obtained, see Fig. 5.2.2-2. Whether this process is reversible or not, is harder to judge. The intensities of the silica overtone bands at 523K (Fig. 5.2.2-1, spectrum D) indicate that this may be the case.

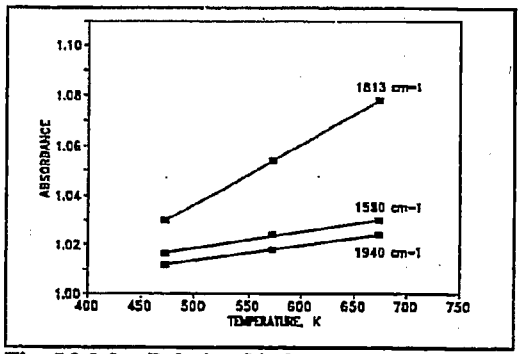

Fig. 5.2.2-2: Relationship between the drying temperature and the intensity of the silica overtone bands.

5.2.3. Hydrogenation of CO over silica supported cobalt catalysts with different metal loading

5.2.3.1. CO spectral region for 0.82% Co/SiO_2

Infrared spectra of CO adsorbed on 0.82% Co/SiO_2 during CO hydrogenation and after various times of flushing with He at 473K are shown in Fig. 5.2.3.1-1. This experiment was

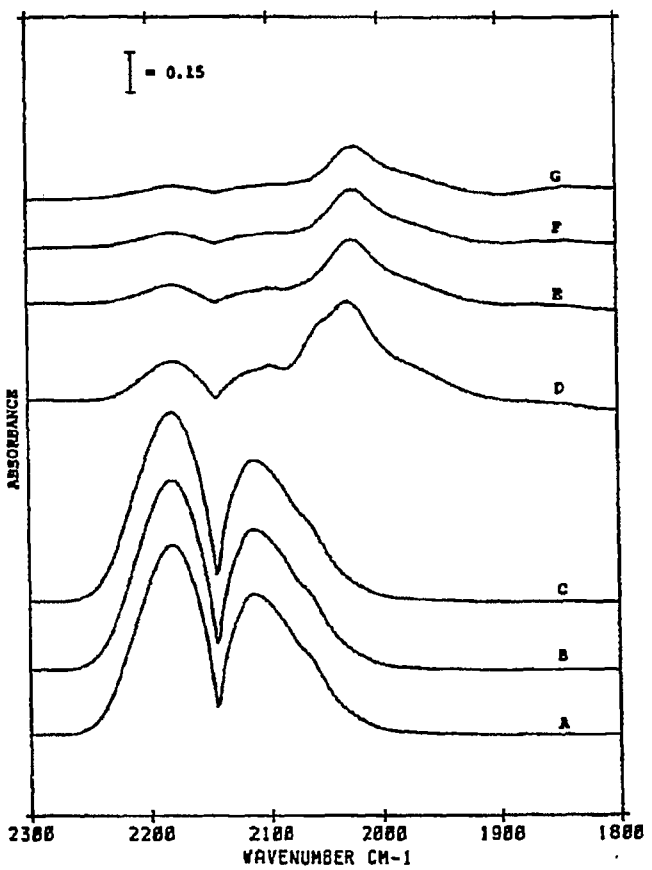

Fig. 5.2.3.1-1: **Infrared absorption bands observed in the CO spectral region during CO hydrogenation over 0.82% Co/SiO_2.**

A: After 11.5 min. in synthesis gas
B: After 13.5 min. in synthesis gas
C: After 26 min. in synthesis gas
D: After 3 min. in He (following CO hydrogenation)
E: After 22 min. in He (following CO hydrogenation)
F: After 38 min. in He (following CO hydrogenation)
G: After 55 min. in He (following CO hydrogenation)

CO hydrogenation conditions:
T = 473K, P_{Tot}= 6 bar, H_2/CO = 2, 100 Nml/min.
("single cell" experiment)

performed as a "single cell" experiment without a reference cell containing blank SiO_2, hence subtraction of the CO gas phase absorption bands was not attempted.

In the presence of gas phase CO, a poorly resolved shoulder could be observed around 2070 cm^{-1}, becoming more distinct with time in synthesis gas. This low frequency shoulder on the gas phase CO doublet becomes the dominent band after elution of synthesis gas with He. The position of the major CO band shifted to lower frequencies and the intensity decreased with time in flowing He. A weakly defined band around 1860 cm^{-1} appears after prolonged exposure of the catalyst to He. The nature and origin of this band will be discussed later in this chapter.

5.2.3.2. CO spectral region for 4.7% Co/SiO_2: $H_2/CO = 2$, $P_{Tot} = 6$ bar, T = 473-573K

Typical infrared spectra of adsorbed species in the region normally expected for molecularly adsorbed CO obtained during CO hydrogenation over 4.7% Co/SiO_2 at 473, 523 and 573K are shown in Fig. 5.2.3.2-1. The spectra at all three temperatures consists of a relatively broad, asymmetric band which does not return to the baseline at low frequencies in the spectral region of current interest. The intensity of the principle absorption band at a fixed temperature and pressure grows with time in synthesis gas until reaching a nearly constant value after approximately 15-30 min. This is illustrated in Fig. 5.2.3.2-2, showing the development of the intensity of the dominating CO absorption band. During this time period the frequency of the band remains essentially unaltered. Assuming that the

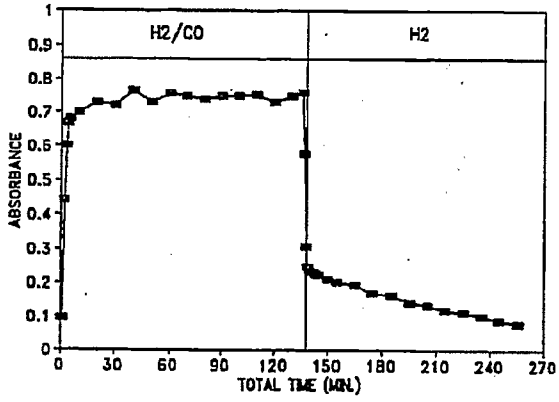

Fig. 5.2.3.2-2: The intensity of adsorbed CO (2072 cm^{-1}) during CO hydrogenation (T=473K, P_{Tot}=6 bar, H_2/CO=2) and H_2-treatment on 4.7% Co/SiO_2.

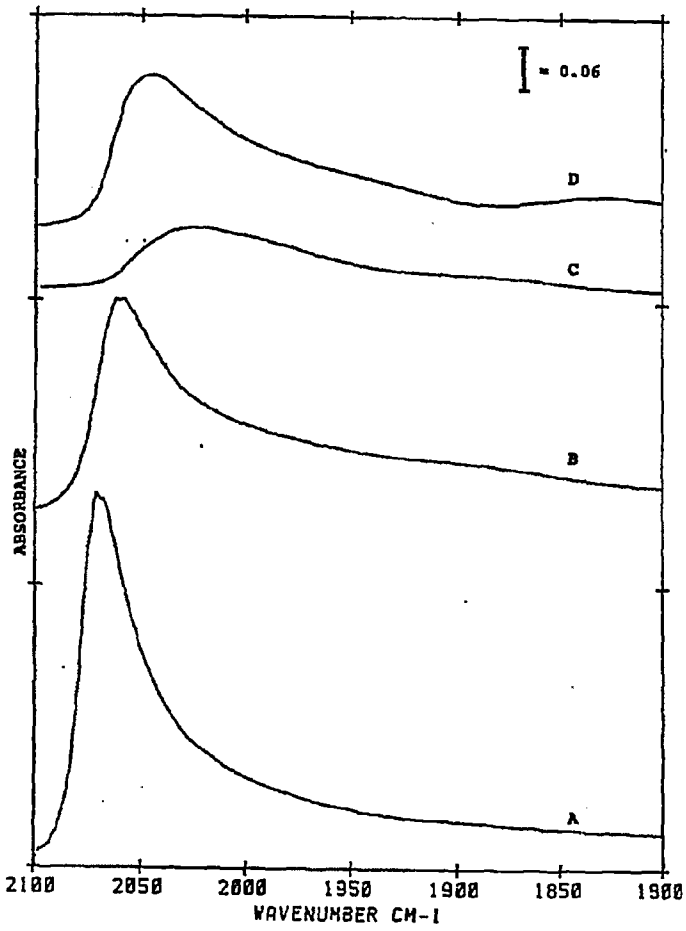

Fig. 5.2.3.2-1: **Infrared spectra of adsorbed CO on 4.7% Co/SiO_2 during CO hydrogenation and subsequent flushing with He at reaction conditions.**

A: **After 120 min. in synthesis gas at 473K**
B: **After 120 min. in synthesis gas at 523K**
C: **After 60 min. in He at 523K (following CO hydrogenation)**
D: **After 130 min. in synthesis gas at 573K**

CO hydrogenation conditions:
P_{Tot} = 6 bar, H_2/CO = 2, 100 Nml/min.

intensity of the band is proportional to the coverage of CO, the constant value then corresponds to saturation coverage of CO. The assumption of a linear relationship between the intensity and coverage of CO is valid as long as the band frequency is invariant with changes in coverage. The saturation coverage is reached at each temperature when the rate of adsorption becomes equal to the rate of desorption.

Both the position and the intensity of the absorption bands were found to depend on the temperature. As the reaction temperature was increased, Fig. 5.2.3.2-1 shows that the peak maximum was shifted to lower frequencies and the intensity of the principal CO band decreased.
Passage of He over the catalyst at reaction temperature resulted in a decline in intensity and a concurrent downscale shift in its position, see Fig. 5.2.3.2-1 spectrum C.

It seems reasonable to assume that the bands located at 2072 cm^{-1} (473K), 2058 cm^{-1} (523K) and 2045 cm^{-1} (573K) can be attributed to linearly adsorbed carbon monoxide on metallic cobalt, since no similar bands are observed over pure silica. This conclusion is based upon previous investigations of CO adsorption on supported cobalt catalysts /49,50,55,69,70,73,74, 85,86/.
Also, the low frequency shoulder on the gas phase CO bands observed in the spectra of the 0.82% Co/SiO_2 catalyst (Fig. 5.2.3.1-1) is assigned to CO adsorbed in a linear mode.
No bands in the 2200-2100 cm^{-1} range were observed in the spectra of either catalysts, except in some spectra, where the "negative" absorption appearing around 2140 cm^{-1} was due to imperfect cancelling of the gas phase CO bands. Infrared bands appearing in this region have generally been assigned to CO linearly adsorbed on cationic cobalt /49,55,70,73/, which would imply incomplete (partial) reduction of the supported catalyst.

5.2.3.3. CO spectral region for 4.7% Co/SiO_2: $H_2/CO = 2$, $P_{Tot} = 11$ bar, T = 473-573K

Increasing the total pressure to 11 bar, but applying otherwise similar reaction conditions as outlined in Fig. 5.2.3.2-1, resulted in the same temperature dependent behaviour of the

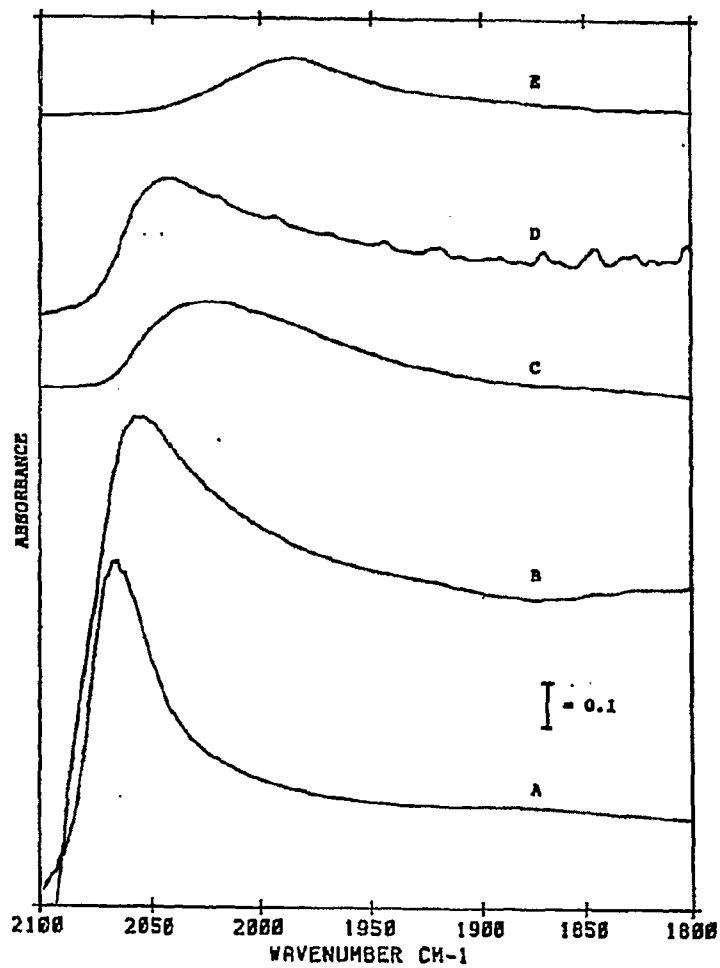

Fig. 5.2.3.3-1: Infrared spectra of adsorbed CO on 4.7% Co/SiO_2 during CO hydrogenation followed by flushing with He and then H_2, or directly by H_2.

A: After 120 min. in synthesis gas at 473K
B: After 120 min. in synthesis gas at 523K (50 Nml/min.)
C: After 60 min. in He at 523K (following CO hydrogenation)
D: After 120 min. in synthesis gas at 573K (30 Nml/min.)
E: After 60 min. in He at 573K (following CO hydrogenation)

CO hydrogenation conditions:
P_{Tot} = 11 bar, H_2/CO = 2, 100 Nml/min. unless otherwise stated.

absorption band corresponding to linearly adsorbed CO, as shown in Fig. 5.2.3.3-1. The frequency of the linear CO band shifted from 2066 cm^{-1} at 473K to 2043 cm^{-1} at 573K.
The effect of flushing with inert gas (He) on the spectra of adsorbed CO was similar to that observed in Fig. 5.2.3.2-1, viz. decreasing intensity and a downscale shift in frequency with time in He.

However, the overall band absorbances are higher at 11 bar at all the investigated temperatures compared to the CO band intensities obtained with a total pressure of 6 bar. This is illustrated more clearly by looking at the spectra presented in Fig. 5.2.3.3-2, which are obtained at the same temperature (473K) but at different reaction pressures. The frequency of the band designated as molecularly adsorbed CO in the linear form is regarded to be constant within analytical significance (which is ± 4 cm^{-1}, the applied resolution) with increasing total pressure. This indicates that the band frequency is apparently independent of the partial pressure of CO, while the opposite is the case for the intensity of the CO absorption band.

The dependence of the CO band intensity on the partial pressure of CO in the gas phase can be explained by an increasing coverage of CO, governed by the adsorption-desorption equilibrium. It is generally believed that increasing coverage (f.ex. by an increase in pressure) induces a upward shift (blue shift) in the frequency of the linear CO band /11,66,91/. The upward shift in frequency has been attributed to the reduced extent of back-donating from metal *d*-orbitals into the $2\pi^*$ antibonding orbital of CO, as a result of competition for metal *d*-electrons with increasing coverage of carbon monoxide. A weakening of the M-C bond and a strengthening of the C-O bond is explained to give an increase in the CO stretching frequency. These kinds of effects are usually termed "chemical" effects (transfer of electrons through the metal).
Secondly, dipole-dipole coupling interactions between adsorbed CO molecules are expected to increase with increasing coverage of CO.
The observed, apparent absence of any frequency shift to higher wavenumbers with increasing CO coverage on the 4.7% Co/SiO_2 catalyst can be discussed in terms of the two effects described above.
Upon adsorption of carbon monoxide, adjacent CO molecules may repel each other, leading

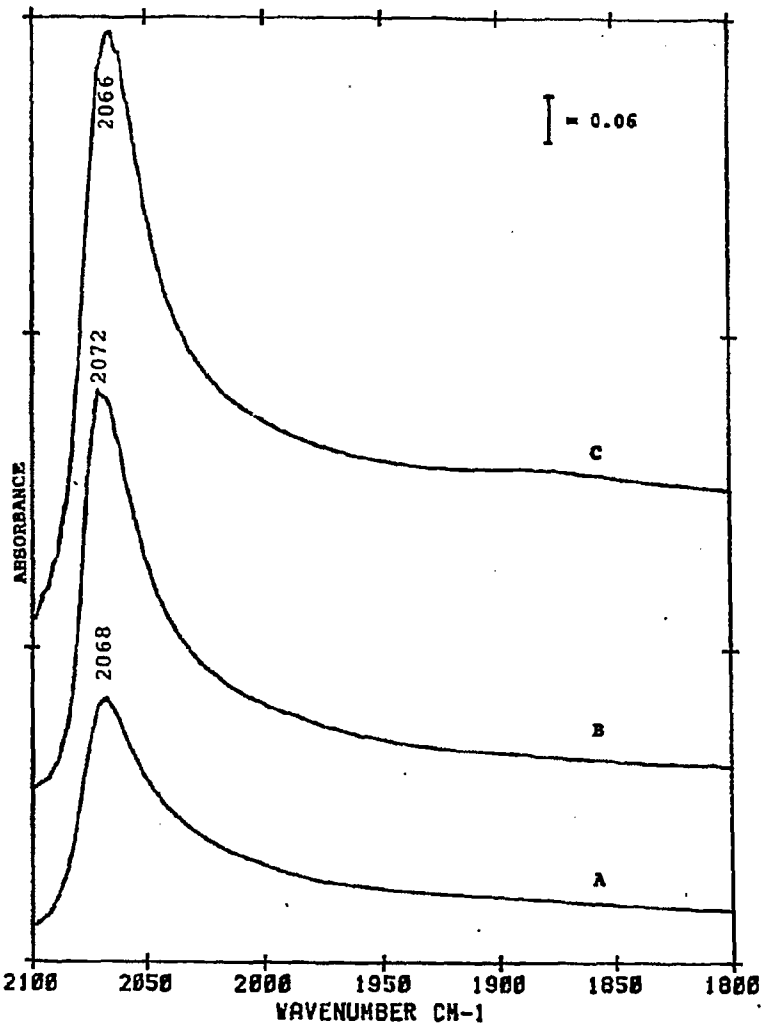

Fig. 5.2.3.3-2: **Effect of total reaction pressure on linearly adsorbed CO on 4.7% Co/SiO_2 during CO hydrogenation.**

A: **After 120 min. in synthesis gas at 2.5 bar total pressure**
B: **After 120 min. in synthesis gas at 6 bar total pressure**
C: **After 120 min. in synthesis gas at 11 bar total pressure**

CO hydrogenation conditions:
T = 473K, H_2/CO = 2, 100 Nml/min.

to a maximization of the distances between them, or attract each other, which would minimize the intermolecular distance resulting in the formation of groups of CO, or clusters of adsorbed CO molecules, that is, CO island formation. In both cases, the coupling forces will be essentially the same, while there will be differences in the physical forces. In the former case, the "repulsive" model, an increase in the coverage of CO would result in a change in the CO stretching frequency. It would be expected that the frequency progressively increases from that of the singleton frequency to a value determined by the magnitude of the coupling interactions /43/.

The second case, the formation of islands of CO is of interest in view of the results shown earlier in this section. In a strongly coupled system, the absorption band arises from islands or domains of adsorbate vibrating in phase, and the CO molecules can not be individually considered to contribute to the band /167/. A very rapid change in the frequency with coverage to a value representing saturation coverage would be expected. Under such conditions, and given the spectral sensitivity, the absorption frequency for a single CO molecule unpertubed by nearest CO neighbour may be difficult to observe, hence it would seem that the detected frequency remains constant with coverage /11/. Crossley et al. /168/ suggested that a lack of any frequency shift upon an increase in coverage could imply CO island formation. The molecular environment experienced by a CO molecule in a large island of CO molecules (interior molecule) will not be severely influenced by changes in the coverage and the frequency can therefore be regarded as constant.

CO molecules located on the edges of the island may give rise to additional bands in the infrared spectrum. Since edge and corner CO molecules have fewer neighbours compared to an interior molecule, the dipole field they experience is different. This will be even more pronounced when the ratio of edge molecules to interior molecules is low, as it will be with increasing dimensions of the CO island. The additional infrared mode due to edge effects will, when the molecules in the island are of the same type, give rise to a low frequency band/shoulder on the main absorption band which represents CO island molecules vibrating in-phase /169/. Thus, CO molecules at the edge of the islands may account for the asymmetric shape of the principal CO band observed in the 2100-1900 cm^{-1} region.

Even though the dispersion of the 4.7% Co/SiO_2 catalyst is not known, it is likely to assume that a value of 7% provides a reasonable estimate. Then, applying the relationship between

dispersion and particle size given by Boudart et al. /170/, $D=0.9/d_p$, a particle diameter of 13 nm would correspond to an 782 CO molecule island. This will of course be the maximum number of CO molecules which can be adsorbed on an Co particle of the given size. This number does not represent the actual size of the island, since adsorption stoichiometry, heat of adsorption etc. is not included in the calculations.

Thus, a possible explanation for the lack of any significant shift in frequency with increasing coverage could mean that the adsorption proceeds by CO island formation, indicative of a coverage independent CO molecular environment.

On the other hand, the constant frequency with increasing coverage of CO could point to the fact that interadsorbate vibrational coupling is absent, or at least very weak. The consequence is that the observed CO frequency at reaction conditions then possibly can be regarded as that belonging to an isolated CO molecule. Since the linear CO band develops at a constant γ_{co}, this would imply that the CO molecules are far apart (spatially isolated) from each other, where each contribute as independent singletons to the infrared absorption band.

Changes in the electronic environment of the molecules ("chemical effects") must also be taken into account when considering the relatively high and constant peak frequency. The two mechanisms operating are, as earlier mentioned, donation of lone pair electrons of the carbon atom into vacant metal *d*-orbitals (5δ-bonding) and back-donating, electrons from filled metal *d*-orbitals into vacant antibonding CO orbitals (2π-bonding). It is generally believed that the positive (upward) shift arising from the 5δ/metal bonding is overcome by the stronger negative metal/2π contribution. In the deduction of the molecular orbital model, Blyholder /66/ assumed constant σ-bonds when considering CO adsorption. However, it is possible that contributions from the 5σ/metal component must be included when trying to explain the lack of any frequency shift with increasing coverage. Hollins et al. /171/ suggested that there could be a change in the balance of the 5σ/2π bonding components in such a way that no competition for *d*-electrons develop as the coverage of CO increases. It was reported that the approximately invariant CO frequency on Cu upon an increase in the coverage of CO was due to a cancelling of the dipole-dipole interactions by a chemical shift in the opposite direction. This may seem reasonable for Group IB metals like Cu, which is characterized by negative work function changes and the metal/CO $2\pi^*$ back-donation is strongly reduced. Increasing θ_{CO} would result in reduced donation from the 5σ orbital, hence a negative shift in frequency

would be expected /172/. The direction of the chemical shift will depend on the applied transition metal. For example, from CO adsorption on Pd(100), a upscale shift in frequency was reported /173/. Thus, one can envisage a shift to higher as well as lower frequencies, or none at all, depending on the extent of electron donation and/or back-donation.

The constant frequency with increasing coverage can then possibly be related to a coverage dependent, bonding induced shift (chemical) acting in the opposite direction of the dipole-dipole interactions, as proposed by Crossley et al. /168/. A similar explanation was given by Hardeveld et al. /174/ to account for the constant frequency of N_2 on nickel.

In the present case, this would imply an increased occupancy of the d-π orbital, contrary to the predictions from the molecular orbital model, which suggests a reduction in the degree of electron back-donation resulting from increased competition for metal d-electrons with increasing CO coverage.

However, the presence of electron-donating adspecies may change the situation. One could then envision a case where the "loss" of electrons/charge (reduction in back-bonding due to increased competition) is compensated for by donation of electrons from coadsorbed species, thus maintaining the relative orbital electron density, despite an increase in the coverage of CO. It is not unlikely that hydrogen or atomic carbon (from the dissociation of carbon monoxide) may act as electron donor ligands. The influence of the donation of electrons from f.ex. hydrogen can be extended to not only include "compensating" donation, but also donation of electrons through the metal, which probably would have the effect of reducing the CO frequency to lower wavenumbers. Thus, it can be speculated if the magnitude of the downscale shift is of such an order that it could counteract the dipole-dipole coupling shift towards higher frequencies. Thus, it is possible that the presence of coadsorbates influence the electron density in the proximity of the metal and enhances the back-donation of electrons into the $2\pi^*$ antibonding orbital of CO. The two interacting effects, dipole-dipole coupling interactions through space, and the electron-donating through the metal, could then on Co be proposed to be of approximately the same magnitude. The slight variations in the observed CO frequency with the different reaction conditions can then be attributed to the imperfect cancelling, either regarding the $5\delta/2\pi$ constellation and/or that of the dipole-dipole/chemical interaction.

5.2.3.4. CO spectral region for 4.7% Co/SiO_2: $H_2/CO = 3$, $P_{Tot} = 6$ bar, T = 473-573K

Since the band intensity was found to be influenced by the partial pressure of CO, it was of interest to investigate a possible relationship between the CO band intensity and/or frequency and the H_2/CO ratio. Spectra recorded with a H_2/CO ratio of 3 at the reaction temperatures 473, 523 and 573K are shown in Fig. 5.2.3.4-1. Prominent absorption bands assigned to linearly adsorbed CO were observed with peak maxima located at 2068 cm^{-1} (473K), 2058 cm^{-1} (523K) and 2045 cm^{-1} (573K). The frequency of the linear CO band shifted downscale with increasing temperature. The frequency shift at each temperature was of approximately the same order of magnitude as with H_2/CO=2. The intensities decreased with increasing reaction temperature; the absorbance at 573K declined to approximately 44% of that at 473K. Furthermore, introduction of He at reaction temperature following CO hydrogenation resulted in a broadening and red shift in frequency with time in He.

From a comparison of the spectra in Fig. 5.2.3.2-1 and Fig. 5.2.3.4-1, it is seen that there are no significant differences in the peak positions of the linear CO band with increasing H_2/CO ratio. Concerning the intensities, these were higher at 473K and a H_2/CO ratio of 2 than at the same temperature but with H_2/CO=3. However, at reaction temperatures of 523 and 573K, the intensities of the CO band were almost identical. It should further be noted that the flow of synthesis gas was varied during the experiments conducted at 523K and 573K, as described in the figure text (Fig. 5.2.3.4-1).

At least two possible effects of adsorbed hydrogen on the spectra of adsorbed CO can be envisaged:

1. Electronic effect, where hydrogen may act as an electron donor increasing the electron density on the metal and consequently additional donation of electrons into the $2\pi^*$-antibonding CO orbital may take place. This lead to a stronger metal-carbon bond strength and a weakened C-O bonding, hence a downscale shift (red shift) in the vibrational frequency of CO is often observed.

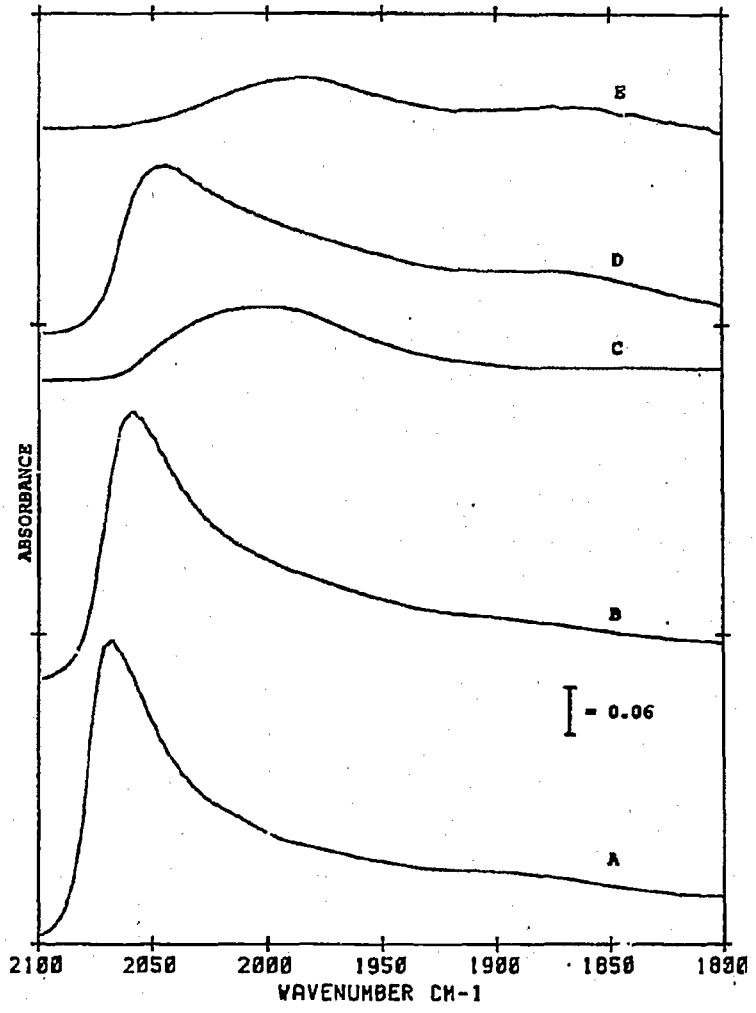

Fig. 5.2.3.4-1: Infrared bands due to linearly adsorbed CO observed during CO hydrogenation and subsequent flushing with He at reaction conditions over 4.7% Co/SiO_2.

A: After 120 min. in synthesis gas at 473K
B: After 90 min. in synthesis gas at 523K (50 Nml/min.)
C: After 60 min. in He at 523K (following CO hydrogenation)
D: After 120 min. in synthesis gas at 573K (200 Nml/min.)
E: After 60 min. in He at 573K (following CO hydrogenation)

CO hydrogenation conditions:
P_{Tot}= 6 bar, H_2/CO = 3, 100 Nml/min. unless otherwise stated

2. Dilution effect, a geometrical effect which can be explained by a reduction of the CO dipole-dipole interactions in coadsorbed layers. Hydrogen is in this case believed to function as a spacer, decoupling the adsorbate interaction resulting in a downscale shift in frequency.

If one acknowledges the structural geometric behaviour of CO, viz. the formation of CO islands, it would be of interest to investigate the adsorption of CO in the absence of hydrogen.

Fig. 5.2.3.4-2 shows the infrared spectra of adsorbed CO obtained over 4.7% Co/SiO_2 upon exposure to a premixed blend of He and CO at 473K and a total pressure of 6 bar. The linear CO band at these reaction conditions was located at 2072 cm^{-1}. Subsequent treatment with He resulted in decreasing band intensities accompanied by a downscale shift in frequency with time. After prolonged exposure to He at reaction temperature (90 min.), the temperature was raised to 598K in flowing He. The resulting spectra at selected temperatures are shown in Fig. 5.2.3.4-3.

The frequency of the band assigned to linearly adsorbed CO is the same both in the presence and absence of hydrogen, see f.ex. Fig. 5.2.3.2-1, 5.2.3.3-2 and Fig. 5.2.3.4-2. This may suggest that the adsorption of hydrogen does not influence CO adsorption, i.e. that coadsorption of hydrogen and carbon monoxide with different ratios apparently does not affect the formation of islands of CO. Since the frequencies can be considered to be constant, it can be suggested that the mutual distance between adsorbed CO molecules are unchanged. If coadsorbates influenced the formation of CO islands, a change in the frequency of the linear CO band should have been observed. Within the confines of the limited available data, it can be suggested that only small amounts of hydrogen is adsorbed on cobalt. The heat of adsorption of CO and hydrogen has been reported to 197 and 101 kJ/mole, respectively /237/. These values imply a low coverage of hydrogen. Thus, it may appear as the adsorption of hydrogen is inhibited in the presence of carbon monoxide, and it does seem that the presence of hydrogen has little or no influence on the strenght of the C-O bond in surface Co-CO. If significant H_2 adsorption does occur, there is little interaction with, or displacement of, adsorbed carbon monoxide. The retention of the 2072 cm^{-1} band shows that a major part of

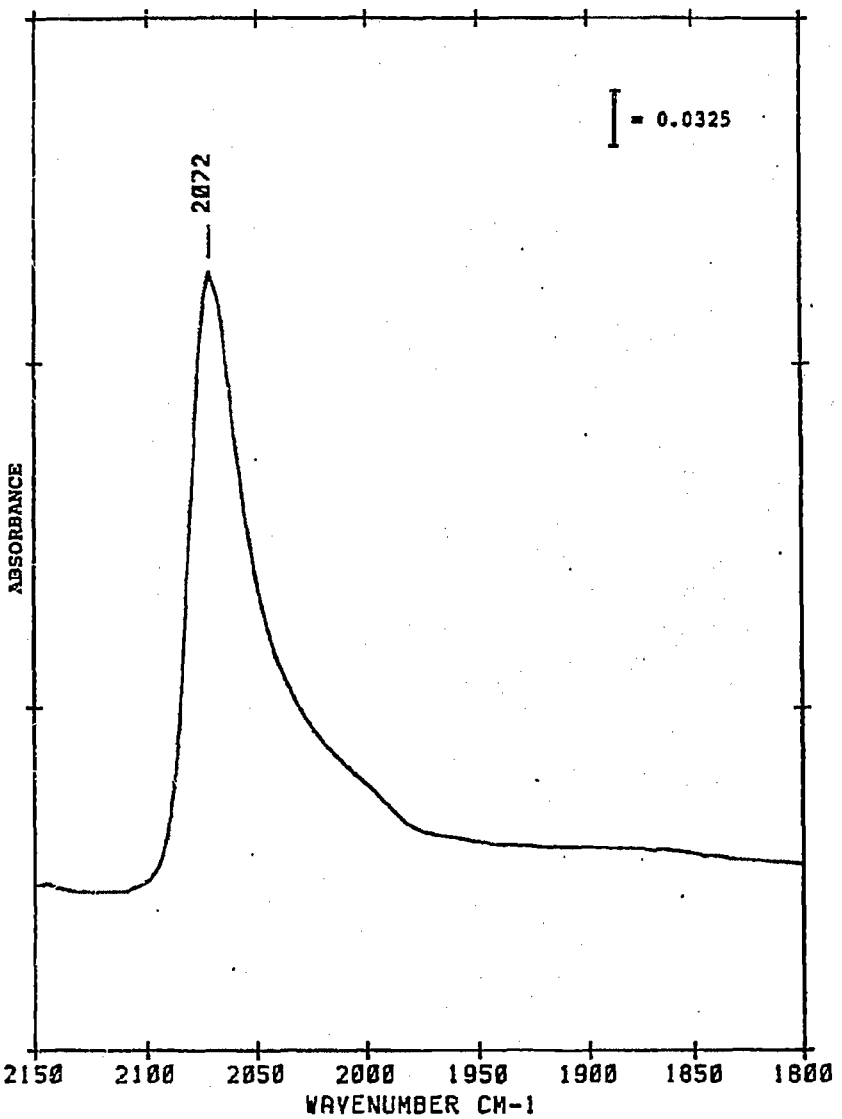

Fig. 5.2.3.4-2: **Infrared spectra of adsorbed CO on 4.7% Co/SiO_2. Spectrum recorded after 140 min. in He:CO**

CO adsorption conditions:
P_{Tot}= 6 bar, T = 473K, He:CO = 9:1, 100 Nml/min.

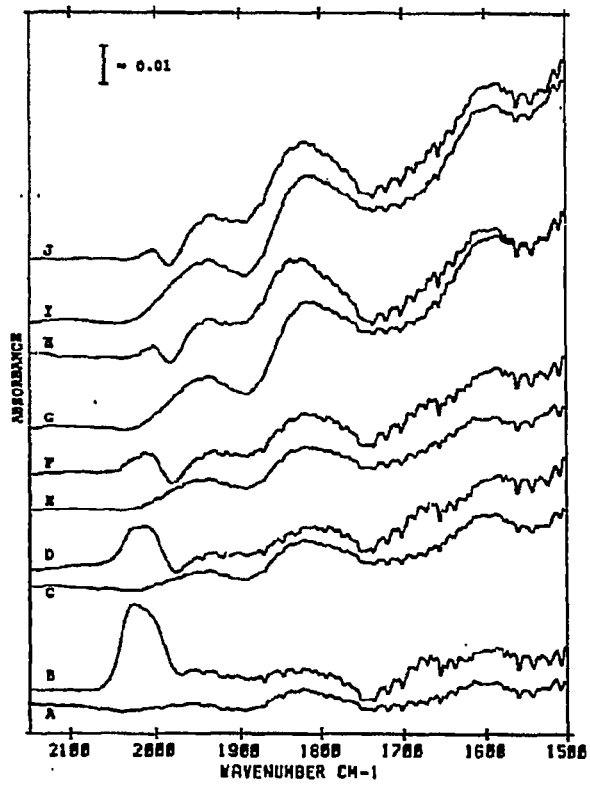

Fig. 5.2.3.4-3: **The effect of temperature on the absorption bands in the spectral region 2150-1500 cm^{-1} of 4.7% Co/SiO_2 and SiO_2.**

4.7% Co/SiO_2: B, D, F, H, J
SiO_2 : A, C, E, G, I

Spectra were recorded in He at the following temperatures after exposure of the pressed disks to He:CO (9:1) for 140 min.:

A, B: 488K
C, D: 508K
E, F: 523K
G, H: 563K
I, J: 573K

Heating rate: 2K/min.

the Co surface retains linearly adsorbed CO in a molecular environment which is essentially unaffected by the presence of adsorbed hydrogen. Upon an increase in the temperature, the linear CO band in H_2/CO decreased in intensity and shifted to lower wavenumbers. If the catalyst had been heated in CO alone, and a similar behaviour was to be observed, these observations taken together could indicate a passive role of hydrogen.
Of further notice is that the above observations exclude the possibility of spatially isolated CO molecules, since in this case one or perhaps both of the possibilities above would be expected. Furthermore, the adsorption of CO has been found to be stronger and faster than that of hydrogen /175,176/. The fact that high surface coverages of CO exists under reaction conditions is in agreement with the partial pressure dependencies, which are near zero or negative for CO and approximately unity for hydrogen (see page 55).

The spectra in section 5.2.3.1-5.2.3.4 indicate that flushing with He following CO hydrogenation at reaction conditions results in a common behaviour of the linear CO band: a downward shift in frequency of the linearly CO band accompanied by a weakening and broadening of the band as a function of He purge time, as illustrated in Fig. 5.2.3.4-4. The width of the principal CO peak is of such a magnitude that it could possibly incorporate several different CO bonding energies, suggesting that the removal of CO molecules occurs more randomly than upon adsorption. It is believed that the general behaviour of the CO band in He can be explained by a reduction in the dipole-dipole coupling interactions, as a result of a decrease in the coverage of CO. The observed shift in frequency is of such a size that this explanation can be considered reasonable.
The downscale shift in frequency can also reasonably well be rationalized in terms of the chemical effect. Decreasing surface coverage of CO would result in an increase in metal *d*-electrons available for backbonding (diminishing competition). This strengthens the Co-C bond and weakens the C-O bond for carbon monoxide chemisorbed on the catalyst surface. The net effect would be a decrease in the vibrational frequency of carbon monoxide.

It has been shown in Fig. 5.2.3.2-2 that the intensity of the principal CO peak remains approximately constant during prolonged exposure to synthesis gas. Such a behaviour was found to be typical at each of the investigated reaction conditions. Since dipole-dipole interactions between adsorbed CO molecules also are accommondated during CO

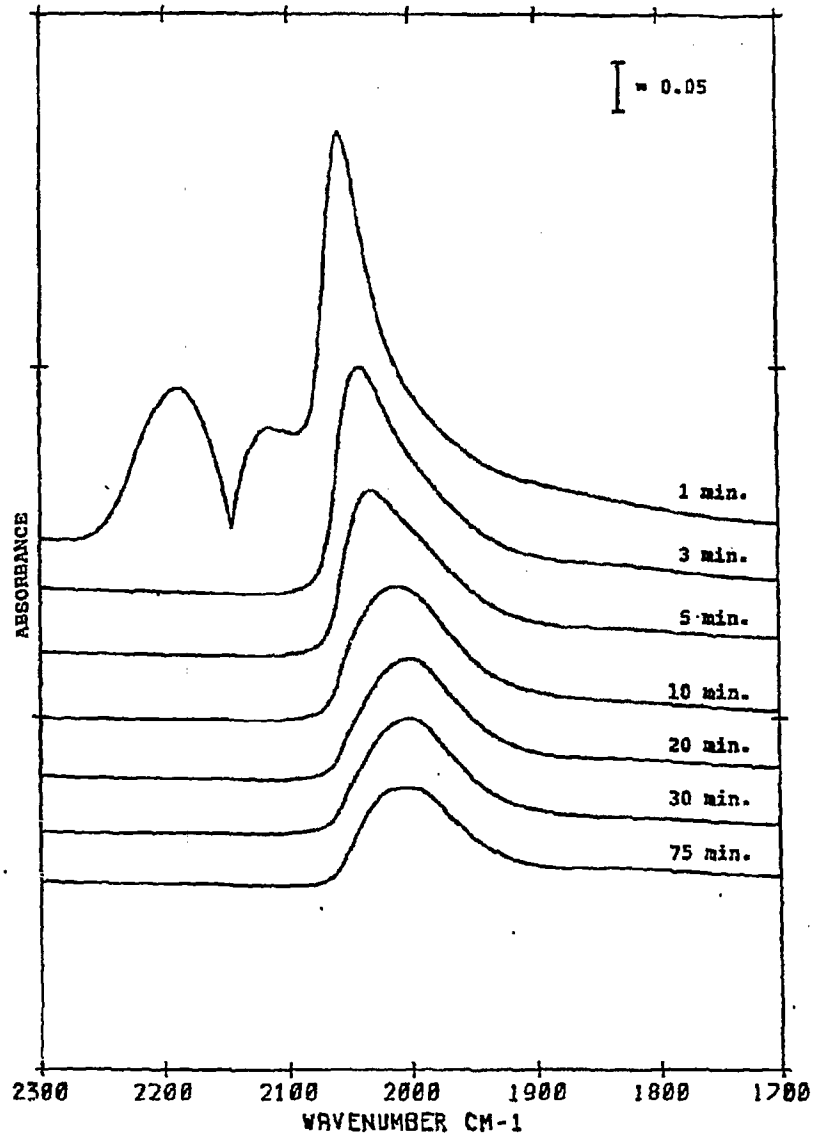

Fig. 5.2.3.4-4: **Effect of He-flushing at reaction conditions on the intensity and frequency of linearly adsorbed CO on 4.7% Co/SiO_2.**

Spectra were taken after various times in He after 1.5 hr. of exposure to synthesis gas (T=523K, P_{tot}=6 bar, H_2/CO=3).

hydrogenation, the possible influence of carbon or carbonaceous deposits with increasing reaction temperature on the vibrational coupling states becomes important. If deposition of such materials are regarded as probable, their likely effect on the dipole-dipole vibrational coupling would might be to reduce (uncouple) the CO dipole-dipole interactions, which would result in a decreasing intensity of the major CO band with time in H_2/CO. In addition, the linear CO band frequency would be affected. Why the intensity of the CO band remains unaltered is not completely known in detail. However, it could be suggested that if the dipole-dipole coupling has a sufficient long range through space character (extending "over" a site covered by carbon/carbonaceous materials), then one could possibly expect a behaviour similar to that observed.

A careful examination of the spectra in Fig. 5.2.3.1-1 to 5.2.3.4-4 reveals the occasional presence of weak features in the 1950-1800 cm^{-1} region during CO hydrogenation and subsequent flushing with He. Bands in this spectral range have generally been attributed to bridgebonded CO /50,73,74,78,85-87/. However, a number of observations disagree with such an assignment for the bands observed in this region in the present study. It will be shown that these bands are not due to bridgebonded (multicoordinated) CO, but that they could rather be associated with changes in one of the Si-O overtone bands of the silica support during reaction. Support for this assumption can be expressed as follows:

It has already been shown that the infrared spectra of SiO_2 alone consists of at least two peaks in the 2000-1800 cm^{-1} frequency range, of which the 1813 cm^{-1} band is by far the most intense. The corresponding band for the silica supported Co-catalysts is located near 1870-1860 cm^{-1}. Fig. 5.2.3.4-5 shows the single beam spectra of a 4.7% Co/SiO_2 catalyst and pure SiO_2 immediately before introduction of synthesis gas. Absorption bands due to silica overtone are evident in the spectra at 1997 and 1871 cm^{-1}. The presence of these bands is due to imperfect cancelling upon dividing the sample spectra on the reference spectra.

During CO hydrogenation as well as in He or H_2, infrared bands in similar positions can be observed in the absorbance spectra of both the sample and reference. Subtracting the reference absorbance spectra from the sample absorbance spectra yielded in most cases a flat baseline, as can be seen in the difference spectra presented in Fig. 5.2.3.2-1, spectrum A. Occasionally, however, weak absorption bands were observed in the difference spectra but their peak positions differed from one spectrum to another. The location of these peaks was found to

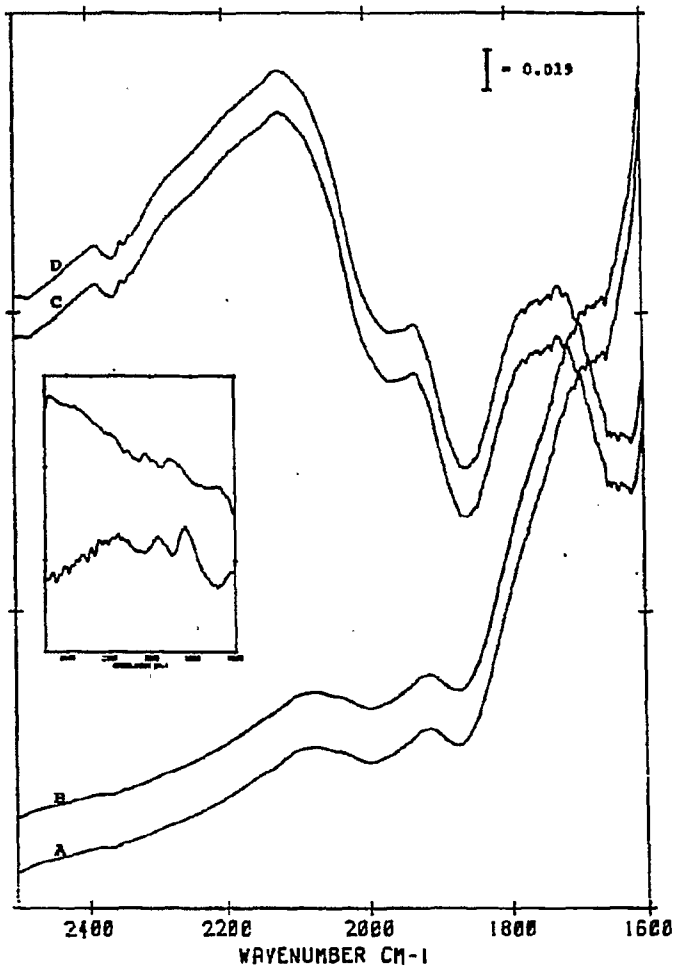

Fig. 5.2.3.4-5: Single beam spectra of 4.7% Co/SiO_2 and SiO_2 alone.

A,B: Single beam spectra of 4.7% Co/SiO_2
C,D: Single beam spectra of SiO_2

Spectra were recorded at 473K and 11 bar total pressure in flowing H_2.
Pretreatment conditions:
Reduction for 16 hours at 673K in flowing hydrogen followed by cooling (in H_2) to 473K.

Bottom spectrum in figure insert: 100% line of 4.7% Co/SiO_2
Upper spectrum in figure insert: 100% line of SiO_2

depend on the quality of the reference spectra recorded during the course of an experiment. Especially at high total reaction pressures, two ill-defined spikes for $CO_{(g)}$ could be detected instead of the usual, distinct doublet. Typical for these spectra were irregular, high absorbances, often accompanied by a shift in the frequency of the bands in the region below 2000 cm^{-1}. Fig. 5.2.3.4-6 illustrates some of the above effects and their influence on the difference spectra.

Using these reference absorbance spectra in the subtracting process resulted in weak peaks appearing at different locations in the 2000-1800 cm^{-1} region, where the peak positions of the bands in this frequency range is directly dependent on the quality of the recorded reference absorbance spectrum. However, if a reference absorbance spectrum exhibiting the earlier described irregularities was substituted with a spectrum containing none of the above features, no absorption bands were detected in the spectral range of current interest.

The appearance of these peaks in the spectra at random times in synthesis gas is shown in Fig. 5.2.3.4-7. If these peaks were due to new adsorbed species, it should be possible to recognize them as new bands appearing at least in the single beam spectra with a characteristic frequency. Scrutinizing the single beam spectra revealed that this was not the case. Fig. 5.2.3.4-8 shows that it is not possible to recognize new bands, which would imply the formation of bridgebonded carbon monoxide. It is believed that changes in the Si-O vibrations of the support may explain the appearance/disappearance of this band. Furthermore, these peaks were often present already in the 100% line, that is, the spectrum obtained by ratioing two single beam spectra of the catalysts, obtained either in H_2 or He, before the introduction of reactant gases, see Fig. 5.2.3.4-5.

If these bands belong to bridgebonded CO, one should also expect that the growth should match the development of the band for linear CO during CO hydrogenation. The intensity of these bands increased with temperature when the catalyst was heated to 598K in flowing He following CO adsorption at 473K (He:CO=9:1), as can be seen from Fig. 5.2.3.4-3. Such a behaviour is analogous to the situation described in Fig. 5.2.2-1 for the temperature dependence of the silica overtone bands. Plots of the changes in absorbance with temperature are shown in Fig. 5.2.3.4-9 and 5.2.3.4-10, illustrating in a convincing manner the increase in the intensity of these bands with increasing temperature.

Even if the frequency occasionally coincides with that of bridgebonded CO, the shape, intensity and half height width of the peaks in the present study differ from peaks in the

Fig. 5.2.3.4-6: **Effect of the quality of the reference absorbance spectra on the CO difference spectra.**

A) **Sample (4.7% Co/SiO_2) absorbance and reference (SiO_2) absorbance spectra after 100 min. in synthesis gas.**

Figure insert: **Difference spectrum in the spectral region 2100-1500 cm^{-1}.**

B) **Sample (4.7% Co/SiO_2) absorbance and reference (SiO_2) absorbance spectra after 110 min. in synthesis gas.**

Figure insert: **Difference spectrum in the spectral region 2100-1500 cm^{-1}.**

CO hydrogenation conditions:
P_{Tot} = 11 bar, H_2/CO = 2, T = 473K

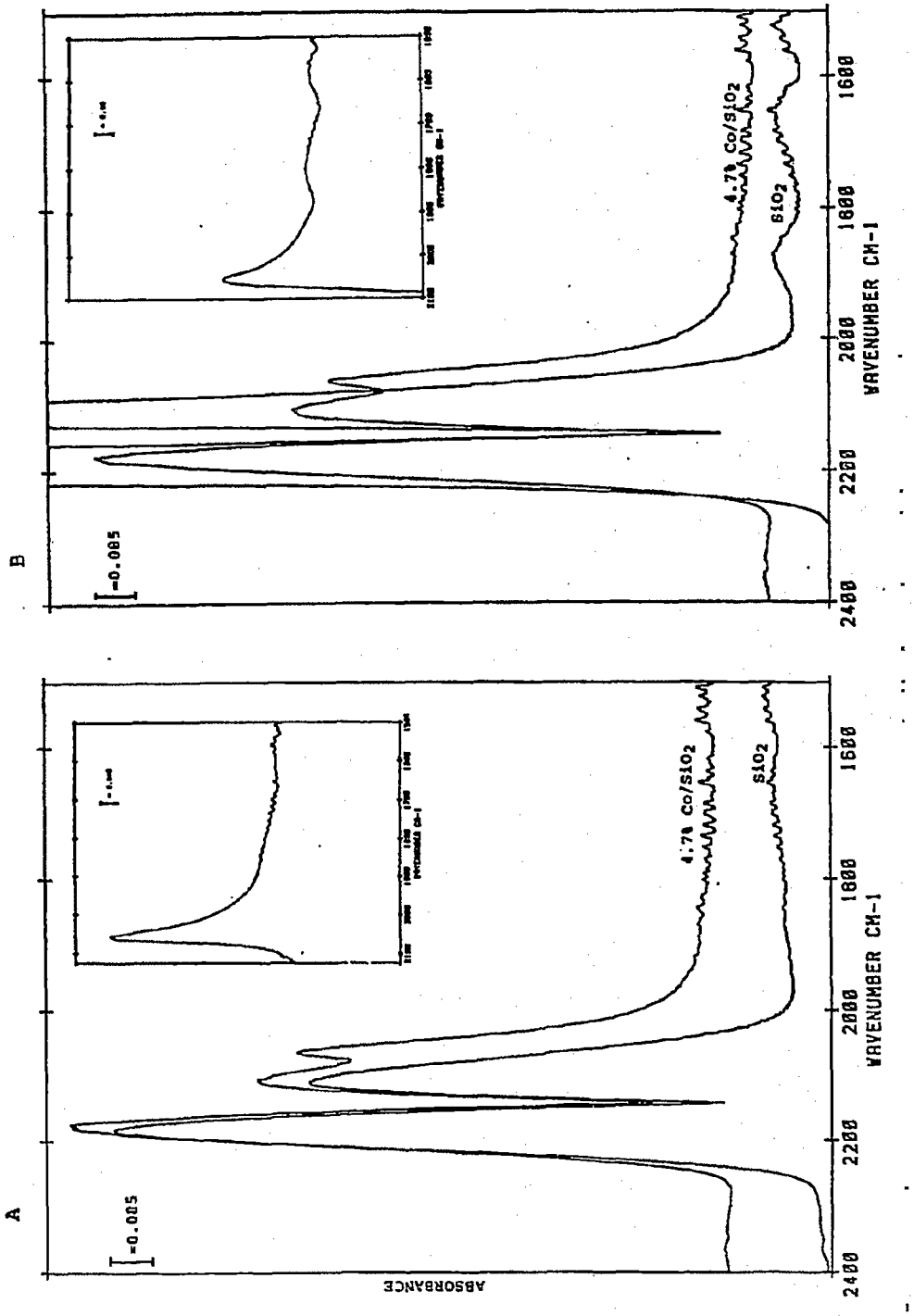
A
B
ABSORBANCE
=0.005
=0.085
4.7% Co/SiO2
SiO2
2400
2200
2000
1800
1600
WAVENUMBER CM-1

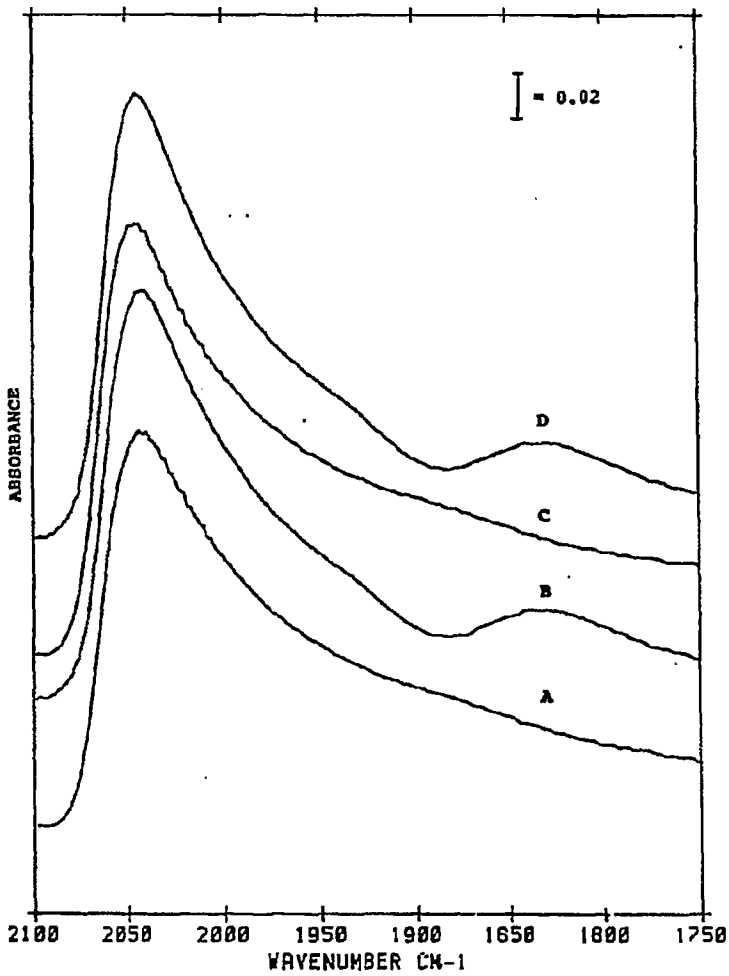

Fig. 5.2.3.4-7: **Appearance of bands in the CO spectral region of 4.7% Co/SiO_2 at different times in synthesis gas.**

A: **After 30 min. in synthesis gas**
B: **After 40 min. in synthesis gas**
C: **After 60 min. in synthesis gas**
D: **After 70 min. in synthesis gas**

CO hydrogenation conditions:
P_{Tot} = 6 bar, T = 573K, H_2/CO = 2, 100 Nml/min.

Fig. 5.2.3.4-8: Single beam spectra of 4.7% Co/SiO_2 obtained at different times during CO hydrogenation.

A: After 30 min. in synthesis gas
B: After 40 min. in synthesis gas
C: After 60 min. in synthesis gas
D: After 70 min. in synthesis gas
E: Reference spectrum 4.7% Co/SiO_2 obtained in hydrogen at 573K

Figure insert: Single beam spectrum of SiO_2 alone at 573K

CO hydrogenation conditions:
P_{Tot} = 6 bar, T = 573K, H_2/CO = 2, 100 Nml/min.

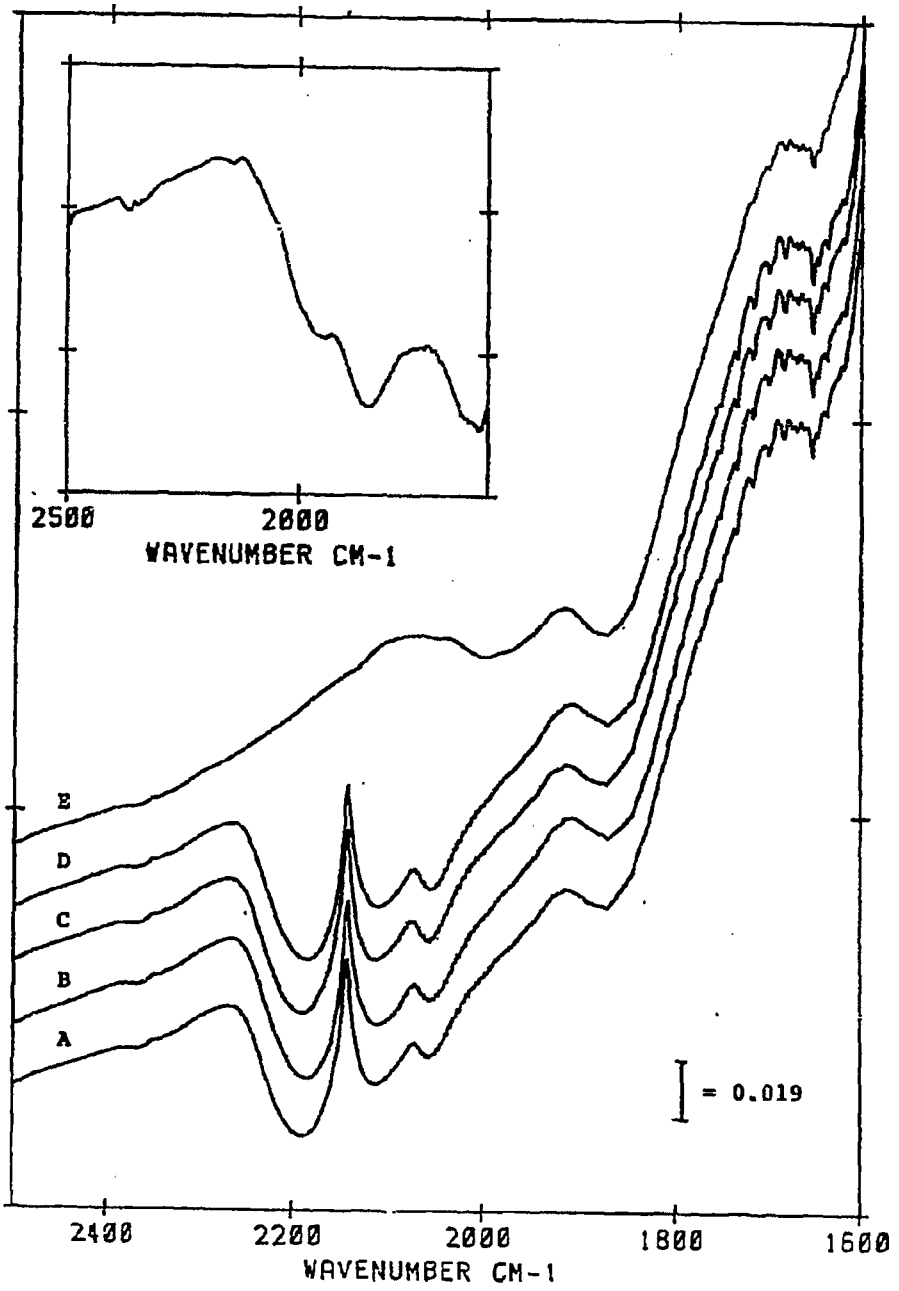
2500
2000
WAVENUMBER CM-1
E
D
C
B
A
= 0.019
2400
2200
2000
1800
1600
WAVENUMBER CM-1

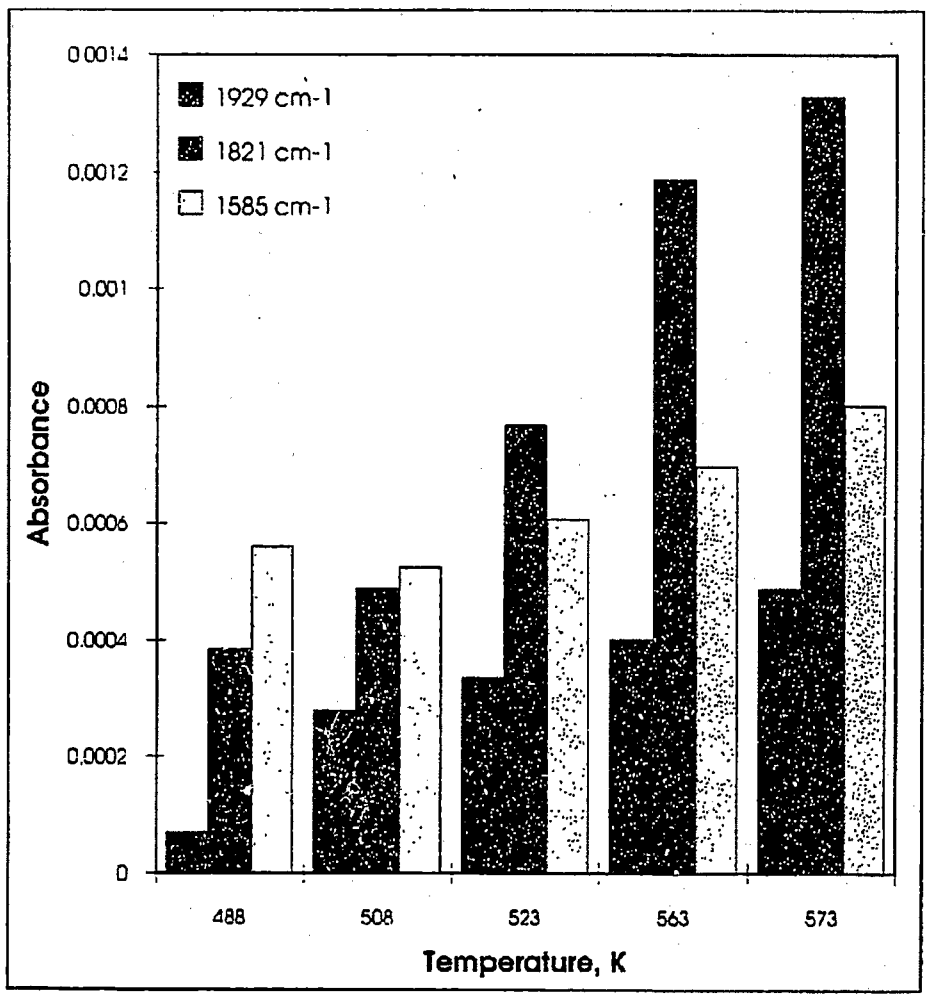

Fig. 5.2.3.4-9: **Development of the intensities of the silica overtone bands with temperature for 4.7% Co/SiO_2.**

Fig. 5.2.3.4-3 constitutes the basis for the estimations of the intensity (as peak heights)

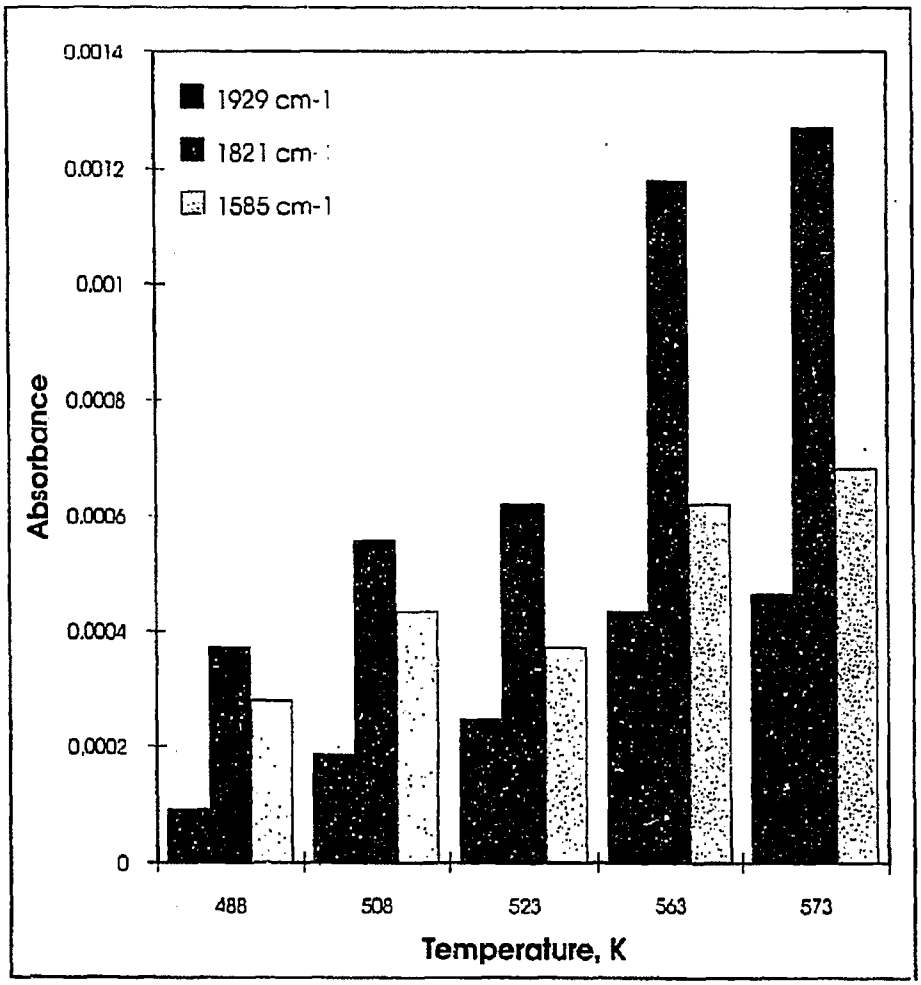

Fig. 5.2.3.4-10: **Development of the intensities of the silica overtone bands with temperature for SiO_2.**

Fig. 5.2.3.4-3 constitutes the basis for the estimations of the intensity (as peak heights)

literature assigned to bridged carbon monoxide. Based on the previous argumentation, bands observed in the 2000-1800 cm^{-1} range for silica supported Co-catalysts in this study are believed not to represent bridgebonded CO, but belong to silica overtone vibrations. Thus, one may conclude that linearly adsorbed CO appears to be the dominant species present on the catalyst surface. The lack of any distinct bands attributable to bridgebonded CO can either be due to a poor dispersion of the 4.7% Co/SiO_2 catalyst, or that its concentration is below the detection limits under the present circumstances.

The reason for the sporadic, poor quality of the reference absorbance spectra could possibly be explained by the procedure applied during collection of the sample and reference spectra, which took advantage of the mirror switching capabilities of the FTIR-instrument. Spectra were in most cases recorded at 5-10 minutes intervals. During this hold time, the IR-beam was always directed through the sample chamber containing the cell with the catalyst disk. After sampling these interferograms, the mirrors were switched over, directing the IR-beam through the reference cell, in which a disk of the pure support was placed. Spectra were taken immediately after the mirror switch without allowing ample time for stabilization of the beam. After the reference spectra had been collected, the mirrors were once again switched back to the sample chamber.

The observation of spikes for gas phase CO instead of the usual distinct doublet can possibly be related to the design of the infrared reactors and the experimental setup. The reacting gases flowed over the pressed disks while the IR beam passed perpendicular through the wafers. Thus, stagnant films of carbon monoxide created by local low-velocity flows parallel to the catalyst surface may be the reason for the periodically detected gaseous CO band spikes.

5.2.3.5. Estimation of the heat of adsorption of CO on 4.7% Co/SiO_2

By considering the intensities of the adsorption band due to linearly adsorbed CO, one would expect that plotting the absorbances as a function of the CO partial pressure would result in data points falling along straight lines, independent of the partial pressure of hydrogen. Using the Langmuir isotherm approach, i.e.

$$\theta_{CO} = \frac{K_{CO} \cdot P_{CO}}{1 + K_{CO} \cdot P_{CO}} \qquad 5.2$$

where $\theta_{CO}=A_s/A_\infty$, θ_{CO} is the coverage of linearly adsorbed CO under reaction conditions, A_s the actual absorbance at the applied reaction conditions, A_∞ is the absorbance (at infinite CO pressure corresponding to) complete monolayer coverage of carbon monoxide, P_{CO} the partial pressure of CO and K_{CO} the effective equilibrium constant for CO adsorption. Modifying the above equation by multiplying both sides with $1/A_s \cdot K_{CO}$ and rearranging leads to the expressions:

$$\frac{A_s}{A_\infty} + \frac{A_s}{A_\infty} \cdot K_{CO} \cdot P_{CO} = K_{CO} \cdot P_{CO} \qquad 5.3$$

$$\frac{P_{CO}}{A_s} = P_{CO} \cdot \left(\frac{1}{A_\infty}\right) + \frac{1}{K_{CO} \cdot A_\infty} \qquad 5.4$$

Plotting P_{CO}/A_s as a function of the partial pressure of CO would then be expected to give a straight line. The slope of the line corresponds to $1/A_\infty$, while the intercept with the y-axis represents the value of $1/(A_\infty \cdot K_{CO})$. Typical results are shown in Fig. 5.2.3.5-1 for the infrared data collected at 473, 523 and 573K over 4.7% Co/SiO_2 ($H_2/CO=2$). The absorbance values are corrected for the differences in disk weights, allowing direct comparison between the catalyst samples. It is seen from the figure that, at least in the case of the reaction carried out

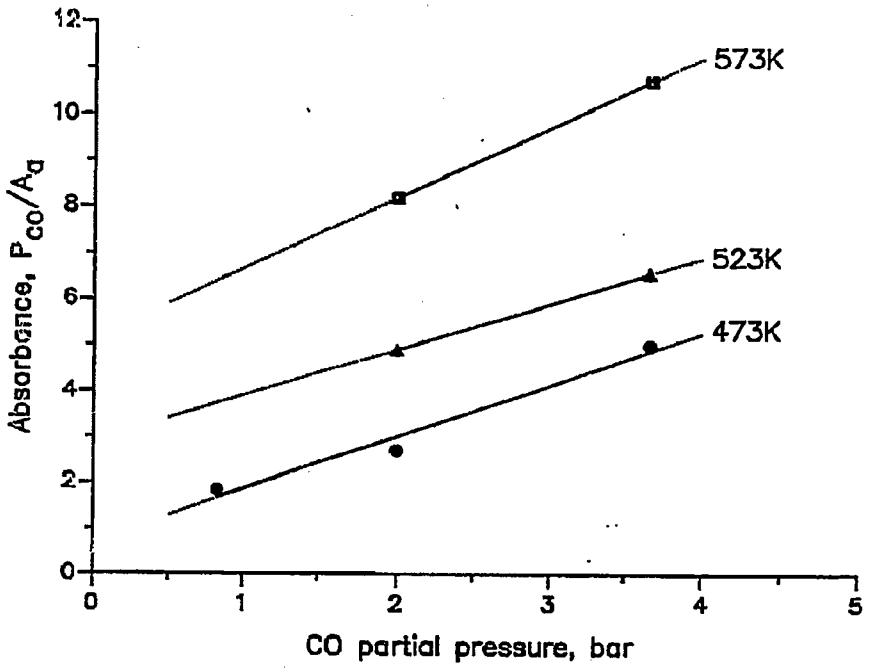

Fig. 5.2.3.5-1: **CO adsorption data plotted according to equation 5.4 for 4.7% Co/SiO_2.**

at 473K, the adsorption of carbon monoxide fairly well follows the Langmuir isotherm. The adsorption constant K_{CO} can now be estimated using the following procedure. From the slope of each line in Fig. 5.2.3.5-1, $1/A_{\alpha}$ is determined. The equilibrium constant K_{CO} can then be calculated applying A_{α} and intercepts from Fig. 5.2.3.5-1. Graphical solution of the van't Hoff equation results in a straight line with a slope corresponding to $-\Delta H/R$. From Fig. 5.2.3.5-2, a heat of adsorption of about 40 ± 30 kJ/mole can be estimated. The value obtained in this way is relatively small with respect to CO adsorption on cobalt single crystals, where values up to 126 kJ/mole has been suggested /120/. The estimated heat of adsorption agrees rather well with that reported in the kinetic study of Huff et al. /177/, 25 kJ/mole. Vannice /120/ assumed that the value for the heat of adsorption of CO on Co was between those of

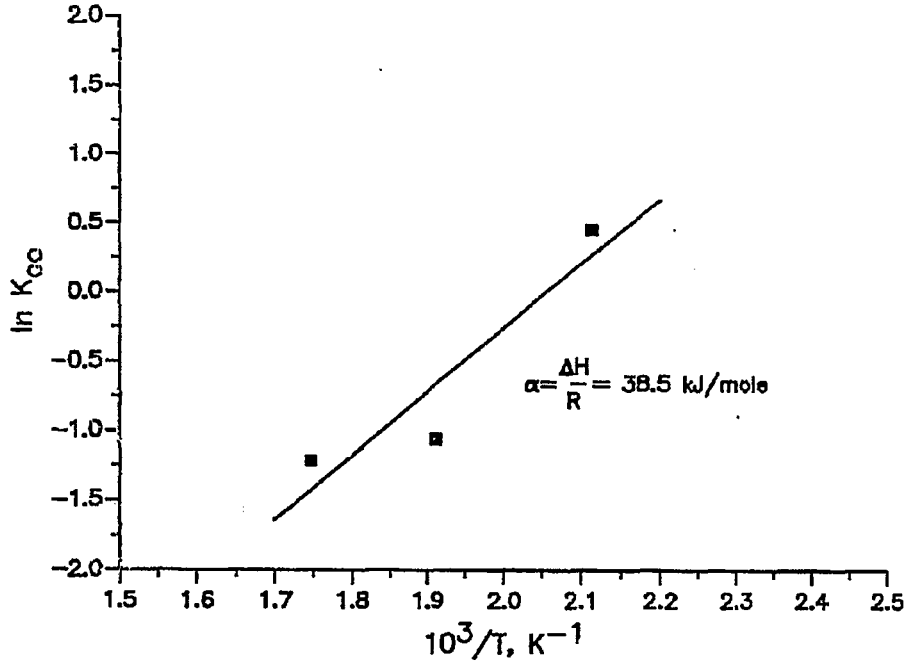

Fig. 5.2.3.5-2: Estimation of the heat of adsorption of CO on 4.7% Co/SiO_2.

Fe and Ni, and assigned a ΔH_a value of 126 kJ/mole for CO on cobalt single crystals. Kantaradage et al. /178/ reported the heat of adsorption of CO on Co-films to 75-84 kJ/mole at 303K, while on Co/γ-Al_2O_3, a value of 70 kJ/mole was found (524-573K) /179/.

The assumptions invoked when deriving the Langmuir-Hinschelwood expression is i) immobile adsorption, ii) each site accommodates one molecule, iii) same adsorption energy on all sites, i.e. energetically uniform, and iiii) the adsorption energy is unaffected by adsorption on neighbouring sites. It could be surmised if point iii) and iiii) correspond to a constant heat of adsorption. Somorjai /180/ reported a decrease in ΔH with increasing coverage ($>\theta=0.5$). The heat of adsorption per molecule at near monolayer coverage is about one-third of that at low coverage, 46-54 kJ/mole versus 105-134 kJ/mole, due to repulsive

CO-CO interactions between adsorbed CO molecules.

Generally, the present obtained value of the heat of adsorption of CO appears to be somewhat low compared to those reported in the literature. It could be suggested that the differences relates to the inherent difficulties in reliable measurements of the heat of adsorption. Factors like temperature, coverage and surface heterogeneity must be taken into consideration. Changes in the bonding or coverage of CO with increasing temperature, or the presence of defect sites, steps and kinks, which adsorb CO with higher heats of adsorption, may influence the determination of ΔH_{CO}.

Appendix A6 outlines the procedure and gives examples of the applied calculation method.

5.2.3.6. Estimations of the amount of adsorbed CO on 4.7% Co/SiO_2 at reaction conditions

The relation generally used to relate the surface concentration of carbon monoxide to infrared peak areas is the Beer-Lambert equation, given by equation 5.5. Applying this equation makes it possible to estimate the amount of adsorbed CO on the catalyst surface during CO hydrogenation at different reaction conditions in the present study:

$$A_{CO} = \frac{1}{L \cdot C_{CO}} \int_{\gamma_1}^{\gamma_2} \log_{10}\left(\frac{I_0}{I}\right) d\gamma = \frac{S_{CO}}{L \cdot C_{CO}} \qquad 5.5$$

where

A_{CO} = molar integrated infrared intensity (cm/mol)

$S_{CO} = \int \log_{10} (I_0/I) d\gamma$ = area under the absorption band ascribed to linearly adsorbed CO (cm^{-1})

C_{CO} = concentration of CO (mol/cm^3)

L = sample thickness or path length (cm)

The term $L \cdot C_{CO}$ is not a convenient notation to use when it comes to the study of gases adsorbing on a catalyst surface. However, the number of moles of surface species in the wafer can be expressed as:

$$A_c \cdot C_{co} \cdot L = m \cdot n_{co} \qquad 5.6$$

where n_{co} = molar uptake of CO (mol/g)

m = weight of the pressed catalyst disk (g)

A_c = cross-sectional area of the pressed wafer (cm^2)

Solving for $L \cdot C_{co}$ and substituting the result into equation 5.5 gives:

$$n_{co} = \frac{S_{co} \cdot A_c}{m \cdot A_{co}} \qquad 5.7$$

The parameter A_i for a species *i* (for example CO) is represented by the integral of the extinction coefficient, ε_γ for a given frequency over the frequency range γ_1 to γ_2 of the infrared band for the species *i*:

$$A_i = \int_{\gamma_1}^{\gamma_2} \varepsilon_\gamma \, d\gamma \qquad 5.8$$

Equation 5.8 may be regarded as averaging the extinction coefficient over the *i* (CO) absorbance peak. The area under the linear CO absorption band was determined following the procedure given by Rasband et al. /181/, further described in Appendix A7. This method was used to provide the upper and lower integration limits, which was subsequently applied in the determination of the integrated absorbance area of the linear CO peak. Thus, the problem is reduced to obtaining values for A_{co}, the integrated absorption intensity. Duncan /182/ used ^{13}C-NMR and IR measurements to estimate the molar integrated infrared intensity, which was reported to $26 \cdot 10^6$ cm/mol for linearly adsorbed CO. Using this value, and assuming that A_{co} is independent of the coverage of CO and of the temperature, the amounts of adsorbed carbon monoxide as indicated by infrared spectroscopy can be estimated. Selected results for the silica supported Co catalysts are presented in Table 5.2.3.6-1.

Table 5.2.3.6-1: **Estimates of the amount of adsorbed CO on 4.7% Co/SiO_2 during CO hydrogenation ($H_2/CO=2$).**

Temperature (K)	*P_{Tot} (bar)*	*Amount of adsorbed CO (µmole/g catalyst)*
473	2.5	41
473	6	63
523		43
573		30

Further details of these calculations are, as already mentioned, provided in Appendix A7.
The amount of adsorbed CO decreases with increasing temperature. Possible reasons for this is discussed later in this chapter.
At a fixed temperature (473K), the lower amount of linearly adsorbed carbon monoxide can be ascribed to the lower partial pressure of CO.

As already mentioned, the dispersion of the 4.7% Co/SiO_2 catalyst is not known. However, in section 5.2.3.3, a dispersion of 7% was assumed and applied in the calculations of the approximate number of CO molecules in islands of carbon monoxide.
The amount of adsorbed CO as determined from the infrared measurements (Table 5.2.3.6-1) can be used to estimate a dispersion for the 4.7% Co/SiO_2 catalyst, assuming an adsorption stoichiometry of 1:1 (linear mode of CO bonding). Applying an average value of 45 µmole CO/g catalyst, the CO:Co ratio on 4.7% Co/SiO_2 can be estimated to 0.056, that is, a dispersion of approximately 6%.